A Subdivision Approach to the Construction of Smooth Differential Forms

Thesis by

Ke Wang

In Partial Fulfillment of the Requirements

for the Degree of

Doctor of Philosophy

California Institute of Technology

Pasadena, California

2008

(Defended August 13th, 2007)

Acknowledgements

I am grateful to my advisor Peter Schröder for his guiding me into this field and for his never-failing support. I started working with Peter in April 2005 when I was a fourth-year PhD student still seeking an advisor. Peter accepted me as his student when my life hit bottom. Looking backward, I have benefited so much from his profession and instruction in many different ways, from my first conference presentation to writing this thesis.

I would like to thank Mathieu Desbrun for his support and valuable suggestions. This project is largely motivated by his original work on discrete differential modeling.

I would also like to thank Yiying Tong for the helpful discussions. I am also grateful to Weiwei for her beautiful artwork presented in this thesis. I also thank Cici Koenig for her teaching me the art of lighting.

Finally, I would like to express my gratitude to my wife, for her love and support during the hard times.

This research has been supported in part by NSF(CCF-0528101, CCR-0133983, and ITR DMS-0453145), DOE (W-7405-ENG-48/B341492 and DE-FG02-04ER25657), the Caltech Center for Mathematics of Information, nVidia, and Autodesk.

Abstract

Vertex- and face-based subdivision schemes are now routinely used in geometric modeling and computational science, and their primal/dual relationships are well studied. In this thesis we interpret these schemes as defining bases for *discrete differential* 0- *resp.* 2-*forms*, and present a novel subdivision-based method of constructing smooth differential forms on simplicial surfaces. It completes the picture of classic primal/dual subdivision by introducing a new concept named *r-cochain subdivision*. Such subdivision schemes map scalar coefficients on r-simplexes from the coarse to the refined mesh and converge to r-forms on the mesh. We perform convergence and smoothness analysis in an arbitrary topology setting by utilizing the techniques of matrix subdivision and the subdivision differential structure.

The other significance of our method is its preserving exactness of differential forms. We prove that exactness preserving is equivalent to the commutative relations between the subdivision schemes and the topological exterior derivative. Our construction is based on treating r- and $(r+1)$-cochain subdivision schemes as a pair and enforcing the commutative relations. As a result, our low-order construction recovers classic Whitney forms, while the high-order construction yields a new class of *high order Whitney forms*. The 1-form bases are C^1, except at irregular vertices where they are C^0. We also demonstrate extensions to three-dimensional subdivision schemes and nonsimplicial meshes as well, such as quadrilaterals and octahedra.

Our construction is seamlessly integrated with surface subdivision. Once a metric is supplied, the scalar 1-form coefficients define a smooth tangent vector filed on the underlying subdivision surface. Design of tangent vector fields is made particularly easy with this machinery as we demonstrate. The subdivision r-forms can also be used as finite element bases for physical simulations on curved surfaces. We demonstrate the optimal rate of convergence in solving the Laplace and bi-Laplace equations of 1-forms.

Contents

List of Figures

Chapter 1

Introduction

Geometric objects (curves, surfaces and volumes) in the physical world are inevitably represented as discrete meshes in computers. The discrete differential modeling approach to computations has been studied in the literature of DEC *(Discrete Exterior Calculus)* by many researchers [Hirani 2003; Desbrun *et al.* 2005a; Elcott *et al.* 2007]. Those models respect intrinsic geometry of the discrete mesh, and as a result, they exhibit great advantages in conserving structures (symmetry, invariants). Further discrete differential modeling is often much easier to implement than its continuous counterpart, which makes it well suited to dealing with computations on complicated geometry.

One of the building blocks of DEC is to use *differential forms* or simply forms as the *intrinsic* representations for continuous objects. Physical quantities often have their geometrical meanings. For instance, an electronic field E is physically measured by the amount of work of moving a charged particle along a particular curve in that field. Therefore the intrinsic discrete representation for E is by no means pointwise. Rather they are integral quantities associated with edges of the mesh primitives. In the language of differential geometry, the field E is represented by 1-forms which are ready to be integrated along one-dimensional curves. From this point of view, differential forms are just coordinate free objects ready to be integrated. Generally speaking, r-forms live on r-manifolds and they associate a scalar (we call it a measurement) with each r-submanifold. Obviously, measurements associated with r-manifolds are the discrete counterparts of r-forms and are called *discrete differential r-forms*, or discrete r-forms for short. While discrete forms are the premises of DEC, we often need to reconstruct the underlying field from the given measurements through differential form bases.

Some properties of such differential form bases are preferred. First we want to perform the usual vector calculus operations simply through local operations on discrete measurements and keep some of the identities of operations on the discrete level, such as $\nabla \times \nabla = 0$. Further such bases need to have enough *pointwise smoothness* in continuum sense so that one can control the error of approximation when the underlying object is smooth. In solving second- or higher-order partial differential equations, certain regularity of the finite element bases is also required by the Galerkin method. Moreover, we want to preserve cohomology groups as mapping measurements to forms. That is to say, exact discrete r-forms should be mapped to exact r-forms.

The goal of this thesis is to initiate a subdivision approach to the construction of smooth form bases, which have the desirable properties listed above. To our knowledge this construction is the first attempt to bridge the subdivision theory with the construction of differential forms. We build required differential structures into the subdivision schemes, and the techniques of matrix subdivision enable us to prove convergence and smoothness of form bases.

In the following sections, we overview the main ideas of discrete differential modeling as well as the main results of this thesis.

1.1 Discrete Differential Geometry

In this section we briefly introduce the main concepts from DEC as needed later in this thesis. We focus on the two-dimensional case only to get the idea across. A more complete introduction can be found in [Hirani 2003; Desbrun *et al.* 2005a].

Instead of smooth surfaces, the underlying domain of DEC is a discrete triangle meshe, or more precisely, a simplicial complex which is a two-manifold and orientable. Abstracly, such a complex $K = (V, E, T)$ is a collection of vertices $V = \{v_i | i = 1, \ldots, n\}$ (0-simplexes), edges $E = \{e_{ij} | i, j \in V\}$ (1-simplexes) and triangles $T = \{t_{ijk} | e_{ij}, e_{jk}, e_{ki} \in E\}$ (2-simplexes). Recall that integration of a differential r-form represents its measurement over an r-manifold. So it is natural to associate discrete 0-forms with pointwise measurements at vertices. Discrete 1-forms are measurements along edges and so they are coefficients stored on edges. Finally discrete 2-forms are measurements over triangles, and they are naturally associated with coefficients living at triangles. Notice we have defined discrete forms without referring

to local coordinates or metric of the domain K. This is what we expected since differential forms are *metric independent*.

DEC introduces a *discrete exterior derivative operator*, or discrete differential, d on K. Its definition is based on Stokes' theorem, which says that the measurement of a form ω on the boundary of a simplex σ is the same as the measurement of the continuous exterior derivative $\boldsymbol{d}$ of this form on the simplex itself

$$\int_{\sigma} \boldsymbol{d}\omega = \int_{\partial\sigma} \omega. \tag{1.1}$$

So the discrete differential operator can be seen as the transpose of the boundary operator and we will use this as the definition of the discrete differential. For a simplicial complex, the boundary operator is given by the oriented incidence matrices. For example, consider the incidence matrix of edges on triangles. Each triangle has a column with 3 nonzero entries, either $+1$ or -1, depending on whether a boundary edge is oriented the same way or opposite to the triangle. With these matrices $d^0 = \partial_1^T$ maps 0-forms to 1-forms while $d^1 = \partial_2^T$ maps 1-forms to 2-forms. We will generally neglect the subscripts as the type of d is implied by its argument. Since $\partial \circ \partial = 0$ (the boundary of a boundary is empty) we immediately get $d \circ d = 0$, as is the case in the standard smooth exterior calculus setting.

So far we have only spoken of discrete r-forms which are scalars associated with r-simplexes, and used mesh topology only to bring in the discrete differential d. The metric comes in through the Hodge-$\star$ operator. In the smooth setting, the Laplace operator on a 2-manifold can be represented by $\boldsymbol{d}$ and $\star$,

$$\Delta = -(\star\boldsymbol{d}\star\boldsymbol{d} + \boldsymbol{d}\star\boldsymbol{d}\star). \tag{1.2}$$

We will discuss Hodge-$\star$ in details in Chapter 5. For now we only need to know that, the definition of Hodge-$\star$ operator on K is induced by a Riemannian metric on K. While the discrete differential d is determined by the mesh topology, the discrete Hodge-$\star$ is induced by a discrete metric on K. Evidently, piecewise linear imbedding of K into an ambient space locally defines a isomorphism to $\mathbb{R}^2$ under which the barycentric coordinates of points within each triangle are invariant. We call it an *affine atlas* of K. The resulting metric of K induced by the embedding are piecewise uniform. A diagonal discrete Hodge-$\star$ operator

is constructed through the *dual complex* of K. The interested reader is referred to [Bossavit 2001; Desbrun *et al.* 2005a]. Due to its simplicity and flexibility, such PL imbedding has been widely used for modeling and computing in spite of its low approximation order. Instead we will introduce in the following a smooth atlas on K through subdivision.

1.2 Subdivision Differential Structure

Recall that a C^r-atlas on a 2-manifold M is a collection $\{(U_\alpha, \psi_\alpha),\ \psi_\alpha \colon U_\alpha \to \mathbb{R}^2\}$ of coordinate systems on M such that the coordinate neighborhoods $\{U_\alpha\}$ cover M, and for any pair (U_1, ψ_1) and (U_2, ψ_2) of coordinate systems, the *transition function* $\psi_1 \circ \psi_2^{-1}$ is a C^r-diffeomorphism. There are two reasons why a smooth atlas on the simplicial complex K is preferred.

First, Galerkin's method for solving partial differential equations often requires certain regularity for the finite element bases. For example, the Laplace operator (1.2) is *metric dependent*. The PL 0-form basis is capable of solving Laplace's equation of scalar fields, but not enough to solve the bi-Laplace equation.

Second, splines together with subdivision schemes have become the major tool for accurate surface modeling through coarse control meshes. Subdivision surfaces are very flexible and easily accommodate the construction of smooth surfaces of arbitrary topology. For example, Loop's subdivision scheme, as described in the following, generates a specific class of subdivision surfaces. These surfaces are C^2, except at a finite set of points where they are C^1 (see Figure 1.1). As the physical domain is represented by subdivision surfaces over which computation is carried out, for instance, simulations of flows over an aerofoil defined by subdivision surfaces, using the smooth structure induced by subdivision to maintain the approximation order is just a natural choice.

Loop's subdivision scheme generalizes quartic box splines to irregular meshes. Recall that a quartic box spline is generated by convolving a PL hat function on regular triangle meshes along the three principal directions. Such splines are C^2 functions on $\mathbb{R}^2$ that are piecewise degree-four polynomials. Further, they are refinable and therefore admit subdivision schemes on coefficients associated with vertices (see Figure 1.2, left and middle). Basically, a subdivision scheme consists of the splitting step that refines the mesh followed by the averaging step that calculates coefficients at the refined level through local linear

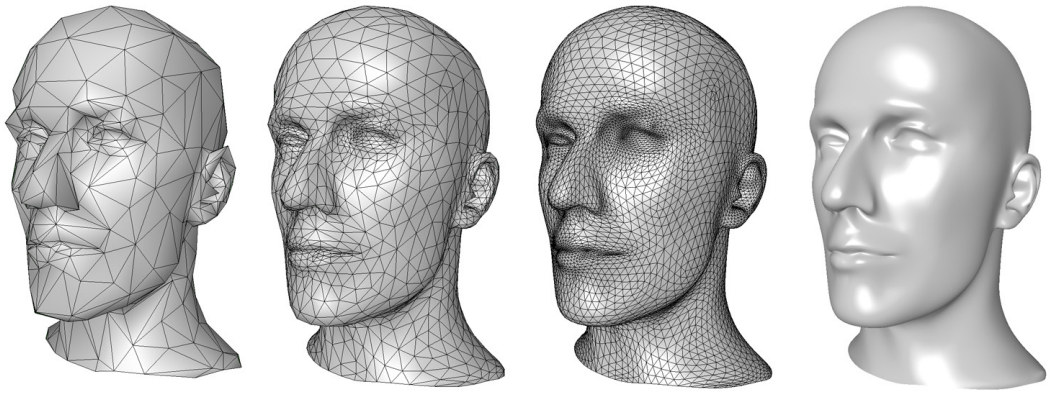

Figure 1.1: *Surface generated by Loop's subdivision scheme. From left to right: initial mesh; subdivision level* 1*; subdivision level* 2*; limit surface.*

combinations of coefficients at the coarser level. Loop generalized subdivision schemes of quartic box splines to irregular setting in his master's thesis [1987] (see Figure 1.2, right). We denote by ϕ_v the basis function generated by Loop's scheme by setting a single coefficient one at the vertex v and zero at other vertices. What is important to us is that Loop's subdivision scheme defines a C^2 atlas $\{(|N_1(v,K)|,\ \phi_v\colon |N_1(v,K)| \to \mathbb{R}^2\}$ on K, where $|N_1(v,K)|$ denotes the 1-ring of triangles of K sharing vertex v.

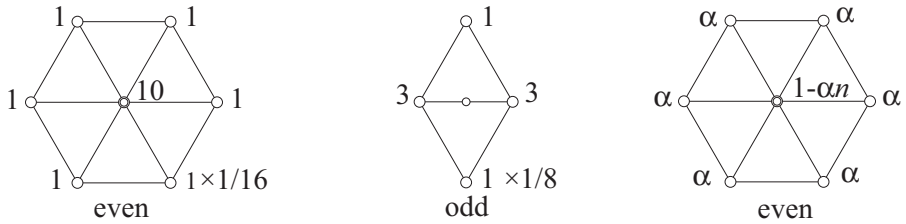

Figure 1.2: *Subdivision stencils of quartic box splines: even stencils at valence* 6 *vertices (left); odd stencils (middle). Stencils of Loop's scheme at irregular vertices of valence* n *(right).*

While Loop's subdivision scheme is concerned with data at vertices, the other class of subdivision schemes, called dual subdivision schemes, map coefficients at triangles from the coarser level to the refined level. Both of them have been widely used for surface modeling as well as physical modeling of scalar fields. The natural question to ask is: what about 1-forms on surfaces? In the following section, we introduce a new class of edge-based subdivision schemes which can be used to construct 1-forms on K.

1.3 Contribution: Subdivision Construction of Smooth Forms

The major contribution of this thesis is to extend the method of subdivision to the construction of smooth differential forms on simplicial complex K. Our work is motivated by the construction of Whitney forms on simplicial complexes (see [Whitney 1957]), which was originally used to build homomorphism between cohomology groups. In the 1970s, Whitney elements were rediscovered in the finite element literature as certain types of mix finite elements. Their connection to Whitney's work were first realized by Bossavit [1988].

On a triangle mesh K, Whitney 0-forms ϕ^v are piecewise linear functions ϕ_i associated with each vertex v_i, and Whitney 2-forms ϕ^t are simply piecewise constants associated with triangle t_{ijk}. Whitney 1-form basis ϕ^e associated with edge e_{ij} is given by

$$\phi_{ij} = \phi_i \boldsymbol{d}\phi_j - \phi_j \boldsymbol{d}\phi_i. \tag{1.3}$$

As mappings from coefficients on r-simplexes to r-forms, Whitney forms satisfy the following commutative relations:

$$\boldsymbol{d}\phi^v = \phi^e d, \quad \boldsymbol{d}\phi^e = \phi^t d. \tag{1.4}$$

The commutative relations (1.4) assures that exact discrete r-forms get mapped to exact r-forms. This property is essential for preserving the structure of the cohomology groups on K. For computational purpose, preserving exactness of mix finite element bases is crucial for annihilating spurious modes (see [Bossavit 1990]). Note that ϕ_{ij} is linear within each triangle but has only tangential continuity across the boundary. How to get 1-form bases of higher order of smoothness? Naively we could replace the 0-form basis ϕ_i in (1.3) by a smoother 0-form basis, say the basis generated by Loop's scheme. Unfortunately this approach does not quite work because it does not assure the commutative relations. Neither does it admit a subdivision scheme.

The key step in our construction is to notice the refinability of Whitney 1-forms. It is well known that both PL hat functions and piecewise constant functions are refinable. It turns out that Whitney 1-forms are refinable as well. We observed the following two-scale refinement equation for the Whitney 1-form associated with the edge e_{ij} (see Figure 3.2, left):

$$\phi_{ij} = \frac{1}{2}\phi_{ip} + \frac{1}{2}\phi_{pj} + \frac{1}{4}\phi_{mn} + \frac{1}{4}\phi_{rq} - \frac{1}{4}\phi_{pm} - \frac{1}{4}\phi_{np} - \frac{1}{4}\phi_{pr} - \frac{1}{4}\phi_{qp}. \tag{1.5}$$

Written in matrix notations

$$\Phi^e = \phi^e S_1^W, \tag{1.6}$$

where Φ^e represents a row vector of Whitney 1-forms on the coarse mesh and ϕ^e the corresponding row vector of Whitney 1-forms on the refined mesh. The refinement coefficients are written as entries of the subdivision matrix S_1^W. As in the refinable scalar functions, these refinement coefficients of Whitney 1-forms naturally defined a subdivision scheme based on edges (see Figure 3.2, middle and right).

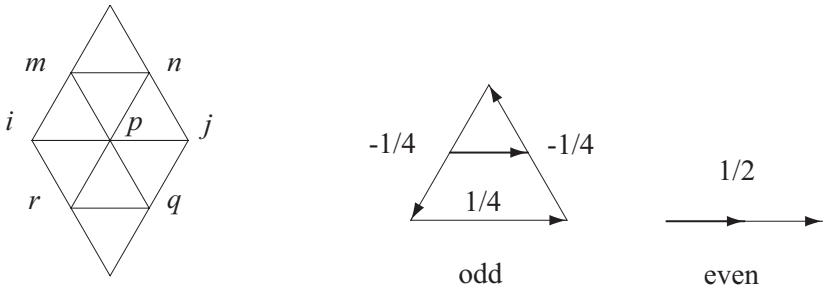

Figure 1.3: *Left: Support of Whitney* 1*-form associated with the central edge ij; Right: the edge-based subdivision scheme for Whitney* 1*-forms.*

Staring with S_1^W, we build edge subdivision scheme S_1 for smooth 1-forms by utilizing the convolution arguments of constructing B-splines. We prove that S_1 is C^1 on regular meshes and satisfies the commutative relations with the subdivision schemes S_0 (quartic box spline) and S_2 (half-box spline scaled by $\frac{1}{4}$)

$$dS_0 = S_1 d, \quad dS_1 = S_2 d. \tag{1.7}$$

We also prove that, the commutative relations (1.7) is equivalent to exactness preserving of S_1. We use (1.7) as the guiding principle to extend S_1 to arbitrary topology setting. We prove that S_1 is C^0 at irregular vertices. Therefore, S_r $(r = 0, 1, 2)$ generate a smooth de Rham complex on simplicial surfaces.

Our method can be naturally extended to three-dimensional subdivision schemes on tetrahedra meshes. We consider subdivision of the uniform mesh consisting of tetrahedra and octahedra, as proposed by [Schaefer *et al.* 2004]. Such mesh structure allows for refinement equations. Again our construction recovers classic Whitney forms on tetrahedra. At the same time, it yields a new class of Whitney forms on octahedra.

1.4 Related Work

Matrix subdivision The theory of matrix subdivision schemes have been studied in the literature of multiwavelets as well as surface modeling [Cohen *et al.* 1995; Heil & Colella 1996; Jiang & Oswald 2003; Charina *et al.* 2005]. We interpret subdivision schemes of r-forms as matrix subdivision schemes. As a result, the theory and techniques of matrix subdivision can be used for convergence and regularity analysis of limit r-forms. Our demonstration has initiated a new category of applications of matrix subdivision.

High order Whitney Forms and Mixed Finite Elements As an extension of Whitney forms which is only PL linear, construction of high order polynomial forms were studied by many researchers (see [Cendes 1991; Hiptmair 1999, 2001; Bossavit 2002; Arnold *et al.* 2006a]). Their constructions are mainly concerned with non-conforming mixed finite elements in the sense that compatibility conditions are imposed on element boundaries while smoothness across boundaries is not assured. They are not mappings from discrete r-forms to r-forms but Whitney forms are. No analogs to the commutative relations are presented in their constructions.

In contrast our construction of high order Whitney forms satisfies the following properties: (a) *Linear mappings from discrete r-forms to r-forms;* (b) *Respect for the commutative relations* (1.4)*;* (c) *Smooth across boundaries of elements;* (d) *Admitting subdivision schemes.*

The immediate consequence of property (b) and (c) is that our method leads to smooth mixed finite element bases that admit the exact sequences of de Rham complex. The exact sequences of de Rham complex are crucial to the stability of mixed finite elements for electromagnetism and elasticity, *e.g.* [Bossavit 1990; Arnold *et al.* 2006b].

Simulations on Surfaces of Arbitrary Topology In order to perform simulations of vector fields on surfaces of arbitrary topology, one way is to track the local coordinate induced by each surface patch and impose continuity across the patch boundaries (*e.g.* [Stam 2003]). On the other hand, discrete differential modeling through Whitney forms has the advantage that it is coordinate free and intrinsic to the mesh structure. For instance, simulations of simplicial fluids were demonstrated by [Elcott *et al.* 2007], where tangential/normal continuity is assured by Whitney form bases and the diagonal discrete Hodge-$\star$ operator is

used. Our construction supplies a new smooth 1-form basis which has higher approximation order and implies a discrete Hodge-$\star$ operator with larger support. At the same time it inherits the advantages of discrete differential modeling. We demonstrate a 1-form Laplace solver using our 1-form bases and verify its optimal rate of convergence in the energy norm.

1.5 Overview

This thesis is organized as follows. In Chapter 2 we detail the subdivision differential structure of simplicial surfaces. We introduce the concept of r-cochain subdivision. In Chapter 3 we build the theory of subdivision forms. We establish convergence and regularity of r-cochain subdivision schemes. We prove that commutative relations are equivalent to exactness preserving of 1-cochain subdivision schemes. In Chapter 4 we design particular subdivision schemes of r-forms following the theory in Chapter 3. We also show the applications of the 1-form scheme to tangential vector field design. In Chapter 5 we solve the Laplace and bi-Laplace equations of 1-forms on Riemannian surfaces using our smooth 1-form bases. In Chapter 6 we extend our method to three-dimensional subdivision on tetrahedra meshes. The conclusion is given in Chapter 7 and the future work is discussed there.

Chapter 2

Subdivision Differential Structures of Simplicial Surfaces

In this chapter we describe the fundamentals of subdivision theory on simplicial surfaces and the differential structures indorsed by subdivision functions. Subdivision schemes are widely used in all areas of geometric modeling and computer graphics [Zorin & Schröder 2000; Warren & Weimer 2001]. Their foremost benefit is the ease with which they accommodate the construction of smooth surfaces in the arbitrary topology setting of meshes. They also offer many favorable computational properties for applications ranging from surface compression to physical modeling [Khodakovsky *et al.* 2000; Grinspun *et al.* 2002]. Their mathematical properties are well understood [Reif 1995, 1999; Zorin 2000a,b]. A large variety of subdivision schemes and extensions have been developed since the 1970s. Generally, subdivision schemes are classified as either primal (*e.g.*, Catmull-Clark [1978], Loop [1987], and $\sqrt{3}$ [Kobbelt 2000]) with data being stored at vertices, or dual (*e.g.*, Doo-Sabin [1978] and dual-$\sqrt{3}$ [Oswald & Schröder 2003] with data being stored at faces.

In DEC the underlying domain is given in the form of *discrete manifold*. In general, a two-dimensional discrete manifold $\mathcal{M}$, or 2-manifold for simplicity, is a simplicial surface that admits local isomorphism to $\mathbb{R}^2$. A 2-manifold has no isolated edges or isolated vertices, and each of their edges is adjacent to two triangles (except for the boundary where the edge is adjacent to only one triangle). We presume that all simplicial surfaces discussed in this thesis are 2-manifolds. In the context of geometric modeling or finite element methods we *approximate* or *discretize* a continuous surface by a simplicial surface embedded into 3D which naturally induces a piecewise linear isomorphism. This isomorphism identifies

each triangle of the mesh with a region on $\mathbb{R}^2$ under which the barycentric coordinates of points within each triangle are invariant. However, the resulting *atlas* formed by the piecewise linear isomorphism is not differentiable across boundaries of triangles. While higher smoothness of a basis function is easy to achieve within triangles, it is highly nontrivial to maintain their smoothness across boundaries of triangles when the mesh topology is complicated. In this chapter we will see that a C^r subdivision scheme naturally induces a C^r atlas on a 2-manifold. As an application, a new paradigm for thin-shell modeling was proposed in [Cirak *et al.* 2000] in which subdivision functions served as H^2 elements needed for a finite Kirchhoff-Love energy. For the purpose of this thesis, the differential structure induced by subdivision paves the way for the construction of smooth differential forms on 2-manifolds.

2.1 Exterior Calculus on Simplicial Complexes

2.1.1 Simplicial Complexes

We review some basics of simplicial complexes. The reader is invited to refer to [Spanier 1989; Wallace 1970; Whitney 1957] for details.

A *simplex* σ in an affine space E is a set of points expressible in the form

$$p = \lambda_0 v_0 + \cdots + \lambda_r v_r, \quad \text{with } \lambda_i \geq 0 \text{ and } \sum_{i=0}^{r} \lambda_i = 1, \tag{2.1}$$

the v_i being independent *vertices*. Then $\dim(\sigma) = r$ and σ is called *r-simplex*. The μ_i are the *barycentric coordinates* of p in terms of v_i. We write $\sigma = v_0 \dots v_r$. Then the simplexes $v_{n_0} \dots v_{n_k}$ are the faces of σ, and the v_i are its vertices.

By the *oriented simplex* $\sigma = v_0 \dots v_r$, we mean the simplex σ oriented by the set of vectors $\{v_1 - v_0, \dots, v_r - v_0\}$, or equivalently, $\{v_1 - v_0, \dots, v_r - v_{r-1}\}$. For any permutation $\{n_0, \dots, n_r\}$ of $\{0, \dots, r\}$, $v_{n_0} \dots v_{n_r}$ has the same or opposite orientation as $v_0 \dots v_r$, according as the permutation is even or odd. We define the *boundary operator* as follows:

$$\partial v_0 \dots v_r = \sum_{j=0}^{r} (-1)^j v_0 \dots \widehat{v_j} \dots v_r, \tag{2.2}$$

where $\widehat{v_j}$ indicates that v_j is removed from the sequence.

Recall that a *simplicial complex* K is a subspace of an affine space E, consisting of a set of simplexes such that the intersection of any two is a face of each. The *dimension* of K is the largest of the dimensions of the simplexes making up K. A two-dimensional simplicial complex K is also called *simplicial surface*. The 0-simplexes in K form a set called $\mathrm{Vertex}(K)$. The sets of 1- and 2-simplexes are called $\mathrm{Edge}(K)$ and $\mathrm{Face}(K)$, respectively.

A *subcomplex* L of a simplicial complex K, denoted by $L \subset K$, is a subset of K that is a simplicial complex. Given any simplex $\sigma \in K$, let $\bar{\sigma} \subset K$ denotes the subcomplex containing σ and all of its subsets. For any subcomplex $L \subset K$ we define its *1-neighborhood* $N_1(L, K)$ by

$$N_1(L, K) = \bigcup \bar{\sigma}, \quad \text{where } \sigma \in K \text{ and } \bar{\sigma} \cap L \neq \emptyset.$$

Larger neighborhoods of L are defined recursively by $N_j(L, K) = N_1(N_{j-1}(L, K))$. We simplify the notation to $N_j(L)$ when the ambient complex K is clear from the context.

Given a simplicial complex K, we can form its *topological realization* $|K|$ in $\mathbb{R}^m$ by identifying the vertices $1, \ldots, m$ with the standard basis vectors $e_1, \ldots, e_m$ of $\mathbb{R}^m$. For each simplex $s \in K$ let $|s|$ denote the convex hull of its vertices in $\mathbb{R}^m$, and let $|K| = \bigcup_{s \in K} |s|$. Then any point $p \in |K|$ can be represented as a convex combination of vertices of K:

$$p = \sum_{v \in K} \lambda_v v, \quad \text{with } \lambda_v \geq 0 \text{ and } \sum_{v \in K} \lambda_v = 1.$$

Next we define piecewise linear maps on K. A *piecewise linear map* $f \colon |K| \to \mathbb{R}^n$ is given by

$$f(p) = \sum_{v \in \mathrm{Vertex}(K)} p_v f(v) \quad \text{for all } p \in |K|.$$

An injective piecewise linear map from $|K|$ into $\mathbb{R}^n$ is called a *geometric realization* of K.

Notice that a piecewise linear map is completely determined by its values on $\mathrm{Vertex}(K)$. A subdivision function, which will be introduced later, is also determined by functions on $\mathrm{Vertex}(K)$, which we call *control nets*. The space of all control nets on K is denoted by

$$\mathrm{CN}(K) = \{u \colon \mathrm{Vertex}(K) \to \mathbb{R}\}. \tag{2.3}$$

While control nets are functions on $\mathrm{Vertex}(K)$, we can define functions on $\mathrm{Edge}(K)$ and $\mathrm{Face}(K)$ as well. They can all be unified with the concept of *cochains*, which will be

discussed in the next section.

2.1.2 Cochains and Forms

In this section we briefly introduce the concept of *Geometric Integration* on simplicial complexes. For more details the reader is referred to [Whitney 1957]. We let K be a complex, and let its simplexes be oriented. An (algebraic) *r-chain* of K is an expression of the form $A = \sum a_i \sigma_i^r$, the a_i being real numbers. We write $\dim(A) = r$. Two chains are added by adding corresponding coefficients; to multiply a chain by a real number, multiply each coefficient by that number. Thus the set of r-chains becomes a linear space $\mathcal{C}_r = \mathcal{C}_r(K)$. The dimension of this space is the number of r-simplexes of K.

An (algebraic) *r-cochain* X of K is an element of the conjugate space $\mathcal{C}^r = \bar{\mathcal{C}}_r$ of $\mathcal{C}_r$. We write $X \cdot A$ in place of $X(A)$. Set $X_i = X \cdot \sigma_i^r$. If we let σ_i^r denote not only an oriented simplex or a chain, but also the cochain defined by $\sigma_i^r \cdot \sigma_j^r = \delta_i^j$, then the σ_i^r form also a base for the r-cochains; for any X as above, clearly $X = \sum X_i \sigma_i^r$.

Remark 2.1. As functions on the vertices of a simplicial surface K, 0-cochains are equivalent to the control nets defined as (2.3). Similarly 2-cochains are equivalent to the control nets defined on triangles. While classic primal/dual subdivision schemes are defined as linear mappings on vertex/face control nets, in Section 2.2 we will generalize subdivision schemes to linear mappings on r-cochains for $r = 0$, 1 or 2.

The boundary operator on a simplex is defined as (2.2). Given an r-chain $A = \sum_i a_i \sigma_i^r$, the *boundary* ∂A is an $(r-1)$-chain defined as

$$\partial \sum_i a_i \sigma_i^r = \sum_i a_i \partial \sigma_i^r.$$

The operation ∂ is a linear mapping of $\mathcal{C}_r(K) \to \mathcal{C}_{r-1}(K)$, for each $r \geq 1$. It follows from (2.2) that

$$\partial \partial A = 0, \quad \text{for all chains } A. \tag{2.4}$$

The *coboundary* dX of the r-cochain X of K is defined by

$$dX \cdot A = X \cdot \partial A, \tag{2.5}$$

dX being an $(r+1)$-cochain of K. Because of (2.4), we have

$$ddX = 0, \quad \text{for all cochains } X. \tag{2.6}$$

Recall that a *differential r-form* ω, or *r-form* for short, in the set $Q \subset \mathbb{R}^n$, is a function defined in Q, whose values are r-covectors; r is the *degree* of ω. We say ω is *s-smooth* if, for each r-vector α, $\omega(p) \cdot \alpha$ is s-smooth.

A *convex polyhedral cell* (or *cell* for short) σ in an affine space E is a non-empty bounded subset of E expressible as the intersection of a finite set of closed half spaces. We call the cell an r-cell if $\dim(\sigma) = r$. Note that r-simplex is also an r-cell.

Given a r-form ω, we can define the *integration of* ω, denoted by $\int_\sigma \omega$, for any oriented r-cell, ω being defined and *continuous* in σ. The definition is based on simplicial subdivisions of σ and the uniform continuity of ω [Whitney 1957, Chapter 3]. Integration of the r-form ω on *cellular* r-chains $\sum a_i \sigma_i^r$, a_i being real coefficients, follows from linearity of integration:

$$\int_{\sum_i a_i \sigma_i^r} \omega = \sum_i a_i \int_{\sigma_i^r} \omega.$$

An r-form ω in the open set $Q \subset \mathbb{R}^n$ is *regular* if it is continuous there, and there is a continuous $(r+1)$-form ω' in Q such that

$$\int_{\partial\sigma} \omega = \int_\sigma \omega', \quad \text{for all } (r+1)\text{-simplexes } \sigma \subset Q. \tag{2.7}$$

Then ω' is uniquely determined due to [Whitney 1957, Lemma 16a]. We call ω' the *derived* form $\boldsymbol{d}\omega$ of ω. If ω is smooth, the operation $\boldsymbol{d}$ is the usual *exterior differential*. Note we used boldfaced $\boldsymbol{d}$ for derivative as it should be distinguished from the coboundary operator d. Given a regular r-form ω, Stokes' Theorem follows from the definition of $\boldsymbol{d}$

$$\int_{\partial\sigma} \omega = \int_\sigma \boldsymbol{d}\omega, \quad \text{all } (r+1)\text{-cells } \sigma. \tag{2.8}$$

Remark 2.2. Cochains are the discrete counterparts of differential forms in the sense that they are both defined as *mappings from chains to real numbers*. This analogy has its physical relevance as well. As physical objects are represented by differential forms, the natural way to *measure* them through sensors is to detect their integrations on manifolds with the same

degree, that is to say, r-forms should be integrated on r-manifolds. When the domain is a simplicial complex, the measurements of forms are represented as cochains.

2.2 Subdivision Schemes on Simplicial Surfaces

2.2.1 Subdivisions of Simplicial Surfaces

Now we focus on two-dimensional simplicial complexes, or simplicial surface for short. Throughout we let K denote a simplicial surface without boundary. Recall that there are three collections of simplexes in K: Vertex(K), Edge(K) and Face(K). The *valence* of a vertex is the number of edges incident to the vertex. We define the "4 to 1" subdivision of K, denoted by $D(K)$, as follows. For each edge e of K, let $m(e)$ be the middle point of $|e|$. We insert $m(e)$ as a vertex of $D(K)$, called a *E-type* vertex, and let

$$EV = \bigcup_{e \in \text{Edge}(K)} m(e).$$

The vertices of $D(K)$ consist of the vertices of K, called *V-type* vertices, and the E-type vertices:

$$\text{Vertex}(D(K)) = \text{Vertex}(K) \bigcup EV.$$

Now each E-type vertex split each edge of K into two edges. We split each face of K into four faces by connecting the three E-type vertices at its edges. It is easy to verify that $D(K)$ is a simplicial complex. By repeating the process, we can define the subdivision sequences of K recursively by letting $K^j = D(K^{j-1})$, for $j \geq 1$ and $K^0 = K$.

2.2.2 Cochain Subdivision Schemes

Subdivision schemes are generally classified into two categories. A primal subdivision scheme S is the linear mapping of coefficients (or control nets) at vertices: S: CN(K) $\rightarrow$ CN($D(K)$). Similarly, a dual subdivision scheme is the linear mapping of coefficients at faces. Primal/dual subdivision schemes can be unified as *r-cochain subdivision schemes*, defined as

$$S_r : \mathcal{C}^r(K) \rightarrow \mathcal{C}^r(D(K)) \quad r = 0,\ 1,\ 2. \tag{2.9}$$

From now on the notation S_r is reserved for r-cochain subdivision schemes. We may simply say *subdivision scheme* S when the dimension of underlying cochains is unimportant or clear from the context.

Fix the simplicial surface K. Given an r-cochain X we can represent the operation of S_r by its mask a

$$(S_r X) \cdot \sigma = a_{\sigma\tau} X \cdot \tau \quad \text{for all } r\text{-simplexes } \sigma. \tag{2.10}$$

Given an integer $m > 0$ and any simplex σ of $D(K)$, we define the *undivided-m-neighborhood*, which is a generalization of [Arden 2001, Definition 5], by

$$U_m(\sigma, K) = \{s \in K \colon |s| \subset N_m(\sigma, D(K))\}. \tag{2.11}$$

Definition 2.3. A cochain subdivision scheme S_r is local if there is an integer $m_w > 0$, called the *mask width*, such that for any pair K and $\widetilde{K}$ of simplicial surfaces without boundary, any simplex $\sigma \in D(K)$, and any embedding $\rho \colon U_{m_w}(\sigma, K) \to \widetilde{K}$, we have

$$a_{\sigma\tau} = \begin{cases} a_{\rho(\sigma)\rho(\tau)} & \text{for all } \tau \in U_{m_w}(\sigma, K), \\ 0 & \text{otherwise.} \end{cases}$$

2.2.3 The n-Regular Complex K_n

All the new vertices introduced by the 4-to-1 subdivision are valence 6, while the original vertices remain the same valence. The n-regular complex is an infinite simplicial surface with a single vertex of valence n surrounded the vertices of valence 6, consisting of n rotated wedges W (Figure 2.1).

Let $e_1 \equiv (0, 1)$ and $e_2 \equiv (1, 0)$. A *wedge* W (Figure 2.1, left) is an infinite oriented simplicial complex defined as

$$\begin{aligned} &\text{Vertex}(W) = \{m = (m_1, m_2) \colon m \in \mathbb{Z}^2 \text{ and } m_1 \geq 0, m_2 \geq 0\}, \\ &\text{Edge}(W) = \big\{\{m, m + e_1\}, \{m, m + e_2\}, \{m + e_1, m + e_2\} \colon m \in \text{Vertex}(W)\big\}, \\ &\text{Face}(W) = \big\{\{m, m + e_1, m + e_2\}, \{m + e_1, m + e_1 + e_2, m + e_2\} \colon m \in \text{Vertex}(W)\big\}. \end{aligned}$$

For each valence $n \geq 3$, we defined the n-regular complex K_n as follows: Let $\{W_i, i \in \mathbb{Z}_n\}$ denote n disjoint copies of W, and denote the vertices of W_i by (i, j) for $i \in \mathbb{Z}_n$ and

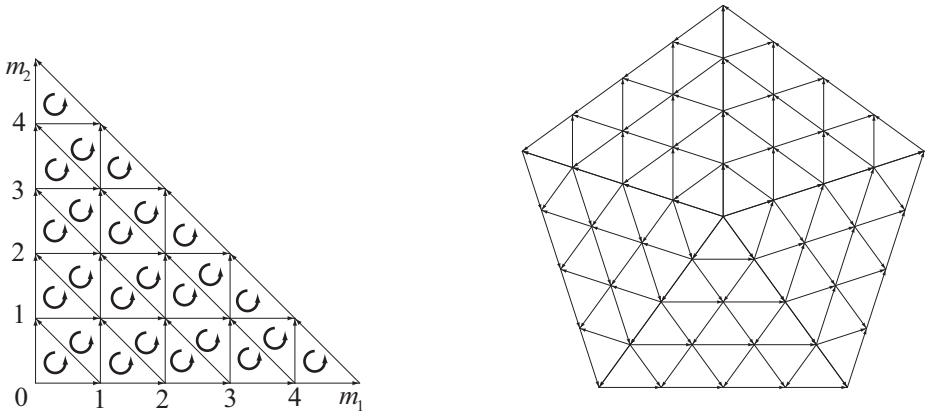

Figure 2.1: *Left: A wedge W with oriented edges and triangles (orientations indicated by arrows); right: the n-regular complex K_n generated from n copies of W ($n = 5$).*

$j \in \mathrm{Vertex}(W)$, where $\mathbb{Z}_n$ is the group of integers modulo n. We then identify vertices by the equivalence relation

$$(i, (j, 0)) \equiv (i - 1, (0, j)) \quad \text{for all } j \geq 0 \text{ and } i \in \mathbb{Z}_n, \tag{2.12}$$

the substraction being taken modulo n. The resulting complex K_n is a simplicial surface without boundary (Figure 2.1, right). The central vertex, denoted by v_0, has valence n and all other vertices have valence 6.

The n-regular complex is self-similar under subdivision. We first define the contraction map on the wedge W. The vertices of W are points of $\mathbb{R}^2$ that define a geometric realization of W, and therefore we have a geometric realization of $D(W)$. The map $c_0 \colon \mathrm{Vertex}(W) \to \mathrm{Vertex}(D(W))$ given, in terms of this realization, by

$$c_0(x) = \frac{x}{2}$$

is a simplicial isomorphism. We can extend the definition of contraction map to r-simplexes of W as follows

$$c_r(v_1 \dots v_r) = c_0(v_1) \dots c_r(v_r) \quad r = 1 \text{ or } 2.$$

We simply denote the contraction map c_r of r-simplexes by c since the dimension r is clear from the argument.

Applying c to each wedge W_i of K_n extends c to a simplicial isomorphism

$$c\colon K_n \to D(K_n),$$

which we call the *contraction map*. Contraction induces a piecewise linear homeomorphism $|c|\colon |K_n| \to |D(K_n)|$, which when composed with the identification induced by subdivision $\imath\colon |D(K_n)| \to |K_n|$, results in a piecewise linear homeomorphism on $|K_n|$, also denoted by c,

$$c\colon |K_n| \to |K_n|. \tag{2.13}$$

2.2.4 The Subdivision Map

The subdivision map represents the operation of stationary 0-cochain subdivision near an extraordinary vertex v_0. Let S be a local subdivision scheme with mask width m_w. For any $m \geq m_w$ we define the *the r-cochain subdivision map* $S_{n,m}$ as the linear transformation

$$S_{n,m,r} = c^* S_r\colon \mathcal{C}^r(N_m(v_0, K_n)) \to \mathcal{C}^r(N_m(v_0, K_n)).$$

We are mainly interested in the special case $S_{n,m_w,r}$, denoted by $S_{n,r}$ for simplicity. The action of $S_{n,m,r}$ is completely determined by $S_{n,r}$ [Arden 2001, Theorem 11][1].

2.2.5 Subdivision Functions

The 0-cochain subdivision schemes have been the major interests of the classic subdivision theory. We review some basics about 0-cochain schemes.

Definition 2.4. A 0-cochain subdivision scheme S_0 is said to be *convergent* if for any simplicial surface K and 0-chain $X \in \mathcal{C}^0(K)$ there exists a continuous function on $|K|$, denoted by $S_0^\infty X$, such that

$$\sup_{v \in \mathrm{Vertex}(K^j)} \left|(S_0^j X)_v - S^\infty X(v)\right| \to 0, \quad \text{as } j \to \infty.$$

We call the limit function $S^\infty X$ a *subdivision function*. S_0 is said to be *affine invariant* if the mask a_{vw} defined as (2.10) satisfy $\sum_w a_{vw} = 1$ for every $v \in \mathrm{Vertex}(D(K))$. A *local and*

[1] The proof is for 0-cochain subdivision map only. But it can be easily generalized to the case of r-cochains.

affine 0-cochain scheme is called *stationary*. A convergent 0-cochain scheme is necessarily affine invariant [Cavaretta *et al.* 1991].

Remark 2.5. To define the convergence of 0-cochain scheme, we only needed the topological structure on $|K|$ since continuity can be defined on a given topology. To define the limit of a r-cochain scheme as a differential r-form on $|K|$, the first step is to build a *smooth atlas* on $|K|$ under which smoothness of r-forms is analyzed. We will utilize subdivision functions to build such atlas.

2.3 The Subdivision Smooth Structure

We first recall the definition of coordinate charts and atlas on a manifold.

Definition 2.6. A coordinate system on an n-dimensional manifold M is a pair (U, ϕ), where U is an open subset of M and $\phi : U \to \mathbb{R}^n$ is continuous and injective. A C^r-atlas on a manifold M is a collection $\{(U_\alpha, \psi_\alpha)\}$ of coordinate systems on M such that the coordinate neighborhoods $\{U_\alpha\}$ cover M, and for any pair (U_1, ψ_1) and (U_2, ψ_2) of coordinate systems, the *transition function* $\psi_1 \circ \psi_2^{-1}$ is a C^r-diffeomorphism.

We are going to construct the affine atlas and the C^r atlas on $|K|$ by utilizing C^r subdivision functions on $|K|$. We will follow the construction in [Arden 2001].

2.3.1 The Affine Coordinates

The vertices of valence other than 6 in a simplicial surface K are called *extraordinary vertices*. We denote the set of such vertices $\mathrm{Ext}(K)$. The *regular complex*, denoted by K_6, is an infinite simplicial surface whose vertices can be identified with $\mathbb{Z}^2$. Each vertex of K_6 is of valence 6 and hence the notation. We first construct an atlas of coordinate charts on $|K| \setminus \mathrm{Ext}(K)$. Let ι: $L \to K_6$ be an embedding of a simplicial subsurface $L \subset K$ into the regular complex, and let $\psi : |K_6| \to \mathbb{R}^2$ be a regular realization of K_6. Then the composition

$$x : |L|^\circ \xrightarrow{\iota} |K_6| \xrightarrow{\psi} \mathbb{R}^2.$$

is a coordinate chart on the coordinate neighborhood $|L|^\circ$, where $|L|^\circ$ denotes the interior of $|L|$. The collection of all such charts forms a C^∞-atlas on $|K| \setminus \mathrm{Ext}(K)$, called the *affine atlas*. Moreover, the transition functions are affine maps.

2.3.2 The Characteristic Map

The *characteristic map*, first introduced by [Reif 1995], plays a pivotal role in the subdivision theory. We adopted the definition in [Arden 2001]:

Definition 2.7. Suppose S_n is a convergent 0-cochain subdivision scheme: $\mathcal{C}^0(K_n) \to \mathcal{C}^0(D(K_n))$. For a fixed valence n, suppose the distinct eigenvalues of the subdivision map $\lambda_0, \lambda_1, \ldots, \lambda_N$, ordered by non-increasing magnitude, satisfy the following conditions:

1. The dominant eigenvalue λ_0 is one, and is an algebraically simple eigenvalue.
2. The sub-dominant eigenvalue λ_1 is real and positive, and is of geometric and algebraic multiplicity 2.
3. The other eigenvalues, λ_j for $j > 1$, are of magnitude strictly less than λ_1.

Let $u_1,\ u_2 \in \mathcal{C}^0(N_{m_w}(K_n))$ be linearly independent λ_1-eigenvectors of S_n. Then the $\mathbb{R}^2$-valued control net $u = (u_1, u_2)$ defines a continuous map

$$S_n^\infty u \colon |N_1(v_0, K_n)| \to \mathbb{R}^2,$$

called a *characteristic map*.

2.3.3 The C^r-atlas

Now we are ready to introduce the C^r smooth atlas on $|K|$. Let ι_v be an identification between $N_1(v, K)$ and $N_1(v_0, K_n)$. Let $\chi : |N_1(v_0, K_n)| \to \mathbb{R}^2$ be a characteristic map. The composition $\psi_v = \chi \circ \iota_v : |N_1(v)|^\circ \to \mathbb{R}^2$ is a *characteristic coordinate chart*,

$$\psi_v : |N_1(v)|^\circ \xrightarrow{\iota_v} |N_1(v_0, K_n)| \xrightarrow{\chi} \mathbb{R}^2.$$

The following result was proved by [Arden 2001, Proposition 15].

Theorem 2.8. *Suppose S is a stationary 0-cochain subdivision scheme such that: (i) subdivision functions are C^r-away-from-extraordinary-verticies and (ii) there are characteristic maps which are injective and regular on $|K| \backslash Ext(K)$. Then for any simplicial surface K without boundary, the collection of characteristic charts $\{(|N_1(v)|^\circ, \psi_v)\}$ for $v \in Vertex(K)$*

is a C^r-atlas on $|K|$. Furthermore, the atlas is C^r-compatible with the affine coordinate charts and with the subdivision smooth structure of $D(K)$.

The C^r-atlas of characteristics charts $\{(|N_1(v)|^\circ, \psi_v)\}$ on a simplicial surface K without boundary is called the *subdivision smooth structure* on $|K|$. We will prove our main results in the following by using such coordinate charts.

Chapter 3

Theory of Subdivision Forms on Simplicial Surfaces

This chapter builds the theoretical foundation of our subdivision construction of smooth forms. In Section 3.1 we introduce Whitney forms as mappings from cochains to forms. In Section 3.2 we introduce the refinement equations of Whitney forms and point out the connection with matrix subdivision schemes. In Section 3.3 we prove convergence criteria for r-cochain subdivision schemes. In Section 3.4 we prove that commutative relations are equivalent to exactness preserving of 1-cochain subdivision schemes and we will use them as the guiding principle for our construction of subdivision schemes. In Section 3.5 we construct a particular smooth subdivision 1-form in arbitrary topology setting and perform regularity analysis.

3.1 Whitney Forms

3.1.1 Definition

Given a simplicial complex K, we let $\Omega^r(K)$ denote the space of r-forms on $|K|$. We can integrate an r-form ω on any r-chain A of K. The integration $\int_A \omega$ is a linear function of r-chains. We define *de Rham map* map $R\colon \Omega^r \to \mathcal{C}^r(K)$ such that, for every $\omega \in \Omega^r(K)$

$$R\omega \cdot A = \int_A \omega \quad \text{all } r\text{-cochains } A \text{ of } K. \tag{3.1}$$

Due to Stokes' Theorem, for an $(r+1)$-chain B, we have

$$R\boldsymbol{d}\omega \cdot B = \int_B \boldsymbol{d}\omega = \int_{\partial B} \omega = R\omega \cdot \partial B = dR\omega \cdot B,$$

and hence

$$R\boldsymbol{d}\omega = dR\omega.$$

The converse is to define an embedding of $\mathcal{C}^r(K)$ into $\Omega^r(K)$. The embedding introduced below was first proposed by Whitney [1957, Chapter 5 §11]. Since the dimension of the r-chain space $\mathcal{C}_r(K)$ is finite and $\mathcal{C}^r(K)$ is its dual space, we may identify the chains with the cochains of K. We denote by λ_i the barycentric coordinate corresponding to the vertex v_i of K.

Definition 3.1. We define the linear mapping $W\colon \mathcal{C}^r(K) \to \Omega^r(K)$ such that, for each r-simplex $\sigma = v_{i_0} \dots v_{i_r}$ of K,

$$W\sigma = r! \sum_{j=0,\dots,r} (-1)^j \lambda_{i_j} \boldsymbol{d}\lambda_{i_0} \wedge \dots \wedge \widehat{\boldsymbol{d}\lambda_{i_j}} \wedge \dots \wedge \boldsymbol{d}\lambda_{i_r}. \tag{3.2}$$

We call W the *Whitney map* and call $W\sigma$ the *Whitney form* of σ. Further we let $\mathcal{W}^r(K)$ be the space of Whitney r-forms on K.

Note that the barycentric coordinates λ_i are C^∞ on the interior of any r-simplex $|\sigma|$ of K while they are not C^1 across $\partial\sigma$. Hence, $W\sigma$ is continuous on the interior of $|\sigma|$ but discontinuous across $\partial\sigma$. What's important for Whitney forms is that, for each r-cell s of $|K|$, the integration $\int_s W\sigma$ is well defined. Some properties of Whitney forms are listed below. See [Whitney 1957; Dodziuk 1976; Dodziuk & Patodi 1976] for details.

Theorem 3.2. *Given an r-simplex σ of K, for each r-cochain X, the Whitney form $W\sigma$ has the following properties*

$$W\sigma = 0 \text{ outside } N_1(\sigma, K), \tag{3.3}$$

$$WdX = \boldsymbol{d}WX, \tag{3.4}$$

$$RWX = X, \tag{3.5}$$

$$WI^0 = \mathbf{1}, \tag{3.6}$$

I^0 being the unit 0-cochain of K and $\mathbf{1}$ being the unit function on $|K|$.

Whitney forms were used in [Whitney 1957] to build isomorphism between the cohomology groups of algebraic cochains and the cohomology groups of differential forms on K. The most remarkable property of Whitney forms is the *commutative relations* given by (3.4). The commutative relations ensure that the Whitney form of a closed cochain X, that is $dX = 0$, is a closed form. Further, an exact $(r+1)$-cochain X, that is $X = dY$ for some r-cochain Y, $r \geq 0$, is mapped to an exact r-form. In Section 3.4 we will exploit the commutative relations in depth. We will see that the commutative relations uniquely determine the Whitney map on simplicial surfaces.

We have the following *de Rham complex* of Whitney forms

$$\mathbb{R} \hookrightarrow \mathcal{W}^0(K) \xrightarrow{\boldsymbol{d}} \mathcal{W}^1(K) \xrightarrow{\boldsymbol{d}} \cdots \xrightarrow{\boldsymbol{d}} \mathcal{W}^n \to 0. \tag{3.7}$$

If the manifold K is contractible, this complex is exact in the sense that the cohomology spaces all vanish, that is to say, the range of each map $\boldsymbol{d}$ is precisely equal to (and not just contained in) the null space of the succeeding map.

As the converse of (3.5), Dodziuk & Patodi [1976] proved the approximation property of W stating that WR is approximately identity.

3.1.2 Whitney Forms on Simplicial Surfaces

We now focus on the Whitney forms on a simplicial surface K. For each vertex v_i of K, we use ϕ_i to denote the Whitney 0-form associated with that vertex. ϕ_i is simply the barycentric coordinate corresponding to the vertex v_i of K. Similarly, we denote by ϕ_{ij} the Whitney 1-form associated with the edge $e_{ij} = v_i v_j$, and ϕ_{ijk} the Whitney 2-form associated with the triangle $t_{ijk} = v_i v_j v_k$. We have

$$\phi_{ij} = \phi_i d\phi_j - \phi_j d\phi_i, \tag{3.8}$$

$$\phi_{ijk} = 2 d\phi_i \wedge d\phi_j. \tag{3.9}$$

As an example, we verify some properties of ϕ_{ij}. It is easy to see that $\int_{e_{ij}} \phi_{ij} = 1$ while its integration over any other edge yields zero. Furthermore, the Whitney 1-form is supported on the two triangles incident to edge e_{ij} and varies linearly over each triangle.

If we fix a metric we may associate the 1-form with a vector field (see Figure 3.1). Note that the vector field is not continuous across the shared edge while its tangential component along the edge is continuous. To see that this definition does indeed admit an expression for the differential of any PL function f in terms of coefficients associated with edges under the commutative relations (3.4), we consider the differential $\boldsymbol{d}f$ over a single triangle t_{ijk},

$$\begin{aligned}\boldsymbol{d}(f_i\phi_i + f_j\phi_j + f_k\phi_k) &= (f_j - f_i)(\phi_i d\phi_j - \phi_j d\phi_i) \\ &+ (f_k - f_j)(\phi_j d\phi_k - \phi_k d\phi_j) \\ &+ (f_i - f_k)(\phi_k d\phi_i - \phi_i d\phi_k) \\ &= (f_j - f_i)\phi_{ij} + (f_k - f_j)\phi_{jk} + (f_i - f_k)\phi_{ki},\end{aligned}$$

where we used the fact that $\phi_i + \phi_j + \phi_k = 1$ and $d\phi_i + d\phi_j + d\phi_k = 0$. The coefficients associated with the $\phi_{ij,jk,ki}$ are the differences (signed sums) of $f_{i,j,k}$ coefficients at the end points of the respective edges, verifying that the coboundary operator d does transform coefficient vectors of 0-forms (with respect to the 0-form basis) into the corresponding coefficient vectors of 1-forms (with respect to the Whitney 1-form basis). In particular Whitney 2-forms are constant forms on each triangle.

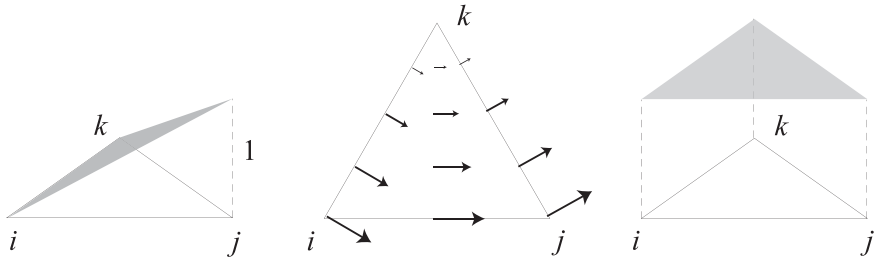

Figure 3.1: *Visualization of Whitney 0-, 1-, and 2-forms. The 0-forms correspond to the usual PL hat functions (left), while 2-forms are piecewise constant over each triangle (right). The 1-forms can be visualized as vector fields if we choose a metric (middle).*

Each triangle of K can be identified with a region in $\mathbb{R}^2$ under the affine coordinate, and hence is equipped with Euclidian metric of $\mathbb{R}^2$ under which we can identify forms with functions and vector fields. The de Rham complex of Whitney forms can be written in terms of operations of vector calculus

$$\mathbb{R} \hookrightarrow \mathcal{W}^0(K) \xrightarrow{\nabla} \mathcal{W}^1(K) \xrightarrow{\nabla\times} \mathcal{W}^2(K) \to 0. \tag{3.10}$$

On a three-dimensional simplicial complex imbedded into $\mathbb{R}^3$, the corresponding de Rham complex is

$$\mathbb{R} \hookrightarrow \mathcal{W}^0(K) \xrightarrow{\nabla} \mathcal{W}^1(K) \xrightarrow{\nabla\times} \mathcal{W}^2(K) \xrightarrow{\nabla\cdot} \mathcal{W}^3(K) \to 0. \tag{3.11}$$

3.1.3 Comparison with Mixed Finite Elements

Whitney forms on 2D and three-dimensional simplicial complexes have been rediscovered in the literature of mixed finite element methods since around 1974. The earliest paper by far pointing out this connection is due to [Bossavit 1988]. For instance the face elements proposed by Raviart & Thomas [1977] are Whitney 2-forms of space-dimension 2. The edge elements proposed by Nédélec [1980] are equivalent to Whitney 1-forms on a tetrahedron. Mixed finite element methods have extensive applications in electromagnetism and elasticity (*e.g.*, [Bossavit 1998; Arnold *et al.* 2006a]). As an extension of Whitney forms which is only PL linear, construction of high-order polynomial forms were studied by many researchers (*e.g.*, [Cendes 1991; Hiptmair 1999, 2001; Bossavit 2002; Arnold *et al.* 2006a]). Their constructions are mainly concerned with non-conforming mixed finite elements in the sense that compatibility conditions are imposed on element boundaries while smoothness across boundaries is not assured. Recall that Whitney forms (3.2) define mappings from cochains to forms. Their constructions of mix finite elements are not mappings of cochains. No analogs to the commutative relations are there in their constructions.

In contrast our construction of high-order Whitney forms through r-cochain subdivision schemes (2.9) satisfies the following properties,

1. *Linear mappings from cochains to forms;*
2. *Respect the commutative relations* (3.4)*;*
3. *Smooth across boundaries of elements;*
4. *Admit r-cochain subdivision schemes.*

Precisely, given an r-cochains X as input, the r-cochain subdivision scheme generates an r-form ω which is finitely supported on $|K|$ and has partition of unity (3.6) if $r = 0$. The interpolating property (3.5) is generally not held by the subdivision schemes. Rather they are *approximation schemes*.

The immediate consequence of property (b) and (c) is that our method leads to smooth mixed finite element bases that admit the exact sequences of de Rham complex give by (3.10). The exact sequences of de Rham complex are crucial to the stability of mixed finite elements for electromagnetism and elasticity, *e.g.*, [Bossavit 1990; Arnold *et al.* 2006b].

3.2 Refinement Equations of Differential Forms

The first step of our construction is to notice *refinement equations of Whitney forms*. In general, a function $f(\boldsymbol{x})$ on $\mathbb{R}^2$ is said to be *refinable* if it is a solution of the refinement equation

$$f(\boldsymbol{x}) = \sum_{\alpha \in \mathbb{Z}^2} c_\alpha f(2\boldsymbol{x} - \alpha), \quad \boldsymbol{x} \in \mathbb{R}^2. \tag{3.12}$$

where c_α are scalar coefficients. In words, in the case of the 4-to-1 subdivision of meshes, $f(x)$ at the coarser scale equals the linear combination of its translated versions on the finer scale. The refinement equation is the key to build hierarchies of refinable functions from coarse to fine, and it plays an important role in the theory of subdivision and wavelets. In this section we will build similar refinement equations for differential forms as well. The consequence of this is twofold. First, it enables us to construct differential forms on simplicial surfaces through subdivision. Second, the subdivision schemes of differential forms can be formally represented as the *matrix subdivision* which will be discussed in Sections 3.2.2 and 3.2.3 in detail. The theory of matrix subdivision has been extensively studied in the literature of multiwavelets but, to my knowledge, no geometric applications of matrix subdivision have been reported. Our construction presents an example with geometric meaning.

3.2.1 Refinement Equations of Whitney Forms

It is well known that, in the regular setting, the Whitney 0-form satisfies a simple linear two-scale relation that yields the piecewise linear interpolation. We note that the definition of Whitney k-forms relies on that of $(k-1)$-forms. Therefore we have a built-in two-scale refinement equation for Whitney 1-forms which is inherited from that of PL functions and leads to PL interpolating of vectors valued at vertices. However this refinement equation may not be satisfying since it is essentially a subdivision scheme of vector fields and we

should not expect it to respect geometry of differential forms (it obviously depends on coordinate systems). Recall the refinement equation (3.12) for 0-forms only involves itself in a recursive way and the topological structure of the mesh. We are therefore seeking a similar refinement equation for 1-forms which *only* depends on the *topological structure* of $|K|$.

The domain where a Whitney 1-form lives upon can be set to be one pair of adjacent triangles, which can be embedded into $\mathbb{R}^2$ through an affine transformation. The 4-to-1 subdivision splits one triangle of $|K|$ into 4 sub-triangles by connecting the middle points of each triangle side. We observed the following two-scale refinement equation for the Whitney 1-form associated with the edge ij (see Figure 3.2):

$$\phi_{ij} = \frac{1}{2}\phi_{ip} + \frac{1}{2}\phi_{pj} + \frac{1}{4}\phi_{mn} + \frac{1}{4}\phi_{rq} - \frac{1}{4}\phi_{pm} - \frac{1}{4}\phi_{np} - \frac{1}{4}\phi_{pr} - \frac{1}{4}\phi_{qp} \tag{3.13}$$

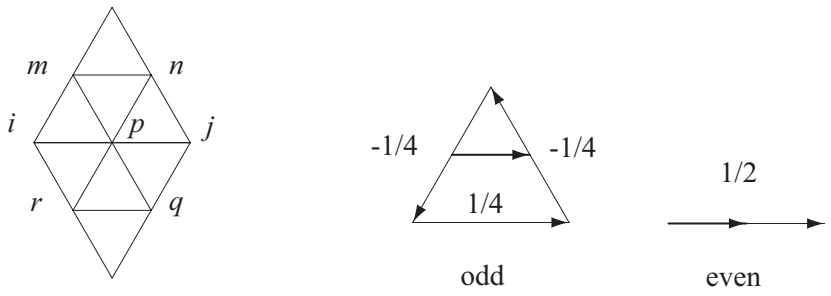

Figure 3.2: *Support of Whitney* 1*-form associated with the central edge* e_{ij} *(left). The edge-based subdivision scheme for Whitney* 1*-forms (middle and right). The two children edges are highlighted. The coefficients at the refined edges are obtained by averaging the coarse edge coefficients with the odd or even stencils. Edge orientations are indicated by arrows.*

Written in matrix notations

$$\Phi^e = \phi^e S_1^W, \tag{3.14}$$

where Φ^e represents a row vector of Whitney 1-forms on the coarse mesh and ϕ^e the corresponding row vector of Whitney 1-forms on the refined mesh. The refinement coefficients are written as entries of the subdivision matrix S_1^W. Similarly the refinement relations of Whitney 0- and 2-forms can be written as

$$\Phi^v = \phi^v S_0^W, \tag{3.15}$$

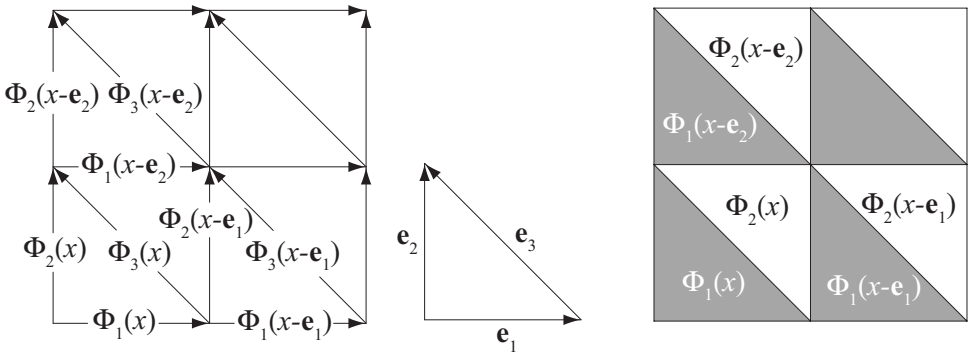

Figure 3.3: *Translations of* 1*-forms associated with* 3 *types of edges (left). Translations of* 2*-forms associated with* 2 *types of triangles (right).*

$$\Phi^t = \phi^t S_2^W. \tag{3.16}$$

As in the refinable scalar functions, these refinement coefficients of Whitney forms naturally defined subdivision schemes on coefficients associated with vertices, edges and triangles. They all fall into the category of *r-cochain subdivision schemes*. While the vertex- and triangle-based subdivision schemes are well known as primal and dual subdivision schemes, respectively, the edge-based subdivision scheme is new (see Figure 3.2).

3.2.2 Matrix Refinement Equations for *r*-Forms

We will build the refinement equation for differential r-forms on $\mathbb{R}^2$. We consider the geometric realization of the regular complex K_6. The vertices of K_6 are identified with $\mathbb{Z}^2$. The oriented edges of K_6 are obtained by translating the three edges denoted by $\mathbf{e}_i$ (see Figure 3.3). While the refinement coefficients c_α in (3.12) are associated with vertices, those for r-forms shall be associated with r-simplexes. We have seen in (3.13) that Whitney 1-forms on the coarser mesh are linear combinations of its scaled and translated version associated with refined edges. The same is true with Whitney 2-forms.

Let $\Phi_i^e(\boldsymbol{x}-\alpha)$ denote the translations of a 1-form associated with the edge aligned with $\mathbf{e}_i$. We can group three types of 1-forms into a 3-vector $\Phi^e(\boldsymbol{x}) \equiv (\Phi_1^e(\boldsymbol{x}), \Phi_2^e(\boldsymbol{x}), \Phi_3^e(\boldsymbol{x}))^T$ and its translations are illustrated in Figure 3.3 (left). We consider *matrix refinement equations* by extending the scalar coefficients c_j in (3.12) to matrices. Formally we have the following.

Definition 3.3. A 1-form Φ^e is said to be refinable if there exist 3×3 matrices P_α^e such

that

$$\Phi^e(\boldsymbol{x}) = \sum_{\alpha \in \mathbb{Z}^2} P^e_\alpha \Phi^e(2\boldsymbol{x} - \alpha). \tag{3.17}$$

The coefficients $\{P^e_\alpha\}$ yield a matrix subdivision scheme S^e. The definition of matrix subdivision schemes is given by (3.24). The *characteristic polynomial*, or *symbol* of the 1-form refinement equation is defined as

$$S^e(\boldsymbol{z}) \equiv \sum_{\alpha \in \mathbb{Z}^2} P^e_\alpha \boldsymbol{z}^\alpha, \quad \boldsymbol{z} = (z_1, z_2). \tag{3.18}$$

Here, by a slight abuse of notations, we use $S(\boldsymbol{z})$ to denote the symbol of subdivision scheme S. Similarly, we can group 2-forms into a 2-vector $\Phi^t(\boldsymbol{x}) \equiv (\Phi^t_1(\boldsymbol{x}), \Phi^t_2(\boldsymbol{x}))^T$ with two components being 2-forms associated the down (gray) and up (white) triangles (Figure 3.3, right).

Definition 3.4. A 2-form Φ^t is said to be refinable if there exist 2×2 matrices P^t_α such that

$$\Phi^t(\boldsymbol{x}) = \sum_{\alpha \in \mathbb{Z}^2} P^t_\alpha \Phi^t(2\boldsymbol{x} - \alpha). \tag{3.19}$$

The symbol of the 2-form refinement equation is defined in a similar way

$$S^t(\boldsymbol{z}) \equiv \sum_{\alpha \in \mathbb{Z}^2} P^t_\alpha \boldsymbol{z}^\alpha. \tag{3.20}$$

Finally the symbols of the coboundary operators are given by

$$d^0(\boldsymbol{z}) = \begin{pmatrix} -1 + z_1^{-1} \\ -1 + z_2^{-1} \\ -z_1^{-1} + z_2^{-1} \end{pmatrix} \quad \text{and} \quad d^1(\boldsymbol{z}) = \begin{pmatrix} 1 & -1 & 1 \\ -z_2^{-1} & z_1^{-1} & -1 \end{pmatrix}. \tag{3.21}$$

Each component Φ^e_i of the 3-vector $\Phi^e(\boldsymbol{x})$ represents a 1-form instead of a scalar function. Given the global coordinates $\{dx, dy\}$ on $\mathbb{R}^2$, Φ^e_i can be represented by its component functions:

$$\Phi^e_i(x, y) = \xi_i(x, y)dx + \eta_i(x, y)dy.$$

By identifying each Φ^e_i with its vector field proxy $(\xi_i(x, y), \eta_i(x, y))^T$, the refinement equa-

tion (3.17) can be written as

$$\xi(\boldsymbol{x}) = \sum_{\alpha\in\mathbb{Z}^2} 2P^e_\alpha \xi(2\boldsymbol{x}-\alpha), \tag{3.22}$$

$$\eta(\boldsymbol{x}) = \sum_{\alpha\in\mathbb{Z}^2} 2P^e_\alpha \eta(2\boldsymbol{x}-\alpha), \tag{3.23}$$

where $\xi = (\xi_1, \xi_2, \xi_3)^T$ and $\eta = (\eta_1, \eta_2, \eta_3)^T$. The component functions of the vector field proxy satisfy the refinement equation with normalized coefficients $\widetilde{P}^e_\alpha = 2P^e_\alpha$. It is important not to confuse the edge coefficients with the vector field coordinates. We will see that the edge coefficients are integral quantities representing circulations of the vector field proxy.

Remark 3.5. From (3.22) and (3.23) we see that the refinement equation (3.17) admits a 1-form solution *only if* the normalized matrix coefficients $\{\widetilde{P}^e_\alpha \colon \alpha \in \mathbb{Z}^2\}$ admit a vector function solution.

3.2.3 Convergence of Matrix Subdivision Schemes

The material in this section is based on [Cohen *et al.* 1995; Heil & Colella 1996]. We consider a uniform stationary matrix subdivision scheme defined by finite number of $n \times n$ matrix coefficients $\{P_\alpha \colon \alpha \in \mathbb{Z}^2\}$. Given $n \times 1$ control vectors at level j $f^j \equiv \{f^j_\alpha \colon \alpha \in \mathbb{Z}^2\}$, the control vectors at level $j+1$ are recursively generated by $f^{j+1} = Sf^j$:

$$f^{j+1}_\alpha = \sum_{\beta\in\mathbb{Z}^2} P_{\alpha-2\beta} f^j_\beta, \quad \alpha \in \mathbb{Z}^2. \tag{3.24}$$

The matrix subdivision scheme S is convergent if for every set of control vectors $f^0 \in \mathbb{R}^n \times \mathbb{Z}$ there is a continuous vector function $f \colon \mathbb{R}^2 \to \mathbb{R}^n$ such that

$$\lim_{j\to\infty} \sup_{\alpha\in\mathbb{Z}^2} \left\| (S^j f^0)_\alpha - f(2^{-j}\alpha) \right\| = 0, \tag{3.25}$$

and $f \neq 0$ for at least one initial datum f^0. We denote the limit function f by $S^\infty f^0$. If $S^\infty f^0 \in C^l$ for all initial data f^0, we say that S is C^l.

Many applications need weaker types of convergence. We interpolate control points $\{f^j_\alpha \colon \alpha \in \mathbb{Z}^2\}$ by constant test functions $\{\chi(2^j\boldsymbol{x} - \alpha) \colon \alpha \in \mathbb{Z}^2\}$ where χ denotes the characteristic functions of $[0,1]^2$. We say that S is convergent in L^p $(1 \leq p \leq \infty)$ if there exists

$f \in L^p$ such that

$$\lim_{j\to\infty} \left\| f - \sum_{\alpha\in\mathbb{Z}^2} (S^j f^0)_\alpha \chi(2^j \boldsymbol{x} - \alpha) \right\|_p = 0. \tag{3.26}$$

It is convenient to consider the $n\times n$ matrix function $\Phi \equiv S^\infty \Delta_0$ where $\Delta_i = \{\delta_{j,i} I_{n\times n}, j \in \mathbb{Z}^2\}$. As in scalar subdivision schemes, the matrix function Φ satisfies the MRE

$$\Phi(\boldsymbol{x}) = \sum_{\alpha\in\mathbb{Z}^2} P_\alpha \Phi(2\boldsymbol{x} - \alpha). \tag{3.27}$$

Transform of both sides of (3.27) gives the following equivalent equation in the Fourier space:

$$\hat{\Phi}(\gamma) = P(\frac{\gamma}{2})\hat{\Phi}(\frac{\gamma}{2}), \tag{3.28}$$

where $P(\gamma)$, called Fourier transform of the matrix subdivision scheme S, is the trigonometric polynomial

$$P(\gamma) = \frac{1}{4} \sum_{\alpha\in\mathbb{Z}^2} P_\alpha e^{-i\alpha\cdot\gamma}, \tag{3.29}$$

where $1/4$ is the dimensional factor. Iterating (3.28) generates

$$\hat{\Phi}(\gamma) = \prod_{j=1}^{n} P(2^{-j}\gamma)\hat{\Phi}(2^{-n}\gamma) \equiv P_n(\gamma)\hat{\Phi}(2^{-n}\gamma). \tag{3.30}$$

We let the infinite product

$$P_\infty(\gamma) \equiv \lim_{n\to\infty} P_n(\gamma).$$

If $P_\infty(\gamma)$ converges for every γ, it is clear that any distributional solution of (3.27) whose Fourier transform is a continuous function must have the form

$$\hat{\Phi}(\gamma) = P_\infty(\gamma)V \tag{3.31}$$

for some vector V. The convergence of $P_\infty(\gamma)$ is determined by the matrix

$$\Delta = P(0) = \frac{1}{4} \sum_{\alpha\in\mathbb{Z}^2} P_\alpha. \tag{3.32}$$

Let

$$\Delta^\infty \equiv \lim_{j\to\infty} \Delta^j.$$

We have the following convergence result from [Heil & Colella 1996, Theorem 3.3].

Theorem 3.6. *The infinite produce $P_\infty(\gamma)$ converges (uniformly on compact sets) if and only if Δ^∞ exits and is nontrivial. In this case, the mapping $V \mapsto \Phi$ induced by* (3.31) *is a linear map of C^r onto the set of all compactly supported distributional solution to the MRE* (3.27)*. Its kernel is the kernel of Δ^∞. It is a bijection when restricted to the* 1*-eigenspace of Δ. In particular, each nontrivial compactly supported solution satisfies $\hat{\Phi}(0) \neq 0$, and there exist exactly s independent solutions of the MRE, where s is the multiplicity of the eigenvalue* 1 *for Δ.*

As an example, the Fourier transforms $P^e(\gamma)$ and $P^t(\gamma)$ of the matrix subdivision schemes of Whitney 1- and 2-forms respectively, after normalization, have the Jordan normal forms

$$2P^e(0) \sim \begin{pmatrix} 1 & 0 & 0 \\ 0 & 1 & 0 \\ 0 & 0 & 1/4 \end{pmatrix} \text{ and } 4P^t(0) \sim \begin{pmatrix} 1 & 0 \\ 0 & 1/2 \end{pmatrix}.$$

3.3 Convergence of r-Cochain Subdivision Schemes

In this section we will establish the sufficient and necessary conditions for an r-cochain subdivision scheme to converge to a limit r-form on $\mathbb{R}^2$. We triangulate $\mathbb{R}^2$ by the regular complex K_6. In particular, we use the standard realization of K_6 described in Section 3.2.2. Since 0-cochain subdivision schemes have been studied in the literature of scalar (primal/dual) subdivision, our main interest will be focused on 1- and 2-cochain subdivision schemes.

3.3.1 Definition of Convergence for 1-Cochain Schemes

We only consider edge subdivision schemes that are invariant under the symmetry group of regular meshes. Therefore the manner we identify edges will not affect the convergence analysis. In particular we set the edge directions $(\boldsymbol{e}_1, \boldsymbol{e}_2)$ (Figure 3.3) to be the standard bases of $\mathbb{R}^2$. By grouping coefficients on edges into 3-vectors $\{f_\alpha \equiv (u_\alpha, v_\alpha, w_\alpha)^T : \alpha \in \mathbb{Z}^2\}$ (Figure 3.4), we can treat an edge subdivision scheme as a matrix subdivision scheme defined as (3.24).

Instead of interpolating coefficients by χ as in the functional setting, we need to properly interpolate coefficients on edges into a vector field $\boldsymbol{V}(\boldsymbol{x}) = (\xi(\boldsymbol{x}), \eta(\boldsymbol{x}))^T$ on $\mathbb{R}^2$ so that we

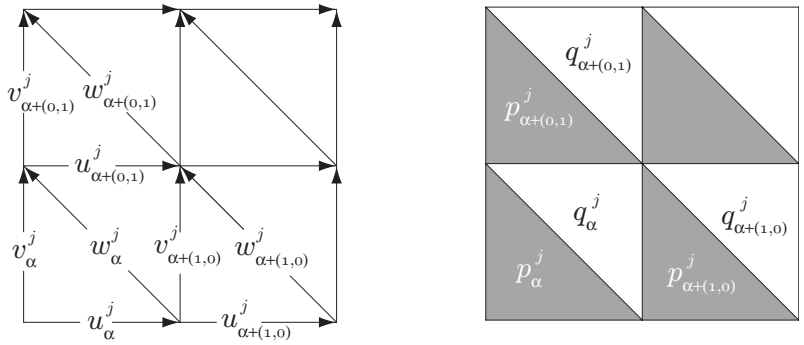

Figure 3.4: *Left: Numbering of edge coefficients* $\{f_\alpha \colon \alpha \in \mathbb{Z}^2\}$ *at level* j*. Right: coefficients on triangles by applying* d *to* f_α*:* $p^j_\alpha = u^j_\alpha - v^j_\alpha + w^j_\alpha$*,* $q^j_\alpha = -u^j_{\alpha+\epsilon_2} + v^j_{\alpha+\epsilon_1} - w^j_\alpha$ *where* $\epsilon_1 \equiv (1,0)$*,* $\epsilon_2 \equiv (0,1)$*.*

can define the corresponding 1-form $\omega(\boldsymbol{x}) = \xi dx + \eta dy$ under the standard bases of $\mathbb{R}^2$. In order for the integration of ω on each 1-cell σ of $|K|$ to be well defined, we require the tangential component of $\boldsymbol{V}(\boldsymbol{x})$ along σ to be continuous when approaching to σ from either side. Interpolation by Whitney 1-forms meets this requirement. Precisely, given vertex positions $\boldsymbol{a}$, $\boldsymbol{b}$, $\boldsymbol{c}$ of the three corners of a triangle together with the scalar coefficients a, b, c on the edges opposite $\boldsymbol{a}$, $\boldsymbol{b}$, $\boldsymbol{c}$, Whitney 1-forms produces a vector field at any point inside the triangle. Given barycentric coordinates λ_a,λ_b, λ_c, we have the restriction of $\boldsymbol{V}$ to the triangle

$$\boldsymbol{V}(\boldsymbol{x})|_{\boldsymbol{abc}} = \frac{1}{2\,\mathrm{Area}(\boldsymbol{abc})}\Big\{[\lambda_b(a+b+c)-b]\boldsymbol{ab}^\perp + [\lambda_c(a+b+c)-c]\boldsymbol{ac}^\perp\Big\}, \tag{3.33}$$

where $^\perp$ indicates a CCW rotation by 90° in the plane of the triangle. Note that the normal (to the edge of K) component of $\boldsymbol{V}$ is discontinuous across the edge while its tangential component is continuous. $\boldsymbol{V}$ is C^∞ within each triangle of K. As a result, we will only be concerned with the piecewise continuous 1-forms whose vector filed proxy has continuous tangential component along the edges of K. Further the vector filed proxy is uniform continuous on the compact set $\overline{T}$ for each triangle $T \in K$.

Definition 3.7. Given the triangulation K of $\mathbb{R}^2$ and the standard bases $\{dx, dy\}$, the space $\mathcal{F}_m(K)$ consists of 1-forms $\omega = \xi(x,y)dx + \eta(x,y)dy$ such that

1. ξ and η are continuous on $\overline{T}$ for each triangle $T \in K$;

2. the tangential component of $(\xi, \eta)^T$ along edges of K is continuous;

3. ξ and η are C^m-continuous functions on $|K|$.

We let $m = -1$ if the normal component of $(\xi, \eta)^T$ to the edges of K is discontinuous

According to Definition 3.7, the piecewise linear interpolation by Whitney 1-forms yields a vector field $\boldsymbol{V} \in \mathcal{F}_{-1}(K)$.

The following lemma shows that a 1-form in $\mathcal{F}_m$ is uniquely determined by its integral over 1-cells. It is a modification of [Whitney 1957, Lemma 16a].

Lemma 3.8. *Let ω_1 and ω_2 be 1-forms in $\mathcal{F}_m$ for some m. Suppose $\int_\sigma \omega_1 = \int_\sigma \omega_2$ for all oriented 1-cells in $|K|$. Then $\omega_1 = \omega_2$.*

Proof. For given triangle $T \in K$, take any $p \in \text{int}(T)$, and any 1-direction α. There is a sequence of oriented 1-cells σ_i in $\text{int}(T)$, with 1-directions $\alpha = \{\sigma_i\}/|\sigma_i|$, such that $\sigma_i \in U_{\rho_i}(p)$, where $U_{\rho_i}(p)$ denotes the ρ_i-neighborhood of p and $\rho_i \to 0$. We have

$$\frac{1}{|\sigma_i|}\int_{\sigma_i} \omega - \omega(p)\cdot\alpha = \frac{1}{|\sigma_i|}\int_{\sigma_i} \big(\omega(q) - \omega(p)\big)dq \to 0.$$

Therefore

$$\omega(p)\cdot\alpha = \lim_{i\to\infty} \frac{1}{|\sigma_i|}\int_{\sigma_i} \omega. \tag{3.34}$$

Applying this to ω_1 and ω_2 shows that $\omega_1(p)\cdot\alpha = \omega_2(p)\cdot\alpha$ for all 1-directions α; hence $\omega_1(p) = \omega_2(p)$ for any $p \in \text{int}(T)$.

In the case that $p \in \partial T$, we divide it into two cases according to the given 1-direction α. If $\alpha = \{\sigma_i\}/|\sigma_i|$ with σ_i being subdivided 1-cells of edges of K, $\omega(p)\cdot\alpha$ is defined by (3.34). The result immediately follows. If otherwise σ_i are 1-cells in $\text{int}(T')$ for the triangle $T' \in N_1(T)$, we can find a sequence $p_i \in \text{int}(T')$, $p_i \to p$, and $\omega(p_i)\cdot\alpha$ is well defined by (3.34). Due to continuity of ω on $\overline{T'}$, we can now define

$$\omega(p)\cdot\alpha = \lim_{i\to\infty} \omega(p_i)\cdot\alpha.$$

Therefore, $\omega_1(p) = \omega_2(p)$ provided that $\omega_1(p_i)\cdot\alpha = \omega_2(p_i)\cdot\alpha$ for all p_i. □

Given an initial 1-cochain X on K, we apply the 1-cochain subdivision S_1 to get $X^j = S_1^j X$ at level j, and then interpolate X^j by Whitney 1-forms at level j to get

$$\boldsymbol{V}^j(\boldsymbol{x}) = WX^j = \xi^j dx + \eta^j dy.$$

We consider the limit of the sequence $\{\boldsymbol{V}^j\}$.

Definition 3.9. A 1-cochain subdivision scheme S_1 is convergent on $|K|$ if, for any 1-cochain X, there exists a 1-form $\omega \in \mathcal{F}_m(K)$ such that

$$\lim_{j\to\infty} \sup_{\sigma\in \mathrm{Edge}(K^j)} \left| \frac{1}{|\sigma|}(S_1^j X)\cdot\sigma - \frac{1}{|\sigma|}\int_\sigma \omega \right| = 0.$$

We denote the limit 1-form by $\omega = S_1^\infty X$.

Lemma 3.10. *If a 1-cochain subdivision scheme S_1 is convergent, then the limit 1-form $S_1^\infty X$ is unique.*

Proof. We need to show that, if a 1-form $\omega \in \mathcal{F}_m(K)$ vanishes on all edges of K^j as $j \to \infty$, then ω itself vanishes. More precisely, we want to establish

$$\lim_{j\to\infty} \sup_{\sigma\in \mathrm{Edge}(K^j)} \frac{1}{|\sigma|}\int_\sigma \omega \to 0 \Longrightarrow \omega = 0.$$

Given any point $p \in |K|$ and 1-direction α, there exist vertex sequence $v_j \in K^j$ such that $|v_j - p| \to 0$. Given any $\epsilon > 0$, choose v_{j_0} such that $|\omega(p)\cdot\alpha - \omega(v_{j_0})\cdot\alpha| < \epsilon$ due to continuity of ω. The 1-direction α can be written in terms of edge directions α_i, $i = 1, 2$, $\alpha = c_1\alpha_1 + c_2\alpha_2$, where $\alpha_i = \{e_i\}/|e_i|$ and e_i are edges in K^{j_0} incident to v_{j_0}. Take large enough j_0 and use the fact that $|\omega(v_{j_0})\cdot\alpha_i| < \epsilon$, we have $|\omega(v_{j_0})\cdot\alpha| < N\epsilon$ for some constant N. Here we assumed that the coefficients c_1 and c_2 are uniformly bounded by a constant. It is indeed the case if the minimal angle of triangles are greater than a positive constant. Finally we have

$$\omega(p)\cdot\alpha < |\omega(p)\cdot\alpha - \omega(v_{j_0})\cdot\alpha| + |\omega(v_{j_0})\cdot\alpha| < (N+1)\epsilon.$$

This finishes the proof by letting $\epsilon \to 0$. □

Definition 3.11. Given a 1-form $\omega = \xi(x,y)dx + \eta(x,y)dy$, its L^∞ norm is defined as

$$\|\omega\|_\infty = \max(\|\xi\|_\infty, \|\eta\|_\infty).$$

Let $\boldsymbol{d}\omega = f(x,y)dx\wedge dy$. The flat norm of ω is defined as

$$\|\omega\|_\flat = \max(\|\omega\|_\infty, \|f\|_\infty).$$

A 1-form ω on $\mathbb{R}^2$ is called *flat* if $\|\omega\|_\flat < \infty$.

Definition 3.12. A flat 1-form ω is called $\mathcal{F}$-regular, or regular for short, if $\omega \in \mathcal{F}_m(K)$ and $\boldsymbol{d}\omega = f(x,y)dx\wedge dy$ with $f(x,y)$ being uniform continuous on each triangle $\overline{T} \in K$.

Remark 3.13. In abstract geometric integration theory, the flat norm is a pivotal concept. Discussion on flat forms is beyond the scope of this thesis. The interested reader is referred to [Whitney 1957] for details. Instead we are mainly interested in a regular form ω whose finite flat norm simply means that both ω and $\boldsymbol{d}\omega$ are uniformly bounded under the maximal norm.

The following lemma shows that $S_1^\infty X$ is determined by the sequence $\{WX^j\}$.

Lemma 3.14. *Given any* 1*-cochain* X*, let* WX^j *be the Whitney map of the cochains* $X^j = S_1^j X$*. On any compact subset* A *of* $|K|$*,*

$$\lim_{j\to\infty} \left\| WX^j - S_1^\infty X \right\|_{\infty,A} = 0. \tag{3.35}$$

Proof. As $\omega = S_1^\infty X$ is uniformly continuous on A, for any $\epsilon > 0$, there exists $\delta > 0$ such that for any p, q satisfying $|p-q| < \delta$, $|\omega(p) - \omega(q)| < \epsilon$. As the maximal distance between points of $|T|$ for a triangle T of K^j is $\frac{\sqrt{2}}{2^j}$, then for any $\epsilon > 0$ there is j_1 such that for all triangles T of K^j, $j > j_1$, for any $p, q \in |T|$, $|\omega(p) - \omega(q)| < \epsilon$. Since A only intersects with finite number of triangles of K, we only need to prove (3.35) on each T.

Take any point $p \in |T|$, we freeze ω on T by $\omega(p) = f_1 dx + f_2 dy$ where f_1 and f_2 are constants on $|T|$. Let e_1 and e_2 be the edges of T parallel with dx and dy, respectively, and $\mu = |e_1| = |e_2|$. Hence $|e_3| = \sqrt{2}\mu$. Let $a_i = \int_{e_i}(f_1 dx + f_2 dy)$, $i = 1, 2, 3$. Clearly $\sum_i a_i = 0$ due to Stokes' Theorem. Then, for $j > j_1$,

$$\left| a_i - \int_{e_i} \omega \right| \le C_1 \epsilon \mu, \quad i = 1, 2, 3.$$

As S_1 is convergent, there exists an integer j_2 such that, for all $j > j_2$,

$$\left| X^j \cdot e_i - \int_{e_i} \omega \right| \leq C_2 \epsilon \mu.$$

Hence, for $j > \max(j_1, j_2)$, we have

$$\left| X^j \cdot e_i - a_i \right| \leq \left| a_i - \int_{e_i} \omega \right| + \left| X^j \cdot e_i - \int_{e_i} \omega \right| \leq C_3 \epsilon \mu.$$

By applying the expression (3.33), we have

$$\left| WX^j - \omega(p) \right| \leq C_4 \epsilon, \quad \text{on } T,$$

and hence

$$\left\| WX^j - \omega \right\|_{\infty,T} \leq C_5 \epsilon, \quad \text{for } j > \max(j_1, j_2).$$

We finish the proof by letting $\epsilon \to 0$. □

3.3.2 Convergence Criteria for 1-Cochain Schemes

We have seen in Section 3.3.1 that, 1-cochain subdivision schemes can be *formally* represented as matrix subdivision schemes. However, the definitions of convergence under the two circumstances are different. In this section we present the conditions under which the 1-form sequence $WX^j = S_1^j X$ converge to the limit of the corresponding matrix subdivision scheme.

We denote by $\boldsymbol{V}^j$ the vector field proxy of WX^j on $\mathbb{R}^2$, given the regular triangulation K of $\mathbb{R}^2$ and standard bases $\{dx, dy\}$. Notice that $\boldsymbol{V}^j$ is not uniquely defined at vertices or along edges. We define a reference vector $\boldsymbol{U}_\alpha$ at each vertex location α which is obtained by interpolating coefficients f_α at that location. At level j, formula (3.33) immediately implies

$$\boldsymbol{U}_\alpha^j = 2u_\alpha^j \boldsymbol{e}_1 + 2v_\alpha^j \boldsymbol{e}_2. \tag{3.36}$$

We define a vector field $\boldsymbol{U}^j(\boldsymbol{x})$ in $\mathbb{R}^2$ interpolating $\boldsymbol{U}_\alpha$ by box functions

$$\boldsymbol{U}^j(\boldsymbol{x}) = \sum_{\alpha \in \mathbb{Z}^2} \boldsymbol{U}_\alpha^j \chi(2^j \boldsymbol{x} - \alpha). \tag{3.37}$$

Let $\chi_{\triangle}$ denote the characteristic function of set $T = \{(x, y) \in [0, 1)^2, x \le y\}$ and $\chi_{\triangledown}$ denote the characteristic function of $[0, 1)^2 \setminus T$. At each vertex α, let

$$\nabla_2 u_\alpha \equiv u_{\alpha+\epsilon_2} - u_\alpha, \quad \nabla_1 v_\alpha \equiv v_{\alpha+\epsilon_1} - v_\alpha,$$

and the piecewise constant functions

$$\nabla_2 u^j(\boldsymbol{x}) \equiv \sum_\alpha \nabla_2 (u)^j_\alpha \chi(2^j \boldsymbol{x} - \alpha),$$

$$\nabla_1 v^j(\boldsymbol{x}) \equiv \sum_\alpha \nabla_1 (v)^j_\alpha \chi(2^j \boldsymbol{x} - \alpha),$$

$$p^j(\boldsymbol{x}) \equiv \sum_\alpha p^j_\alpha \chi_{\triangle}(2^j \boldsymbol{x} - \alpha),$$

$$q^j(\boldsymbol{x}) \equiv \sum_\alpha q^j_\alpha \chi_{\triangledown}(2^j \boldsymbol{x} - \alpha).$$

Theorem 3.15. *Suppose $\boldsymbol{U}^j(\boldsymbol{x})$ uniformly converge to $\boldsymbol{U}(\boldsymbol{x}) \in \mathcal{F}_m$ on $|T|$ for each triangle of K. Then $\boldsymbol{V}^j(\boldsymbol{x})$ uniformly converge to $\boldsymbol{U}(\boldsymbol{x})$ on any compact set $A \subset \mathrm{int}(|T|)$ if*

$$\lim_{j\to\infty} 2^j |p^j|_{\infty,A} = 0. \tag{3.38}$$

Proof. Give vertex location α, we have

$$\|(\boldsymbol{V}^j - \boldsymbol{U}^j)\chi_{\triangle}(2^j \boldsymbol{x} - \alpha)\|_\infty = 2^j |p^j_\alpha|,$$

$$\|(\boldsymbol{V}^j - \boldsymbol{U}^j)\chi_{\triangledown}(2^j \boldsymbol{x} - \alpha)\|_\infty \le 2^j (|q^j_\alpha| + |\nabla_2 u^j_\alpha| + |\nabla_1 v^j_\alpha|),$$

$$|2^j q^j_\alpha| \le 2^j |\nabla_2 u^j_\alpha - \nabla_1 v^j_\alpha| + |2^j p^j_\alpha|.$$

Since $\boldsymbol{U}(\boldsymbol{x})$ is uniform continuous on A, for any $\epsilon >$, there is an integer $N > 0$ such that for any $j > N$,

$$2^j (|\nabla_2 u^j|_{\infty,A} + |\nabla_1 v^j|_{\infty,A}) < \epsilon \quad \text{and} \quad |2^j p^j|_{\infty,A} \le \epsilon.$$

Moreover,

$$|2^j q^j|_{\infty,A} \le 2^j(|\nabla_2 u^j|_{\infty,A} + |\nabla_1 v^j|_{\infty,A} + |p^j|_{\infty,A}) \le 2\epsilon.$$

Therefore

$$\begin{aligned}\|\boldsymbol{V}^j - \boldsymbol{U}^j\|_{\infty,A} &\le 2^j(|p^j|_{\infty,A} + |q^j|_{\infty,A} + |\nabla_2 u^j|_{\infty,A} + |\nabla_1 v^j|_{\infty),A} \\ &\le 4\epsilon\end{aligned}$$

for all $j > N$. This completes the proof by letting $\epsilon \to 0$. □

While Theorem 3.15 gives a sufficient condition for convergence to a 1-form $\omega \in \mathcal{F}_m$, we have the following sufficient and necessary conditions for converging to a regular 1-form under the flat norm.

Theorem 3.16. *Suppose the sequence $\boldsymbol{U}^j(\boldsymbol{x})$ converge to $\omega \in \mathcal{F}_m$ on $|T|$ for any triangle T of K. Further, suppose that ω is a regular 1-form with $\boldsymbol{d}\omega = f(\boldsymbol{x})dx\wedge dy$ being continuous 2-form on $|T|$. Then the sequence $\boldsymbol{V}^j(\boldsymbol{x})$ uniformly converge to ω on any compact set $A \subset \mathrm{int}(T)$ under the flat norm if and only if*

$$\lim_{j\to\infty}\Big\|f(\boldsymbol{x}) - \sum_{\alpha}\big(4^j p^j_\alpha \chi_{\triangle}(2^j\boldsymbol{x} - \alpha) + 4^j q^j_\alpha \chi_{\triangledown}(2^j\boldsymbol{x} - \alpha)\big)\Big\|_{\infty,A} = 0. \tag{3.39}$$

Proof. In order to prove convergence under the flat norm, it is equivalent to show

$$\lim_{j\to\infty}\big\|\boldsymbol{V}^j - \omega\big\|_{\infty,A} = 0, \tag{3.40}$$

$$\lim_{j\to\infty}\big\|d\boldsymbol{V}^j - d\omega\big\|_{\infty,A} = 0. \tag{3.41}$$

By applying the standard Lebesgue theory (*e.g.*, [Whitney 1957, Chapter 9]), the 2-form $\boldsymbol{d}\omega(\boldsymbol{x})$ can be identified with the uniformly continuous function $f(\boldsymbol{x})$ on A. Recall that $\boldsymbol{V}(\boldsymbol{x})$ is piecewise linear. We have

$$d\boldsymbol{V}(\boldsymbol{x}) = \sum_{\alpha}\big(4^j p^j_\alpha \chi_{\triangle}(2^j\boldsymbol{x} - \alpha) + 4^j q^j_\alpha \chi_{\triangledown}(2^j\boldsymbol{x} - \alpha)\big). \tag{3.42}$$

Therefore (3.41) is equivalent to (3.39). It is clear that (3.39) implies there exists constant M and integer N such that $4^j|p^j|_{\infty,A} < M$ for $j > N$. Therefore the condition (3.38) is satisfied and (3.40) follows from Theorem 3.15. The necessity is obvious. □

Theorem 3.16 implies the following property of refinement symbols of edge subdivision schemes:

Proposition 3.17. *Suppose the edge MRE* (3.17) *admits a convergent* 1*-cochain subdivision scheme* $S_1 \in \mathcal{F}_1(K)$ *under the flat norm and the* 3×3 *matrix* $P^e(\boldsymbol{z})$ *denotes the symbol of refinement coefficients. Then* $P^e(0)$ *has the Jordan normal form*

$$\begin{pmatrix} 1/2 & 0 & 0 \\ 0 & 1/2 & 0 \\ 0 & 0 & \rho \end{pmatrix} \tag{3.43}$$

with $\rho < 1/4$*. Furthermore,* $P^e(0)$ *has two* $1/2$*-eigenvectors* $\mu_i = (u_i, v_i, w_i)^T$ *(*$i = 1, 2$*) with the constraints:*

$$u_i + v_i - w_i = 0, \quad \textit{for } i = 1, 2. \tag{3.44}$$

Proof. C^1-smoothness of S_1 implies that, the two linearly independent constant 1-cochains corresponding to the de Rham map of $\{dx, dy\}$ must be the two $1/2$-eigenvectors of S_1 [Charina *et al.* 2005, Lemma 2], and hence they must also be the two $1/2$-eigenvectors of $P^e(0)$. The Jordan normal follows form (3.43) [Heil & Colella 1996, Theorem 3.3]. Suppose $(u, v, w)^T$ is one of the $1/2$-eigenvector of $P^e(0)$. Theorem 3.16 shows that $4^j(u + v + w)$ must be bounded as $j \to \infty$. Therefore $u + v + w = 0$, and it indeed admits two linearly independent solutions of (u, v, w). The condition $\rho < 1/4$ follows from C^1-smoothness of S_1 and Theorem 5.4 by Cohen *et al.* [1995]. □

Remark 3.18. In the proof of Proposition 3.17, C^1-smoothness is sufficient for S_1 to have the Jordan normal form (3.43). We will see in the future that C^1-smoothness is not a necessary condition. For instance, the subdivision scheme of Whitney 1-forms is not continuous, but it still has the Jordan normal form (3.43). The key property is the *commutative relations* held by Whitney forms, which we will discuss in detail in Section 3.4.

3.3.3 Convergence Criteria for 2-Cochain Schemes

We can identify a 2-form $\omega = f(x, y)dx \wedge dy$ on $\mathbb{R}^2$ with the function $f(x, y)$. Therefore convergence analysis of 2-cochain subdivision schemes is straightforward. Given 2-cochain $X \in \mathcal{C}^2(K)$, we interpolate $X^j = S_2^j X$ by Whitney 2-forms to yield a piecewise constant

function on K^j. Following the notations in Section 3.3.2, we group coefficients on triangles into 2-vectors $\{f_\alpha^j \equiv (p_\alpha^j, q_\alpha^j)^T, \alpha \in \mathbb{Z}^2\}$ (see Figure 3.4). We have

$$WX^j = \sum_\alpha \big(4^j p_\alpha^j \chi_\triangle(2^j \boldsymbol{x} - \alpha) + 4^j q_\alpha^j \chi_\triangledown(2^j \boldsymbol{x} - \alpha)\big). \tag{3.45}$$

Definition 3.19. A 2-cochain subdivision scheme S_2 is convergent on $|K|$ if, for any 2-cochain X, there exists a 2-form $\omega = f(x,y)dx\wedge dy$ such that $f(x,y)$ is continuous on each triangle $T \in K$ and

$$\lim_{j\to\infty} \sup_{\sigma\in \mathrm{Face}(K^j)} \left| \frac{1}{|\sigma|}(S_2^j X)\cdot\sigma - \frac{1}{|\sigma|}\int_\sigma \omega \right| = 0.$$

We denote the limit 2-form by $\omega = S_2^\infty X$.

Lemma 3.20. *If a 2-cochain subdivision scheme S_2 is convergent, then the limit 2-form $S_2^\infty X$ is unique, and on any compact subset $A \subset |K|$,*

$$\lim_{j\to\infty} \left\| WX^j - S_2^\infty X \right\|_{\infty, A} = 0.$$

Proof. It is analogous to the proof of the results for 1-cochains.

Lemma 3.20 shows that the convergence of S_2 to a piecewise continuous 2-form is equivalent to the convergence of the matrix subdivision sequence $\{f_\alpha^j\}$ to a piecewise continuous function. It follows from [Heil & Colella 1996, Theorem 3.3] that the symbol of S_2 has the Jordan normal form of $\left(\begin{smallmatrix} 1/4 & 0 \\ 0 & \rho \end{smallmatrix}\right)$ with $\rho < 1/4$.

3.4 Commutative Relations of Subdivision Schemes

3.4.1 Whitney Forms

We have defined the convergence and uniqueness of a r-form subdivision scheme. In addition to the Whitney 1-form subdivision scheme, the well-known barycentric interpolation and piecewise constant dual scheme can be naturally reinterpreted as 0- and 2-form subdivision schemes, respectively. We have now a triple of subdivision schemes S_0^W, S_1^W and S_2^W (Figure 3.5), based on vertices, edges and triangles, respectively. They converge to the corresponding linear Whitney forms.

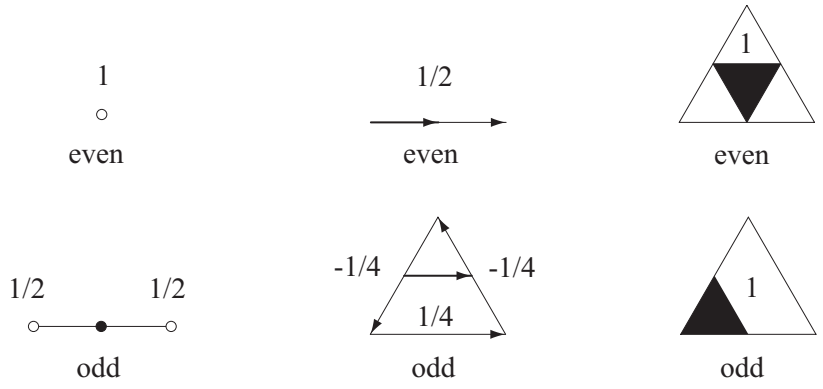

Figure 3.5: *Left:* 0*-form scheme* S_0^W*; middle:* 1*-form scheme* S_1^W*; right:* 2*-form scheme* S_2^W*.*

Lemma 3.21. *Whitney forms are linearly independent,* i.e.*, if* $WX = 0$ *then* $X = 0$*.*

Proof. This is a straightforward result from (3.5). Let R be the de Rham map. We have $RWX = X$ for any r-cochain X. It is easy to see that $R0 = 0$. Hence $WX = 0$ implies $X = 0$. □

Recall the commutative relations (3.4). The remarkable property of the triple subdivision schemes is that they are linked by *discrete* commutative relations through the discrete exterior differential operator d.

Proposition 3.22. *The Whitney subdivision schemes* S_0^W*,* S_1^W*,* S_2^W *satisfy commutative relations:*

$$dS_0^W = S_1^W d, \tag{3.46}$$

$$dS_1^W = S_2^W d. \tag{3.47}$$

Proof. The refinement equations for basis forms at the coarser (Φ) and finer (ϕ) levels follow as

$$\Phi^v = \phi^v S_0^W, \quad \Phi^e = \phi^e S_1^W, \quad \text{and} \quad \Phi^t = \phi^t S_2^W. \tag{3.48}$$

Using (3.48) together with (3.4) we can now prove that the associated subdivision operators satisfy the following relations

$$\phi^e d S_0^W X = \boldsymbol{d}(\phi^v S_0^W X) = \boldsymbol{d}(\Phi^v X) = \Phi^e dX = \phi^e S_1^W dX$$

for any 0-cochain X. Now $\phi^e(dS_0^W X - S_1^W dX) = 0$ implies $dS_0^W X = S_1^W dX$ due to linear

independence of Whitney 1-forms (see Lemma 3.21). Hence we have proved $dS_0^W = S_1^W d$ for S_0^W and S_1^W. The proof is entirely analogously for S_1^W and S_2^W. □

The 1-cochain subdivision scheme S_1 satisfying (3.46) and (3.47) has the property that it maps an exact 1-cochain to another exact 1-cochain, and it maps a closed 1-cochain to another closed 1-cochain. Recall that a cochain subdivision map is defined on the n-regular complex K_n which is a contractible manifold. Poincaré Lemma says that, on a contractible manifold, every closed form is also exact. The discrete Poincaré Lemma generalizes the same result to discrete manifold and algebraic cochains (*e.g.*, [Desbrun *et al.* 2005b]). Hence the r-cochain subdivision schemes that map exact cochains to exact cochains are of particular interest.

In the context of primal subdivision theory, the property (3.6) is called *affine invariant* property, that is to say, the unit 0-cochain on K is invariant under the 0-cochain subdivision map $S_0\mathbf{1} = \mathbf{1}$. Affine invariance is necessary for a 0-cochain subdivision scheme to converge (*e.g.*, [Cavaretta *et al.* 1991; Warren 1994]). On K_n the unit 0-cochain $\mathbf{1}$ is the unique (up to a multiplier) closed 0-cochain. Therefore we reinterpret affine invariance as preserving exact cochains, and generalize this property to 1-cochains in the next section. We will also see that the discrete commutative relations uniquely determine the Whitney 1-form.

3.4.2 1-Cochain Subdivision Schemes Preserving Exactness

We consider a finite portion of the infinite simplicial complex K_n. We define W_l as follows

$$\begin{aligned}
&\text{Vertex}(W_l) = \{m = (m_1, m_2) \colon m \in \mathbb{Z}^2 \text{ and } 0 \le m_1 + m_2 \le l\},\\
&\text{Edge}(W_l) = \big\{\{m, m+e_1\}, \{m, m+e_2\}, \{m+e_1, m+e_2\} \colon m \in \text{Vertex}(W_l)\big\},\\
&\text{Face}(W_l) = \big\{\{m, m+e_1, m+e_2\}, \{m+e_1, m+e_1+e_2, m+e_2\} \colon m \in \text{Vertex}(W_l)\big\}.
\end{aligned}$$

The finite simplicial complex of $K_{n,l}$ is generated from n copies of W_l in the same manner as K_n is from W, by the equivalence relation

$$(i, (j, 0)) \equiv (i = 1, (0, j)) \quad \text{for all } 0 \le j \le l \text{ and } i \in \mathbb{Z}_n, \tag{3.49}$$

$K_{n,l}$ is a finite simplicial complex with boundaries (see Figure 3.6).

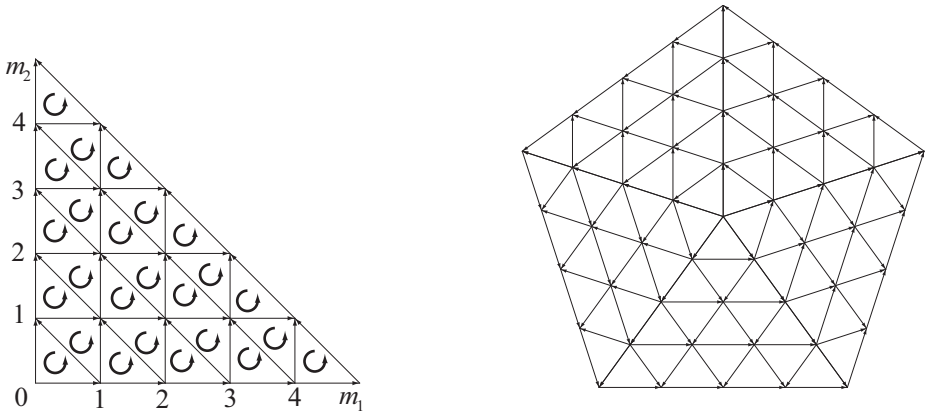

Figure 3.6: *Left: A wedge W_l with oriented edges and triangles (orientations indicated by arrows); right: the n-regular complex $K_{n,l}$ generated from n copies of W ($n = 5$).*

We consider the subdivision of $K_{n,l}$:

$$D\colon K_{n,l} \to K_{n,2l}.$$

Here we abused the notation D which also refers to the subdivision of K_n. The difference is that $D(K_{n,l})$ is not a simplicial isomorphism of $K_{n,l}$.

We have the *discrete Poincaré Lemma* on the complex K_n:

Lemma 3.23. *Given a closed* 1*-cochain X on K_n, that is $dX = 0$, there exists a* 0*-cochain Y on K_n such that $dY = X$.*

Proof. The proof is elementary. We first assign a real number c_0 to the central vertex v_0 of K_n. It is straightforward to integrate X on each wedge W_i for $i \in \mathbb{Z}_n$. The resulting 0-cochain Y_i is defined on W_i and $dY_i = X$ on W_i for $i \in \mathbb{Z}_n$. Notice that Y_i is uniquely determined by c_0 and X. We only need to show that Y_i's coincide along the shared boundaries of two adjacent wedges. This is obvious because we have the equivalence relations (3.49) of vertices and the same initial value c_0 for integration. Therefore we have obtained a 0-cochain Y such that $Y \equiv Y_i$ on W_i and $dY = X$ on K_n. Furthermore, Y is unique up to a constant. □

Remark 3.24. While it is straightforward to prove the discrete Poincareé Lemma on the finite n-regular complex $K_{n,l}$, to prove it on more general discrete manifold is more involving. The interested reader is referred to [Desbrun *et al.* 2005b] for details.

Proposition 3.25. *Let $\mathcal{C}_l^r$ denote the r-cochain space on $K_{n,l}$. We have*

$$\dim \mathcal{C}_l^0 = \frac{n(l^2+l)}{2} + 1, \quad \dim \mathcal{C}_l^1 = \frac{n(3l^2+l)}{2}, \quad \dim \mathcal{C}_l^2 = nl^2. \tag{3.50}$$

Therefore

$$\dim \mathcal{C}_l^1 = \dim \mathcal{C}_l^0 + \dim \mathcal{C}_l^2 - 1. \tag{3.51}$$

Furthermore

$$\operatorname{Ker} d^1 = d^0 \mathcal{C}_l^0, \quad \dim \operatorname{Ker} d^1 = \dim \mathcal{C}_l^0 - 1 \tag{3.52}$$

$$\operatorname{Im} d^1 = \mathcal{C}_l^2, \quad \dim \operatorname{Im} d^1 = \dim \mathcal{C}_1^2. \tag{3.53}$$

Proof. It is trivial to verify (3.50) by counting the number of vertices, edges and faces in $K_{n,l}$. Since $d^1 \circ d^0 = 0$, we have $d\mathcal{C}_l^0 \subset \operatorname{Ker} d^1$ and hence $\operatorname{Ker} d^1 \geq \dim d^0 \mathcal{C}_1^0$. Lemma 3.23 shows that $\operatorname{Ker} d^1 \subset d\mathcal{C}_1^0$ and $\operatorname{Ker} d^1 \leq \dim d^0 \mathcal{C}_1^0$. Therefore $\operatorname{Ker} d^1 = d\mathcal{C}_1^0$ and $\operatorname{Ker} d^1 = \dim d^0 \mathcal{C}_l^0 = \dim \mathcal{C}_l^0 - 1$ since $d^0 \mathbf{1} = 0$. The classic theory of algebra tells us that $\dim \mathcal{C}_l^1 = \dim \operatorname{Ker} d^1 + \dim \operatorname{Im} d^1$. It follows from (3.51) that $\dim \operatorname{Im} d^1 = \dim \mathcal{C}_l^2$. Since $\operatorname{Im} d^1 \subset \mathcal{C}_l^2$, we have $\operatorname{Im} d^1 = \mathcal{C}_l^2$. □

Remark 3.26. The Proposition 3.25 is an immediate conclusion from the fact that, the de Rham complex of algebraic cochains on a contractible manifold is exact.

The stationary k-cochain subdivision operator S_k with finite support can now be described as a mapping

$$S_r \colon \mathcal{C}^r(K_{n,l}) \to \mathcal{C}^r(K_{n,l}) \quad \text{for } l \geq m_w - 1,$$

where m_w is the mask width of S_r. We call $K_{n,l}$ an *invariant neighborhood* of S_r. Therefore S_r is fully determined by its action on its minimal invariant neighborhood K_{n,m_w} and it can be reduced to a finite subdivision matrix. In all that follows we assume that S_r represents a stationary r-cochain subdivision operator with invariant neighborhood $K_{n,l}$.

Theorem 3.27. *Given a 1-cochain subdivision matrix S_1 and its invariant neighborhood $K_{n,l}$. $\operatorname{Ker} d^1$ is an invariant subspace of S_1 if and only if there exists a 0-cochain subdivision*

matrix S_0 with invariant neighborhood $K_{n,l}$ such that the commutative diagram holds

$$d^0 S_0 = S_1 d^0. \tag{3.54}$$

Proof. The proof of sufficiency is straightforward. Given a 1-cochain X such that $dX = 0$. Lemma 3.23 implies that there exists a 0-cochain Y such that $X = dY$. We have $S_1 X = S_1 dY = dS_0 Y$ provided the commutative diagram (3.54). Therefore $dS_1 X = d \circ dS_0 Y = 0$ and $\operatorname{Ker} d^1$ is an invariant subspace of S_1.

We will use a constructive approach to prove necessity. Given any 0-cochain X and the exact 1-cochain $Y = d^0 X \in \operatorname{Ker} d^1$. Since $\operatorname{Ker} d^1$ is an invariant subspace of S_1 we have $S_1 Y \in \operatorname{Ker} d^1$ and

$$S_1 d^0 X = d^0 Z \quad \text{for some } Z \in \mathcal{C}_l^0 \tag{3.55}$$

due to Lemma 3.23. Recall that $\operatorname{Ker} d^0$ is a one-dimensional space consisting of all constant 0-cochains on $K_{n,l}$. Therefore (3.55) defines a unique, up to a constant, 0-cochain $Z \equiv S_0 X$ for any given $X \in \mathcal{C}_l^0$. Plugging it back into (3.55), we have reached $d^0 S_0 = S_1 d^0$. We can fix the constant by requiring S_0 to preserve constant 0-cochains, *i.e.*$S_0 \mathbf{1} = \mathbf{1}$. □

Corollary 3.28. *Given a 1-cochain subdivision scheme S_1 with invariant neighborhood $K_{n,l}$. If $\operatorname{Ker} d^1$ is an invariant subspace of S_1, then there exists a unique 0-cochain scheme S_0 satisfying $S_0 \mathbf{1} = \mathbf{1}$, and a unique 2-cochain scheme S_2, both with invariant neighborhood $K_{n,l}$, such that the following commutative diagrams hold:*

$$d^0 S_0 = S_1 d^0, \quad d^1 S_1 = S_2 d^1. \tag{3.56}$$

Proof. The first commutative diagram is directly from Theorem 3.27. We only need to show the second one. Let the 2-cochain scheme S_2 be defined as follows. Given any 2-cochain $X \in \mathcal{C}_l^2$, there must exist a 1-cochain $Y \in \mathcal{C}_l^1$ satisfying $d^1 Y = X$ due to (3.53). If we define S_2 such that $S_2 X = d^1 S_1 Y$, then we have $S_2 d^1 = d^1 S_1$. We need to show that $S_2 X$ is well defined. If there exists another 1-cochain $Z \in \mathcal{C}_l^1$ such that $d^1 Z = X$, then $Z - Y \in \operatorname{Ker} d^1$. Since $\operatorname{Ker} d^1$ is an invariant subspace of S_1, we have $d^1 S_1 (Z - Y) = 0$. Therefore $d^1 S_1 Z = d^1 S_1 Y$. This proves the uniqueness of $S_2 X$ for any given X. □

Remark 3.29. Given the 0- and 2-cochain subdivision schemes at the two ends, the 1-cochain subdivision scheme satisfying the commutative diagrams is not necessarily unique. However,

we find that we do have a unique 1-cochain subdivision scheme solving the commutative relations in most of the cases we considered.

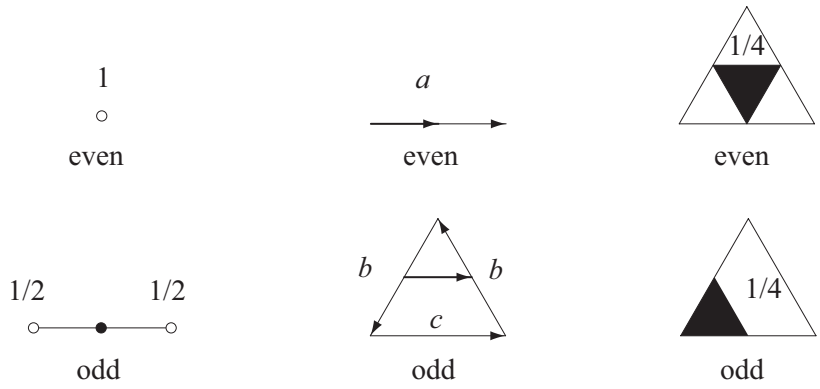

Figure 3.7: *The barycentric interpolation works as S_0 (left); the fully parameterized mask of S_1 (middle); S_2 is the piecewise constant down sampling (right). The unique solution for the commutative relations is $a = 1/2$, $b = -1/4$ and $c = 1/4$ which rediscovers the refinement masks of Whitney 1-form.*

Corollary 3.30. *Given the barycentric subdivision scheme S_0 and the piecewise constant dual subdivision scheme S_2. The subdivision scheme of Whitney 1-form is the only edge subdivision scheme S_1 satisfying the commutative diagrams.*

Proof. The commutative diagrams add constraints to the size of support of potential edge subdivision schemes. Therefore the mask of S_1 can be fully parameterized by a, b and c by symmetry, as is shown in Figure 3.7 . Due to linearity we only need to verify the commutative diagrams with the initial dirac, *i.e.*, a single coefficient 1 at a vertex or edge. Algebraic calculations give the unique solution of the commutative diagrams

$$a = \frac{1}{2}, \quad b = -\frac{1}{4}, \quad c = \frac{1}{4}.$$

This is exactly the mask of Whitney 1-forms. □

The consequence of Theorem 3.27 and Corollary 3.28 implies that we can design an exactness preserving 1-form scheme by imposing the commutative relations. Indeed Corollary 3.30 shows that the commutative relations uniquely characterized Whitney forms in the two-dimensional case. Since scalar subdivision schemes (primal and dual) are extensively studied, this new viewpoint allows us to discover 1-form schemes simply by solving commutative relations. We will show how to construct generalized Whitney forms of higher order

of smoothness in Section 3.5.

Proposition 3.31. *Given the* 1*-cochain subdivision scheme* S_1 *satisfying the commutative relations with* S_0 *and* S_2*. Consider the triangulation* K_6 *of* $\mathbb{R}^2$ *under the coordinates* $\{dx, dy\}$*. Suppose that* S_0 *has linear precision, that is to say, it admits the* 0*-cochains of* $\{x, y\}$ *as its two* $1/2$*-eigenvectors. Further, suppose that* S_2 *admits the constant* 2*-cochain as its dominant* $1/4$*-eigenvector. Then the Jordan normal forms of* $P^e(0)$ *and* $P^t(0)$ *are*

$$P^e(0) \sim \begin{pmatrix} 1/2 & 0 & 0 \\ 0 & 1/2 & 0 \\ 0 & 0 & \rho \end{pmatrix} \text{ and } P^t(0) \sim \begin{pmatrix} 1/4 & 0 \\ 0 & \rho \end{pmatrix}, \ \rho < 1/4. \tag{3.57}$$

Moreover, the ρ*-eigenvector of* $P^t(0)$ *is* $(1, -1)^T$*.*

Proof. The commutative relations can be written in symbols

$$d(\boldsymbol{z})S_0(\boldsymbol{z}) = S_1(\boldsymbol{z})d(\boldsymbol{z}), d(\boldsymbol{z})S_1(\boldsymbol{z}) = S_2(\boldsymbol{z})d(\boldsymbol{z}). \tag{3.58}$$

Since

$$S_0 x = 1/2x,$$
$$S_0 y = 1/2y,$$

we have

$$dS_0 x = S_1 dx = 1/2dx,$$
$$dS_0 y = S_1 dy = 1/2dy.$$

Here we used x, y, dx and dy to represent the cochains corresponding to the de Rham map of x, y, dx and dy, respectively. Hence S_1 admits 1-cochains $\{dx, dy\}$ as its $1/2$-eigenvectors. It follows that $P^e(0)$ has the Jordan normal form (3.57), and there exists 3×3 matrix V

consists of columns of $\{dx, dy\}$ and the ρ-eigenvector, such that

$$V^{-1}P^e(0)V = \begin{pmatrix} 1/2 & 0 & 0 \\ 0 & 1/2 & 0 \\ 0 & 0 & \rho \end{pmatrix}.$$

Recall the symbol of coboundary operator

$$d^1(\boldsymbol{z}) = \begin{pmatrix} 1 & -1 & 1 \\ -z_2^{-1} & z_1^{-1} & -1 \end{pmatrix}.$$

Note that

$$d^1(0)V = \begin{pmatrix} 0 & 0 & \gamma \\ 0 & 0 & -\gamma \end{pmatrix}$$

where γ is a real number. Here we abused notation d^1 to denote the Fourier transform of symbol $d^1(\boldsymbol{z})$. Therefore (3.58) implies that

$$\begin{pmatrix} 0 & 0 & \gamma \\ 0 & 0 & -\gamma \end{pmatrix} \begin{pmatrix} 1/2 & 0 & 0 \\ 0 & 1/2 & 0 \\ 0 & 0 & \rho \end{pmatrix} = P^t(0) \begin{pmatrix} 0 & 0 & \gamma \\ 0 & 0 & -\gamma \end{pmatrix}.$$

By compacting those zero blocks, we get

$$P^e(0) \begin{pmatrix} \gamma \\ -\gamma \end{pmatrix} = \rho \begin{pmatrix} \gamma \\ -\gamma \end{pmatrix}.$$

Since the dominant 1/4-eigenvector of $P^t(0)$ is $(1,1)^T$, the ρ-eigenvector $(\gamma, -\gamma)^T$ of $P^t(0)$ cannot be the dominant 1/4-eigenvector. Therefore we must have $\rho < 1/4$. □

3.4.3 Eigenstructures of Subdivision Matrix

Suppose subdivision matrix S_0, S_1 and S_2 satisfy the commutative relations on K_n. Let λ_i^k $(1 \le i \le J_k)$ be different eigenvalues of the subdivision matrix S_k. Specifically we reserver λ_0^0 for the eigenvalue 1 of S_0. We assume that λ_i^0 are in the order of nonincreasing magnitude and so are λ_i^2. We will describe how to order λ_i^1 in the following.

For λ_i^k, let J_{ij}^k, $j = 1 \dots P_i^k$ be the complex cyclic subspaces corresponding to this

eigenvalue.

Let n_{ij}^k be the orders of these cyclic subspaces; the order of a cyclic subspace is equal to its size minus one.

Let b_{ijr}^k, $r = 0 \dots n_{ij}^k$ be the complex generalized eigenvectors corresponding to the cyclic subspace J_{ij}^k.

Lemma 3.32. *If $b_{ijr}^0 \neq \mathbf{1}$, then $d^0 b_{ijr}^0$ is a generalized eigenvector of S_1; if $d^1 b_{ijr}^1 \neq 0$, then $d^1 b_{ijr}^1$ is a generalized eigenvector of S_2. Furthermore we can enumerate J_{ij}^1 such that*

$$\begin{aligned} d^0 J_{ij}^0 &= J_{ij}^1, \quad \textit{for } i = 1, \dots, J_0, \\ d^1 J_{i'j}^1 &= J_{ij}^2, \quad \textit{for } i' \equiv i + J_0 \textit{ and } i = 1, \dots, J_2. \end{aligned}$$

Proof. The vectors b_{ijr}^0 satisfy

$$\begin{aligned} S_0 b_{ijr}^0 &= \lambda_i^0 b_{ijr}^0 + b_{ijr-1}^0 \quad \text{if } r > 0, \\ S_0 b_{ij0}^0 &= \lambda_i^0 b_{ij0}^0. \end{aligned}$$

Applying d^0 to the equations above, we have from the commutative relations

$$\begin{aligned} d^0 S_0 b_{ijr}^0 = S_1 d^0 b_{ijr}^0 &= \lambda_i^0 d^0 b_{ijr}^0 + d^0 b_{ijr-1}^0 \quad \text{if } r > 0, \\ d^0 S_0 b_{ij0}^0 = S_1 d^0 b_{ij0}^0 &= \lambda_i^0 d^0 b_{ij0}^0. \end{aligned}$$

We claim that $d^0 J_{ij}^0$ is a cyclic subspace of S_1 corresponding to the eigenvalue $\lambda_{i'}^1 = \lambda_i^0$ due to the uniqueness of Jordan decomposition on the complex domain. We can re-order λ_i^1 such that $\lambda_i^1 = \lambda_i^0$ for $i = 1, \dots, J_0$. Therefore we have $dJ_{ij}^0 = J_{ij}^1$ and

$$\bigoplus_{ij} d^0 J_{ij}^0 = \bigoplus_{ij} J_{ij}^1.$$

Repeat the same procedure as above, we can show that $d^1 J_{i'j}^1$ is a cyclic subspace of S_2 corresponding to the eigenvalue $\lambda_{i'}^1 = \lambda_i^2$ where $i' \equiv i + J_0$. Therefore $d^1 J_{i'j}^1 = J_{ij}^2$ for some $1 \leq i \leq J_2$. $i = 1, \dots, J_2$. At the same time the dimensionality relation (3.51) shows that

$\dim \operatorname{Im} d^1 = \sum_{ij} \dim J^2_{ij}$. Therefore we have

$$\bigoplus_{i'j} d^1 J^1_{i'j} = \bigoplus_{ij} J^2_{ij}.$$

□

Lemma 3.32 is general enough to deal with complex eigenvectors, but we will only be interested in the spectrum of Loop's scheme for S_0. It is well known that Loop's scheme is C^1 on the atlas given by the characteristic map. While the convergence criteria of S_0 only needs the affine structure, we do need a metric to discuss convergence and regularity of S_1 and S_2. Throughout this thesis we will use the metric induced by the characteristic map.

Due to its cyclic structure, we can apply Discrete Fourier Transformation (DFT) to the control coefficients. In our cases, the 0-cochain subdivision can be written as

$$X^{j+1} = S_0 X^j, \quad X^j \equiv [\dots, A^j_m, B^j_m, C^j_m, \dots]' \in \mathbb{R}^{3\times n}.$$

The Fourier coefficients of $\{A^j_m\}$, $m = 0, \dots, n-1$ ($\{B^j_m\}$ and $\{C^j_m\}$ *etc.*) are given by

$$\hat{A}^j_k = \sum_{m=0}^{n-1} A^j_m \exp(2\pi\sqrt{-1}mk/n).$$

Let $\hat{X}^j_k \equiv [\hat{A}^j_k, \hat{B}^j_k, \hat{C}^j_k]'$ for $k = 0, \dots, n-1$. Therefore the action of S_0 can be represented as a matrix whose diagonal blocks are matrices $\hat{S}_{0,k}$, $k = 0, \dots, n-1$:

$$\hat{X}^{j+1}_k = \hat{S}_{0,k} \hat{X}^j_k.$$

Similarly, in the Fourier domain S_1 and S_2 can be diagonalized to $S_{1,k}$ and $S_{2,k}$ for $k = 0, \dots, n-1$, respectively. The commutative relations in terms of Fourier coefficients are written as

$$\hat{d}^0 \hat{S}_{0,k} = \hat{S}_{1,k} \hat{d}^0, \quad \hat{d}^1 \hat{S}_{1,k} = \hat{S}_{2,k} \hat{d}^1, \quad k = 0, \dots n-1,$$

where $\hat{d}$ denotes the matrix representation of d in the Fourier domain. It is easy to see that the proof of Lemma 3.32 can be repeated line by line if the cyclic subspace J^k_{ij} of S_k is replaced by the cyclic subspace $\hat{J}^k_{ij}$ of $\hat{S}_k$. Formally we have the following.

Lemma 3.33. *Fix the Fourier mode k. If $\hat{b}^0_{ijr} \neq \mathbf{1}$, then $\hat{d}^0 \hat{b}^0_{ijr}$ is a generalized eigenvector*

of $\hat{S}_{1,k}$; if $\hat{d}^1\hat{b}^1_{ijr} \neq 0$, then $\hat{d}^1\hat{b}^1_{ijr}$ is a generalized eigenvector of $\hat{S}_{2,k}$. Furthermore we can enumerate $\hat{J}^1_{ij}$ such that

$$\hat{d}^0\hat{J}^0_{ij} = \hat{J}^1_{ij}, \quad \textit{for } i = 1, \ldots, J_0,$$
$$\hat{d}^1\hat{J}^1_{i'j} = \hat{J}^2_{ij}, \quad \textit{for } i' \equiv i + J_0 \textit{ and } i = 1, \ldots, J_2.$$

Proof. The proof is essentially the same as that of Lemma 3.32. □

3.5 Construction of Smooth Subdivision Forms

3.5.1 The Regular Setting

A well-known fact from subdivision [Warren & Weimer 2001] states that, in the *regular* setting, a given subdivision scheme can be transformed into a subdivision scheme of higher regularity through convolution. Since we are working with triangle meshes, convolution along the three principal directions is appropriate and we denote its discrete representation with C. With such an additional convolution Whitney 0-forms yield quartic box splines (with subdivision operator $S_0^L = CS_0^W$) while Whitney 2-forms, after normalization by factor 4, give rise to half-box splines ($S_2^H = CS_2^W$). A quartic box spline basis is supported on 2-ring of triangles around the the central vertex while a half-box spline basis is supported on 1-ring of triangles around the central triangle (see Figure 3.8, top). Convolution of the Whitney 1-forms gives a new, smooth 1-form basis with subdivision scheme

$$S_1^E := CS_1^W. \tag{3.59}$$

However, the above definition of S_1 is merely a formal definition before we know how to convolve a 1-form in practice. Metric will come into play in the first place but the final definition has no need for metric, as expected. We first fix a uniform geometric realization of K_6 on $\mathbb{R}^2$, which is equivalent to have the three principal directions, $\boldsymbol{e}_1, \boldsymbol{e}_2$ and $\boldsymbol{e}_3 = \boldsymbol{e}_2 - \boldsymbol{e}_1$ (see Figure 3.3). The vector field proxy $\boldsymbol{V}(\boldsymbol{x})$ of Whitney 1-form basis associated with edge σ is supported on the two triangles incident to σ, and is linear within each triangle. It is now straightforward to convolve $\boldsymbol{V}(\boldsymbol{x})$ along the three principal directions to get a smoother vector field denoted by $\widetilde{\boldsymbol{V}}(\boldsymbol{x})$ (see Figure 3.8, bottom). The component functions of $\widetilde{\boldsymbol{V}}(\boldsymbol{x})$

satisfy a matrix refinement equation (MRE) and the refinement coefficients are given by the symbol S_1^E in (3.59). Notice that the refinement coefficients do *not* depend on the current coordinate system $\{\boldsymbol{e}_1, \boldsymbol{e}_2, \boldsymbol{e}_3\}$ although $\widetilde{\boldsymbol{V}}(\boldsymbol{x})$ itself does (see the Bézier representation in the appendix). Hence a MRE of 1-form is well defined through the symbol S_1^E. After a metric is fixed, this MRE admits component functions of the vector field $\widetilde{\boldsymbol{V}}(\boldsymbol{x})$ as its solution. The support of the smooth 1-form basis is now contained in $N_1(\sigma)$, the 1-ring of triangles around the two triangles incident to σ. Over this support the 1-form is piecewise polynomial (quartic) in terms of barycentric coordinates. The Bézier representation of polynomial patches can be found in the appendix. The subdivision stencils for S_0^L, S_1^E, and S_2^H (in the regular setting) are summarized in Figure 3.9.

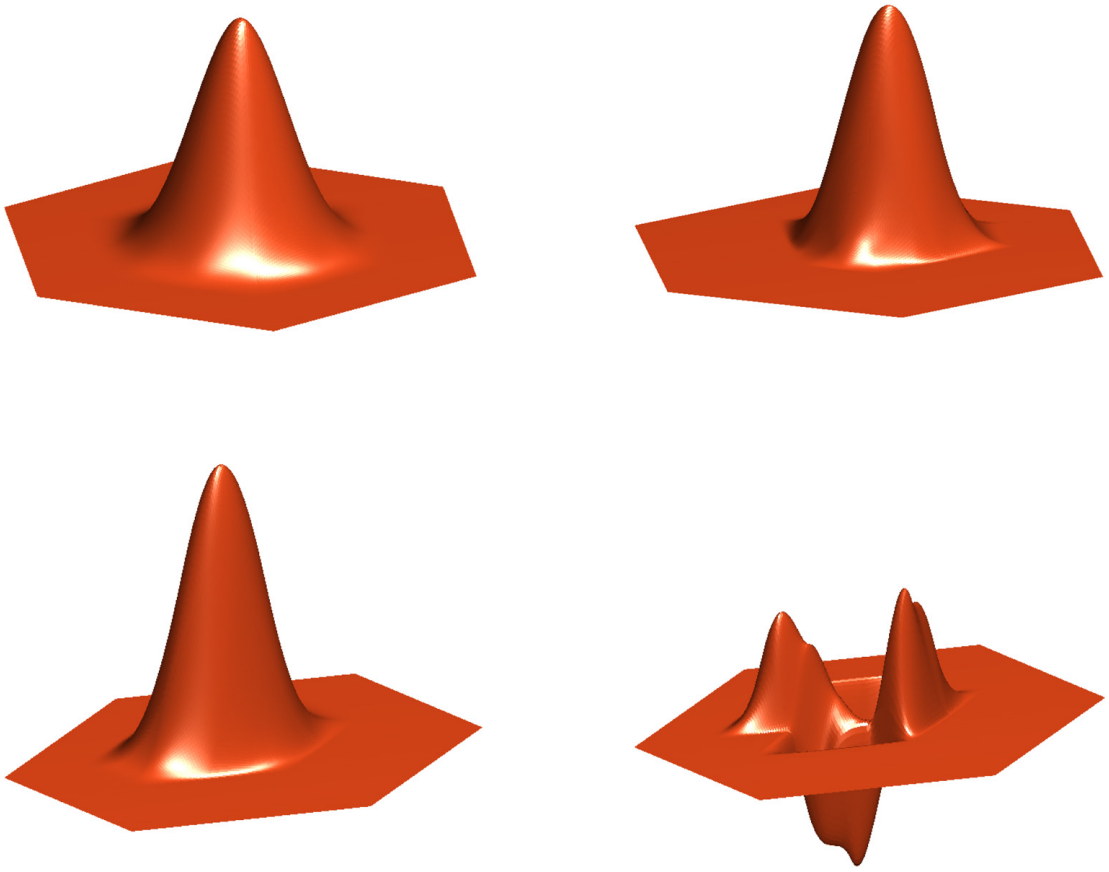

Figure 3.8: *Smooth bases of* 0-, 1- *and* 2-*forms. Bases of quartic box splines (top left) and half-box splines (top right). Visualization (x resp. y component of vector proxy) of smooth* 1-*form bases under the affine atlas (bottom).*

To check that the new subdivision schemes still satisfy the commutative relations (3.56) we consider the subdivision process in the Fourier domain over the $\mathbb{Z}^2$ lattice with diagonals.

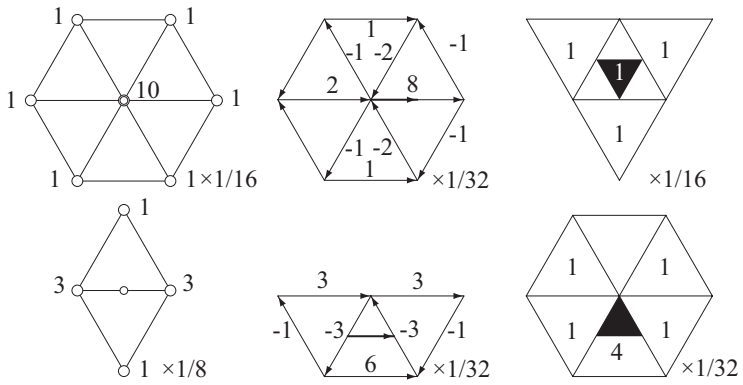

Figure 3.9: *Even (top) and odd (bottom) stencils (regular setting) for smooth 0-, 1-, and 2-forms for 3-direction convolved Whitney forms.*

For $\boldsymbol{z} = (z_1, z_2)$ let $S(\boldsymbol{z})$ denote the symbol of the subdivision scheme S as usual. Recall that the symbols of the co-boundary operators are given by (3.21):

$$d^0(\boldsymbol{z}) = \begin{pmatrix} -1 + z_1^{-1} \\ -1 + z_2^{-1} \\ -z_1^{-1} + z_2^{-1} \end{pmatrix} \quad \text{and} \quad d^1(\boldsymbol{z}) = \begin{pmatrix} 1 & -1 & 1 \\ -z_2^{-1} & z_1^{-1} & -1 \end{pmatrix}.$$

The symbol of three direction convolution is $C(\boldsymbol{z}) = 1/8(1 + z_1)(1 + z_2)(1 + z_1 z_2)$. While $S_0(\boldsymbol{z})$ is a scalar polynomial, $S_1(\boldsymbol{z})$ is a 3×3 matrix valued polynomial, grouping the coefficients associated with the three edge types into a 3-vector, and $S_2(\boldsymbol{z})$ is a 2×2 matrix valued polynomial, with coefficients of "up"/"down" triangles gathered into a 2-vector. Importantly, $C(\boldsymbol{z})$ is *scalar* and thus "pulls through" the relevant products in the Fourier domain

$$\begin{aligned} d^0(\boldsymbol{z}) S_0^L(\boldsymbol{z}) &= d^0(\boldsymbol{z}) C(\boldsymbol{z}) S_0^W(\boldsymbol{z}) = C(\boldsymbol{z}) d^0(\boldsymbol{z}) S_0^W(\boldsymbol{z}) \\ &= C(\boldsymbol{z}) S_1^W(\boldsymbol{z}) d^0(\boldsymbol{z}) = S_1^E(\boldsymbol{z}) d^0(\boldsymbol{z}). \end{aligned}$$

An entirely analogous calculation shows that the commutative relation between S_1^E and S_2^H holds as well (with respect to d^1). Hence we have

$$dS_0^L = S_1^E d, \quad dS_1^E = S_2^H d. \tag{3.60}$$

Suppose $f(x)$ is a function on $\mathbb{R}$, we have the simple expression for the derivative of its

convolution $\widetilde{f}(x)$ with the box function $B(x)$ supported on the interval $[0,1]$:

$$\frac{d}{dx}\widetilde{f}(x) = \frac{d}{dx}\int_{-\infty}^{\infty} f(x-u)B(u)du = \int_{-\infty}^{\infty} \frac{d}{dx} f(x-u)B(u)du. \tag{3.61}$$

In words, the above equation shows that derivative operation commutes with convolution operator. This is also true for partial derivatives and multiconvolution. If we denote by Φ^L, Φ^E and Φ^H the solutions of the refinement equations obtained by convolving Whitney 0-, 1- and 2-form basis, respectively, we have

$$\boldsymbol{d}\Phi^L = \Phi^E d, \quad \boldsymbol{d}\Phi^E = \Phi^H d. \tag{3.62}$$

due to the commutative relations (3.4) of Whitney forms and (3.61).

It is well known that that S_0^L and $4S_2^H$ are convergent C^2 and C^1 subdivision scheme respectively on a regular triangle mesh. The following theorem shows that S_1^E is convergent C^1 1-cochain subdivision scheme. We will suppress the subscripts for simplicity and use notation S_r only.

Theorem 3.34. *Given arbitrary* 1*-cochain* X*,* WS_1^jX *converge to a smooth* 1*-form* $\omega \in \mathcal{F}_1(K)$ *under flat norm:*

$$\|WS_1^jX - \omega\|_\infty \to 0,$$

$$\|\boldsymbol{d}WS_1^jX - \boldsymbol{d}\omega\|_\infty \to 0,$$

as $j \to \infty$*. Moreover,* ω *is a linear combination of the* 1*-form basis* Φ^E *in* (3.62)*.*

Proof. Recall that the symbol of S_1 is given by

$$S_1(\boldsymbol{z}) = 1/8(1+z_1)(1+z_2)(1+z_1z_2)S_1^W(\boldsymbol{z}),$$

where $S_1^W(\boldsymbol{z})$ denotes the symbol of Whitney 1-form subdivision scheme. We have the difference schemes with respect to direction $\boldsymbol{e}_1$ and $\boldsymbol{e}_2$, respectively,

$$\nabla_1 S_1(\boldsymbol{z}) = 1/4(1+z_2)(1+z_1z_2)S_1^W(\boldsymbol{z}),$$

$$\nabla_2 S_1(\boldsymbol{z}) = 1/4(1+z_1)(1+z_1z_2)S_1^W(\boldsymbol{z}).$$

A 1-cochain scheme can be considered as a matrix subdivision scheme whose subdivision sequence are given by (3.37). Since $WS_1^{W,j}X = WX$ for any j, S_1^W has bounded spectral radius, *i.e.*,

$$\rho_\infty(S_1^W) := \lim_{r\to\infty} \sup \|S_1^{W,r}\|_\infty^{\frac{1}{r}} < \infty.$$

It follows from [Charina *et al.* 2005, Theorem 4] that $\nabla_1 S_1$ and $\nabla_2 S_1$ are both continuous difference subdivision schemes. Hence S_1 is a C^1 matrix subdivision scheme. Further $dS_1 = S_2 d$ and the convergence of $4S_2$ implies that condition (3.39) holds. It follows from Theorem 3.16 that WS^jX converge to a C^1 1-form ω under flat norm. It is clear that S_1 is the average scheme of S_1^W. Given an edge σ, $S_1^j\sigma$ converge to the convolution Φ^E of the Whitney 1-form $W\sigma$. Therefore ω is a linear combination of Φ^E. □

3.5.2 Irregular Setting: The Subdivision Metric

In the following sections, we generalize the 1- and 2-cochain subdivision scheme S_1^E and S_2^H to irregular meshes. The generalization of S_0^L is well known as Loop's scheme. Throughout this section we will use S_0, S_1 and S_2 to denote S_0^L, S_1^E and S_2^H, respectively. A generalized half-box spline in irregular setting was proposed in [Oswald & Schröder 2003], and it was used for the schemes in [Wang *et al.* 2006]. However we realized that a variant of the generalization is needed to get highest regularity in the irregular setting. Recall that in the regular setting, $4S_2$ is a C^1 dual subdivision scheme where the factor 4 is reciprocal of the rate that triangle areas shrink along with subdivision. This factor is uniform in the regular setting thanks to the affine atlas where area of each triangle is reduced by 1/4. Therefore we first need to introduce the metric under which the regularity of 1-cochain scheme will be established.

We are only concerned with the 1-cochain subdivision map S_1 that has closed 1-cochains as its invariant subspace. Theorem 3.27 and Corollary 3.28 shows that there must exists a unique 0-cochain scheme S_0 such that $dS_0 = S_1 d$. Suppose we have a C^r-atlas $\{U_\alpha\}$ on $|K|$. Fix a chart $U_\alpha \subset \mathbb{R}^2$ with the coordinates $\{\boldsymbol{dx}, \boldsymbol{dy}\}$. Further we assume S_1 reproduces constant 1-forms $\boldsymbol{dx}, \boldsymbol{dy}$ on the chart U_α, that is to say, there exists 0-cochains X and Y such that

$$S_1^\infty dX = \boldsymbol{dx}, \quad S_1^\infty dY = \boldsymbol{dy} \text{ on } U_\alpha.$$

Due to the commutative relations we have

$$\boldsymbol{d}S_0^\infty X = \boldsymbol{d}x, \quad \boldsymbol{d}S_0^\infty Y = \boldsymbol{d}y \text{ on } U_\alpha.$$

This is equivalent to

$$S_0^\infty X = x + \text{constant}, \quad S_0^\infty Y = y + \text{constant, on } U_\alpha$$

since each U_α is a contractible region. Therefore we have the following result

Proposition 3.35. *Suppose S_1 is an exactness-preserving 1-cochain subdivision map. If $\{U_\alpha\}$ is the C^r-atlas under which S_1 reproduces the constant 1-form $\{\boldsymbol{d}x, \boldsymbol{d}y\}$ on each chart U_α, then U_α must be induced by the unique 0-cochain scheme S_0 such that $dS_0 = S_1 d$.*

We use the C^2 atlas $\{(|N_1(v)|^\circ, \psi_v)\}$ induced by the characteristic map of S_0. In what follows we assume that S_1 commutes with S_0 and S_2 through the coboundary operator.

3.5.3 Some Geometric Properties of Characteristic Map

In this section we study convergence of the r-cochain subdivision schemes S_0, S_1 and S_2 on the n-regular simplex K_n. In what follows we assume that S_r converges in the regular setting. The scalar subdivision scheme S_v has been extensively studied for the constructions of smooth subdivision surfaces. In our setting S_0 equips K_n with a differential structure as introduced in Chapter 2. The convergence of subdivision operators on 1- and 2-cochains will be performed on this differential structure. The key concept for the subdivision differential structure is the *characteristic map*. We adopted the definition in [Arden 2001]:

Definition 3.36. Suppose S_0 is a stationary scalar subdivision scheme: $\mathcal{C}^0(K_n) \to \mathcal{C}^0(D(K_n))$. For a fixed valence n, suppose the distinct eigenvalues of the subdivision map $\lambda_0, \lambda_1, \ldots, \lambda_N$, ordered by non-increasing magnitude, satisfy the following conditions:

1. The dominant eigenvalue λ_0 is one, and is an algebraically simple eigenvalue.

2. The sub-dominant eigenvalue λ_1 is real and positive, and is of geometric and algebraic multiplicity 2.

3. The other eigenvalues, λ_j for $j > 1$, are of magnitude strictly less than λ_1.

Let $u_1,\ u_2 \in \mathcal{C}^0(N_{m_w}(v_0, K_n))$ be linearly independent λ_1-eigenvectors of S_v. Then the $\mathbb{R}^2$-valued control net $u = (u_1, u_2)$ defines a continuous map

$$S_v^\infty u\colon |N_1(v_0, K_n)| \to \mathbb{R}^2,$$

called a *characteristic map*.

As given in [Arden 2001], we define the fundamental annular simplicial surface $\Omega_0 \subset K_n$ by

$$\Omega_0 = N_2(v_0, K_n) \setminus N_1(v_0, K_n).$$

The region $|\Omega_0|$ is shown in Figure 3.10.

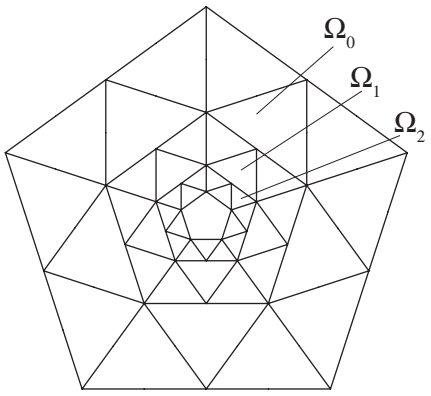

Figure 3.10: $K_n \setminus v_0$ *is decomposed into annuli.*

Recall that the contraction map induces a piecewise linear homeomorphism $|c|\colon |K_n| \to |D(K_n)|$, which when composed with the identification induced by subdivision $\imath\colon |D(K_n)| \to |K_n|$, results in a piecewise linear homeomorphism on $|K_n|$, which is also denoted by c in an abuse of notations

$$c\colon |K_n| \to |K_n|.$$

Let $\Omega_j = c^j\Omega_0 \subset K_n^j$ for $j \geq 0$. For each face $T \in K_n^k$, we let j_T be the unique integer of j satisfying $|T| \subset |\Omega_j|$, and if $T \in N_1(v_0, K_n^k)$, we let $j_T = k$. Notice we have the identity $j_T \leq k$. For instance, in Figure 3.10, given any triangle $T \in K_n^2$, $j_T = 2$ for $|T| \subset |\Omega_2|$ and $j_T = 0$ for $|T| \subset |\Omega_0|$. We recap the geometric properties in the neighborhood of v_0 under the characteristic map. The following is an outline of Section 2.7 of [Arden 2001]. We will need those technical results.

For each valence n, we fix a characteristic map $y\colon |K_n| \to \mathbb{R}^2$, and use it as a global

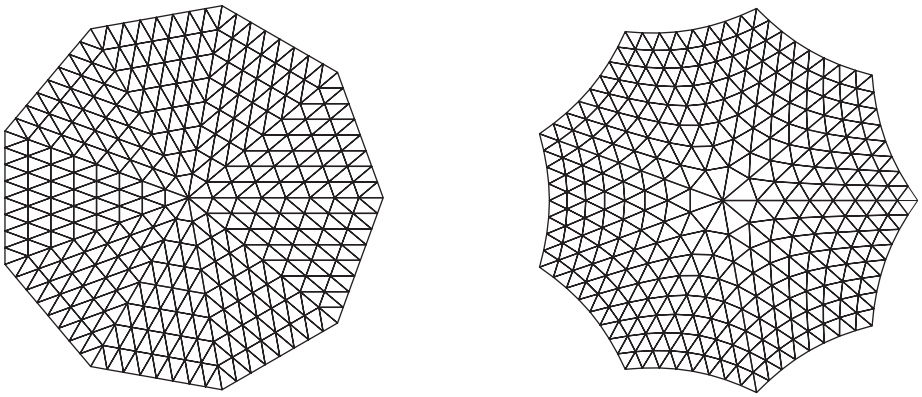

Figure 3.11: *Left: the n-regular complex* $K_9 \subset \mathbb{R}^2$*; right: the image of* K_9 *under the characteristic map of* S_0*.*

chart on K_n. Let λ be the sub-dominant eigenvalue of the subdivision matrix of valence n. We denote, by the subscript Λ, geometric properties of domains in K_n with respect to the Euclidean metric in characteristic coordinates. For example, we define the *diameter* of a set $\Omega \subset |K_n|$ by $\mathrm{diam}_\Lambda \Omega = \sup\{|y(p) - y(q)| : p, q \in \Omega\}$.

Proposition 3.37. *For an fixed integer* $d \geq 0$*, there exists constants* C_0 *through* C_3 *such that for any* $T \in Face(K_n^k)$ *and* $k \geq 0$ *we have*

$$C_0 \lambda^{2j_T} \Big(\frac{1}{2}\Big)^{2(k-j_T)} \leq area_\Lambda |N_d T| \leq C_1 \lambda^{2j_T} \Big(\frac{1}{2}\Big)^{2(k-j_T)}$$

and

$$C_0 \lambda^{2j_T} \Big(\frac{1}{2}\Big)^{k-j_T} \leq diam_\Lambda |N_d T| \leq C_1 \lambda^{2j_T} \Big(\frac{1}{2}\Big)^{k-j_T}$$

Proof. See [Arden 2001, Proposition 26]. □

Proposition 3.37 provides guideline on constructing convergent S_2 on the characteristic atlas. We define the curved simplicial surface $K_{n,\Lambda}^j$ to be the image of K_n^j under the characteristic map and accordingly $\Omega_{j,\Lambda}$ be the image of Ω_j (see Figure 3.11). For instance, a triangle $T = \{a, b, c\} \in K_n^j$ is mapped to the curved triangle $T_\Lambda = \{y(a), y(b), y(c)\} \in K_{n,\Lambda}^j$. Similarly an edge $E = \{a, b\} \in K_n^j$ is mapped to the curved edge $E_\Lambda = \{y(a), y(b)\}$. In characteristic coordinates, the contraction map c can be written as

$$c(y) = \lambda y. \tag{3.63}$$

Given an r-cochain X on $|K_n|$, let $X^j = S_r^j X$ be the r-cochain on $|K_n^j|$. The r-cochain

X^j_Λ on $K^j_{n,\Lambda}$ is defined by the pull-back,

$$X^j_\Lambda \cdot \sigma_\Lambda = X^j \cdot \sigma \quad \text{for any } r\text{-simplex } \sigma \in K^j_n.$$

where σ_Λ denotes the image of σ under the characteristic map. We let r-form $\omega^j = WX^j$ on $|K^j_n|$ be the interpolation of X^j by Whitney r-forms. The corresponding r-form ω^j_Λ on $K^j_{n,\Lambda}$ is defined through the pull-back

$$\omega^j_\Lambda \cdot \alpha_\Lambda = \omega^j \cdot \alpha \quad \text{for any } r\text{-vector } \alpha \text{ on } |K^j_n|.$$

Let $\omega_\Lambda = S^\infty_r X$ be the limit r-form on the characteristic domain. It follows from Lemma 3.14 and Lemma 3.20 that

$$\omega_\Lambda = \lim_{j\to\infty} WX^j_\Lambda = \lim_{j\to\infty} \omega^j_\Lambda.$$

Suppose that X is an eigenvector of S_r with eigenvalue μ. It is easy to see that

$$\omega^{j+1}_\Lambda(\lambda y) = \frac{\mu}{\lambda^r}\omega^j_\Lambda(y). \tag{3.64}$$

Letting $j \to \infty$, we have the following *contraction identity* for ω

$$\omega_\Lambda(\lambda y) = \frac{\mu}{\lambda^r}\omega_\Lambda(y). \tag{3.65}$$

Given the bases $\{dy_1, dy_2\}$ of the characteristic coordinates, the subdivision 2-form ω^j_Λ can be written as

$$\omega^j_\Lambda = f^j(y) dy_1 \wedge dy_2,$$

where f^j is a piecewise constant function on each curved triangle $T_\Lambda \in K^j_{n,\Lambda}$ such that

$$\int_{T_\Lambda} \omega^j_\Lambda = X^j_\Lambda \cdot T_\Lambda.$$

If ω^j_Λ is uniformly bounded, that is to say, there exists a constant $M > 0$ such that $\int_{T_\Lambda} \omega^j_\Lambda \le M|T_\Lambda|$ for all j, then we have from Proposition 3.37 that

$$X^j \cdot T_\Lambda \le M_1 \lambda^{2j},$$

for $T_\Lambda \in K^j_{n,\Lambda} \cap \Omega_{j,\Lambda}$, and

$$X^j \cdot T_\Lambda \leq M_2 \Big(\frac{1}{4}\Big)^j,$$

for fixed $j_T \leq j$ and $T_\Lambda \in K^j_{n,\Lambda} \cap \Omega_{j_T,\Lambda}$. We summarize the observation above as follows.

Lemma 3.38. *Assume that S_2 converges on the regular complex. Then S_2 is a continuous and non-flat (nonzero at the central vertex v_0) 2-cochain scheme under the characteristic coordinate only if $\lambda = 1/2$.*

Proof. With no loss of generality, we assume that X is the eigenvector of S_2 with dominant eigenvalue μ. For $T^j_\Lambda \in K^j_{n,\Lambda} \cap \Omega_{j,\Lambda}$, we have $X^j \cdot T^j_\Lambda = \mu^j X \cdot T_\Lambda \leq M_1 \lambda^{2j}$ as $j \to \infty$, which implies $\mu \leq \lambda^2$. Non-flatness at v_0 implies $X^j \cdot T^j \geq C_1 \lambda^{2j}$ for some constant C_1. Hence we must have $\mu = \lambda^2$.

For $T^j_\Lambda \in K^j_{n,\Lambda} \cap \Omega_{j_T,\Lambda}$ with fixed j_T and $j \to \infty$, we can use the local affine coordinate A which contains T^j_Λ for all $j \geq J$. It is known that X^j converge to a continuous 2-form under the affine coordinate A if and only if the constant 2-cochain $\mathbf{1}$ is the eigenvector with dominant eigenvalue μ. Assume $X^j = \mu^j W S_2^j \mathbf{1}$. We have $C_2 4^{-j} \leq \mu^j \leq C_3 4^j$ from Proposition 3.37. Hence $\mu = 1/4$. Finally we conclude that $\lambda^2 = \mu = 1/4$ and therefore $\lambda = 1/2$. □

3.5.4 Smoothness Analysis of S_1 and S_2

We assume in what follows that S_0 has the dominant eigenvalue $\lambda = 1/2$. The following Lemma gives a sufficient condition for S_2 to be convergent.

Lemma 3.39. *Suppose S_2 has dominant eigenvalue $1/4$. The normalized scheme $Q_2 = 4S_2$ can be reinterpreted as a dual scheme. If Q_2 is a C^1 scheme with an injective and regular characteristic map, then for arbitrary initial 2-cochain X, $WS_2^j X$ converge to a continuous 2-form $\omega = f(y)dy_1 \wedge dy_2$ under the characteristic coordinates $\{dy_1, dy_2\}$ induced by S_0. Further, $f(y)$ is C^1 away from the irregular vertex v_0 and $\partial_{y_i} f(y)$ are uniformly bounded on $N_1(v_0, K_n)$ provided that Q_2 has subdominant eigenvalue $\mu = 1/2$.*

Proof. The characteristic map of S_0 induces the coordinate system

$$\chi \colon |N_1(v_0)| \to \mathbb{R}^2,$$

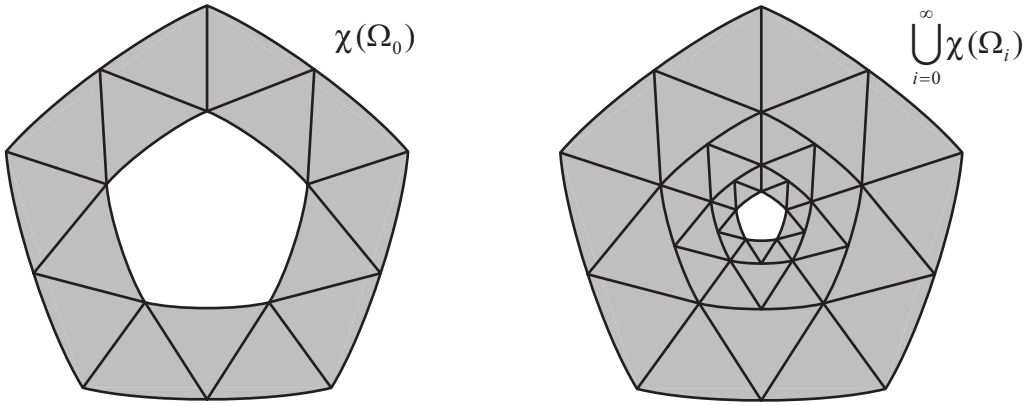

Figure 3.12: *Left: Representation of annulus Ω_0 by the charactersitic map; right: a characteristic chart is represented by $\bigcup_{i=1}^{\infty}\chi(\Omega_i)$.*

and the characteristic map of Q_2 induces another coordinate system

$$\chi_Q\colon |N_1(v_0)| \to \mathbb{R}^2.$$

The action of χ or χ_Q can be decomposed into their actions on annuli (see Figure 3.12):

$$\chi(N_1) = \bigcup_{i=1}^{\infty} \chi(\Omega_0) \cup \chi(v_0),$$

$$\chi_Q(N_1) = \bigcup_{i=1}^{\infty} \chi_Q(\Omega_0) \cup \chi_Q(v_0).$$

Each surface layer $\hat{\Omega}_i \equiv \chi(\Omega_i)$ consists of smoothly joined patches. The scaling relation reads

$$\chi(c(z)) = \lambda\chi(z),\ \chi_Q(c(z)) = \mu\chi_Q(z), \quad \text{for all } z \in |N_2(v_0, K_n)|, \tag{3.66}$$

where $c(z)$ is the contraction map. Therefore $\hat{\Omega}_i$ joined smoothly since we can regard any finite number of layers of patches as a single layer of macro patches. Similarly we can define $\hat{\Omega}_{Q,i} \equiv \chi_Q(\Omega_i)$, and $\hat{\Omega}_{Q,i}$ are smoothly joined patches as well. If both χ and χ_Q are injective and regular, we consider the composition

$$q(y) \equiv \chi_Q \circ \chi^{-1}(y)\colon \hat{\Omega}_0 \to \hat{\Omega}_{Q,0}.$$

For any C^1 function $q(y)$, we have

$$F(q) = F(\chi_Q \circ \chi^{-1}(y)) = f(y).$$

From the chain rule we have $\partial_y f(y) = \partial q/\partial y \cdot \partial F(q)/\partial q$. Notice that

$$\partial q/\partial y = \partial u/\partial \chi \cdot \partial \chi_Q(u)/\partial u$$

is continuously defined on $\hat{\Omega}_0$ due to the Inverse Function Theorem. Here u denotes the affine coordinate defined on each triangle $T \in \Omega_0$. Therefore $f(y)$ is C^1 with respect to y provided that $F(q)$ is C^1 with respect to q. Let D denote the Jacobi matrix. We have the following scaling relations

$$D\chi(u/2) = 2\lambda D\chi(u), \quad D\chi_Q(u/2) = 2\mu D\chi_Q(u).$$

Therefore

$$\partial \chi_Q/\partial \chi(y/2) = \partial u/\partial \chi \cdot \partial \chi_Q/\partial u = \frac{\mu}{\lambda}\partial \chi_Q/\partial \chi(y).$$

Since $\mu = \lambda = 1/2$, we have the recurrence

$$\partial \chi_Q/\partial \chi(y/2) = \partial \chi_Q/\partial \chi(y). \tag{3.67}$$

Notice that $\partial \chi_Q/\partial \chi$ is continuous on $\bigcup_i \hat{\Omega}_i$ and uniformly bounded on $|N_1(v_0)|$ due the recurrence (3.67). Therefore $\partial \chi_Q/\partial \chi$ is continuous at v_0 only if it is a constant [Warren 1994, 7.2.3 Lemma 2], which implies that χ_Q is up to a linear transformation of χ. This condition, however, does not hold in general. For instance, it is certainly not the case when χ_Q and χ consist of cubic and quartic polynomial patches, respectively. As a result, $\partial \chi_Q/\partial \chi$ is not continuous at v_0. Therefore $f(y)$ is C^1 away from v_0, and its derivatives are uniformly bounded due to the chain rule. □

Theorem 3.40. *Suppose the cochain subdivision schemes S_0, S_1 and S_2 satisfy the commutative relations* (3.56)*. Suppose they are C^r ($r \geq 1$) on the regular complex, and the characteristic maps of S_0 and S_2 are regular and injective with subdominant eigenvalue* $1/2$*. Let $\{U_\alpha\}$ be the C^r-atlas induced by the characteristic map of S_0. Then, on each chart U_α that contains an irregular vertex v_0, S_1 and S_2 are continuous at v_0. Further the subdi-*

vision 1*-forms are* H^1*, and the coordinate derivatives of subdivision* 2*-forms are uniformly bounded.*

Proof. We only need to prove that S_1 is continuous and belongs to H^1. Given an eigen 1-cochain X of S_1, we have either $X = d\alpha^0$ with α^0 being an eigen 0-cochain of S_0, or $dX = \beta^2$ with β^2 being an eigen 2-form of S_2, according to Lemma 3.32. For the former case, we have $\omega = \nabla_y \alpha$ with α being a subdivision function generated by S_0 and hence ω is C^0 at v_0 provided that S_0 is C^1 at v_0. It follows from [Reif & Schröder 2001] that $\omega \in H^1$. For the latter case, we assume that, with no loss of generality, dX is the dominant eigenvector of S_2 with eigenvalue $1/4$. It follows from Lemma 3.32 that X is is the dominant eigenvector among all non-exact eigenvectors of S_1. From the contraction identity (3.65) and $\lambda = 1/2$, we have

$$D\omega(\lambda y) = \frac{1}{4\lambda^2} D\omega(y) = D\omega(y).$$

Therefore $D\omega$ is uniformly bounded on U_α, and hence $\omega \in H^1$. □

Remark 3.41. Recall that 0- and 2-forms both represent scalar fields on manifolds. S_0 and S_2 are C^1 on their own characteristic coordinates. However, represented by the characteristic coordinate y of S_0, S_2 is only C^0. Instead we can use the characteristic coordinate q induced by S_2 so that S_2 becomes C^1. Accordingly S_0 becomes C^0 under coordinate q and hence has less regularity than under coordinate y. As a result of commutative relations which link S_1 with S_0 and S_2 through $dS_0 = S_1 d, dS_1 = S_2 d$, it is clear that S_1 has less regularity too.

Chapter 4

Designing Subdivision Schemes of r-Forms

The next question is how to design S_0, S_1 and S_2 according to the conditions in Theorem 3.40. With slight abuse of notations, we use S_2 to denote both the 2-cochain subdivision scheme with dominant eigenvalue $1/4$ and the dual subdivision scheme with dominant eigenvalue 1, up to a multiplier $1/4$. Our design strategy is to first find the proper S_0 and S_2, then solve the commutative relations (3.56) for the mask of S_1. On the regular mesh, they are given by S_0^L, S_1^E and S_2^H, known as schemes for quartic box splines, quartic edge splines and cubic half box splines. We modify the stencils surrounding an irregular vertex so that conditions in Theorem 3.40 still hold.

4.1 Weight Modification for S_0 and S_2

For the choice of S_0 surrounding irregular vertices, we follow the modification of Loop's subdivision scheme proposed by [Biermann *et al.* 2000; Zorin & Schröder 2000] (see Figure 4.1). The odd stencil for edges adjacent to an irregular vertex is modified by ϵ which is independent of the valence n. The even stencil for irregular vertices is the same as Loop's scheme. The subdivision matrix S_0 is similar to the block-diagonal matrix $\{\hat{S}_{0,k} \colon k = 0, 1, \ldots, n-1\}$ under Discrete Fourier Transform. The resulting subdominant eigenvalue of $\hat{S}_{0,1}$ is given by

$$\lambda = \frac{3}{8} + \frac{1}{4}\cos(2\pi/n) + \epsilon.$$

We take $\alpha = \frac{-8\lambda^2+8\epsilon+5}{8n}$ according to [Loop 1987] so that the 0th block $\hat{S}_{0,0}$ has eigenvalue λ^2. Theorem 3.40 requires $\lambda = 1/2$, and hence

$$\epsilon = \frac{1}{8} - \frac{1}{4}\cos(2\pi/n).$$

Rigorous verifications of injectivity and regularity of characteristic maps are the important topic in the theory of subdivision and have been extensively studied in the literature, *e.g.*, [Reif 1995; Peters & Reif 1998; Zorin 1998; Umlauf 2000]. Discussions on those methods are beyond the scope of this thesis. Instead, we only visually check linear approximations of characteristic maps after certain steps of subdivisions. Figure 4.2 shows characteristic maps of modified Loop's subdivision scheme surrounding irregular vertices of different valences. We assume they are all regular and injective.

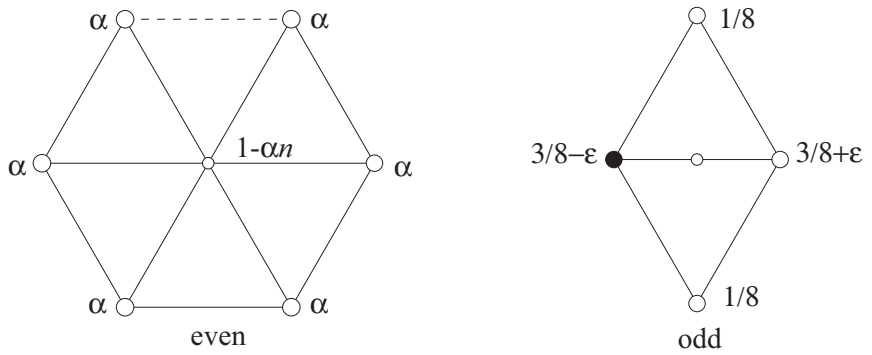

Figure 4.1: *Modified Loop's scheme: the even stencil is the same as Loop's scheme (left); the odd stencil (right) is modified by ϵ, where the irregular vertex is marked in black.*

A generalized half-box spline is proposed in [Oswald & Schröder 2003] and was used as the dual scheme in [Wang *et al.* 2006]. In that case, at most five triangles adjacent to the irregular vertex have nonzero weights. This type of scheme appears simpler but is not able to make the subdominant eigenvalue of S_2 to be $1/2$ for all valences at irregular vertices. Besides, odd children triangles depending on a few parent triangles only in the central 1-ring does not seem right in high valence case. Due to Theorem 3.40, subdominant $1/2$-eigenvalue is also required for S_2. Therefore, we assume the following parameterized stencils for S_2 surrounding irregular vertices (see Figure 4.3).

On the invariant neighborhood (Figure 4.3, right), S_2 is similar to the block-diagonal matrix $\{\hat{S}_{2,k} \colon k = 0, \ldots, n-1\}$ under DFT. Let $\{\hat{\beta}_k \colon k = 0, \ldots, n-1\}$ denote the discrete

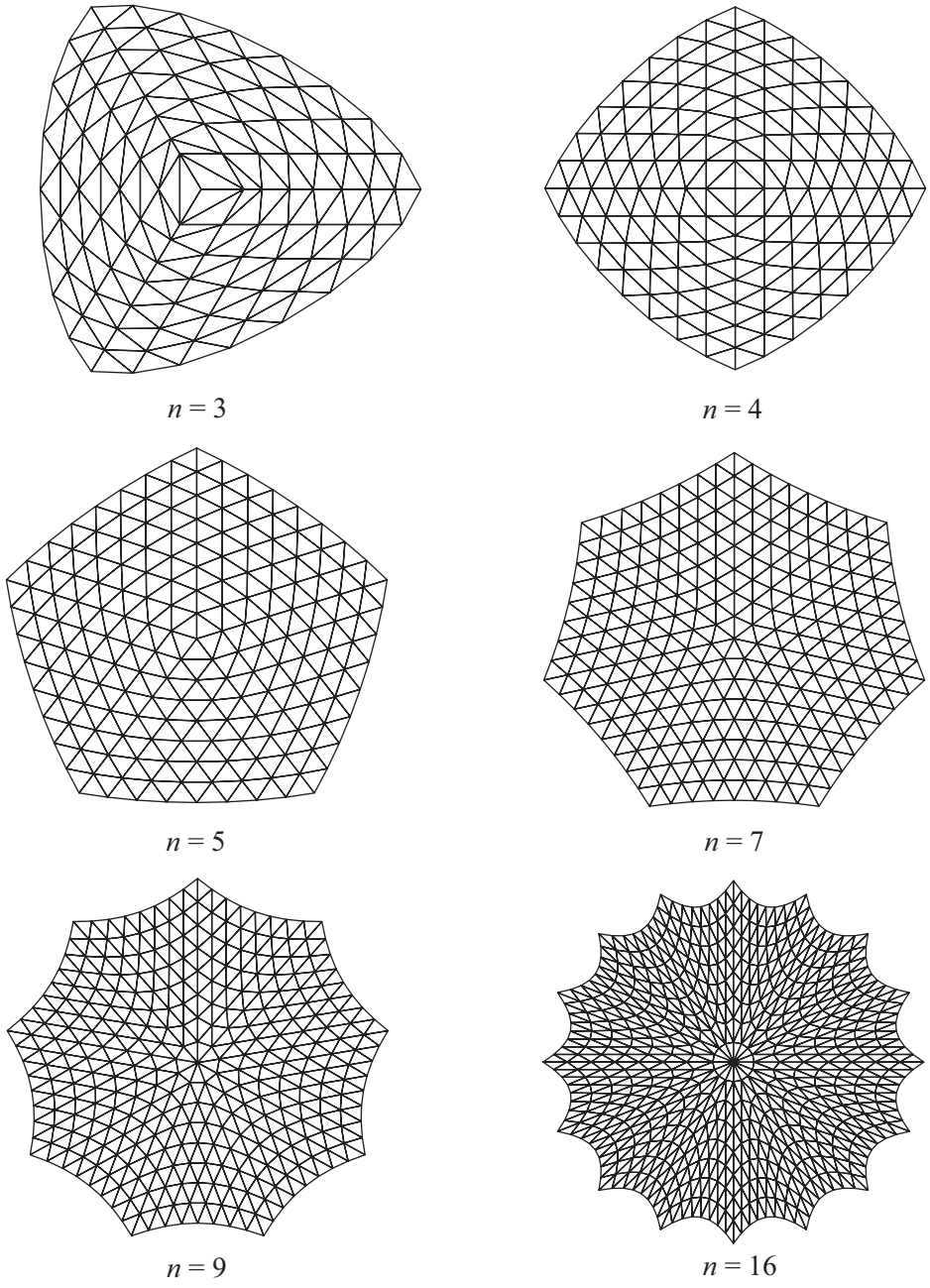

Figure 4.2: *Modified Loop's scheme S_0: characteristic maps surrounding irregular vertices of different valences n.*

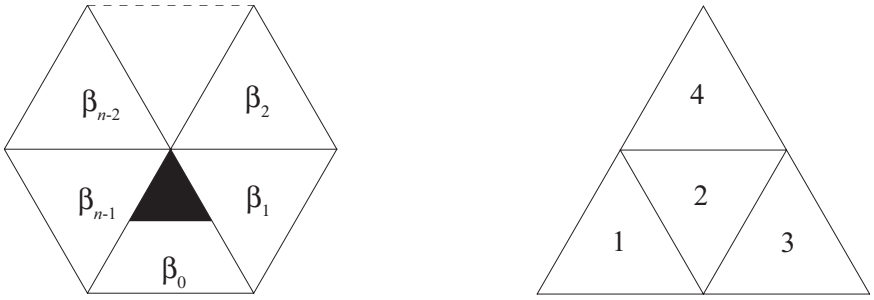

Figure 4.3: *Modified stencil for S_2 at irregular vertices (left). Invariant neighborhood numbering (right).*

Fourier modes of $\{\beta_j \colon j = 0, \ldots, n-1\}$:

$$\hat{\beta}_k = \sum_{j=0}^{n-1} \beta_j e^{2\pi i k j/n}.$$

We have

$$\hat{S}_{2,k} = \begin{pmatrix} \hat{\beta}_k & 0 & 0 & 0 \\ \frac{1}{4}\left(z + 1 + \frac{1}{z}\right) & \frac{1}{4} & 0 & 0 \\ \frac{1}{2} + \frac{1}{8z} & \frac{1}{8}\left(1 + \frac{1}{z}\right) & \frac{1}{8} & 0 \\ \frac{z}{8} + \frac{1}{2} & \frac{z+1}{8} & 0 & \frac{1}{8} \end{pmatrix}, \quad z = e^{2\pi i k/n}. \tag{4.1}$$

Evidently, the four eigenvalues of each submatrix $\hat{S}_{2,k}$ are

$$\left\{\hat{\beta}_k,\ \frac{1}{4},\ \frac{1}{8},\ \frac{1}{8}\right\}.$$

We choose the eigenvalues $\hat{\beta}_k$ such that the subdominant eigenvalue $\frac{1}{2}$ is of multiplicity 2:

$$\hat{\beta}_k = \hat{\beta}_{n-k} = 2^{-k}, \quad k = 0, \ldots, \left\lfloor \frac{n}{2} \right\rfloor,$$

and, for consistence with the regular case, $\hat{\beta}_{\frac{n}{2}} = 1/2$ for $n = 6$. The resulting weights are

$$\beta_j = \frac{1}{n}\Big(1 + 2\sum_{k=1}^{\lfloor \frac{n}{2} \rfloor} \cos(2\pi k j/n)\hat{\beta}_k\Big) \quad \text{for } n \text{ odd}, \tag{4.2}$$

$$\beta_j = \frac{1}{n}\Big(1 + \cos(\pi j)\hat{\beta}_{\frac{n}{2}} + 2\sum_{k=1}^{\frac{n}{2}-1} \cos(2\pi k j/n)\hat{\beta}_k\Big) \quad \text{for } n \text{ even}. \tag{4.3}$$

The characteristic maps of S_2 surrounding irregular vertices of different valences are visu-

alized in Figure 4.4. Evidently, injectivity fails for valence $n = 3$ and 4. Notice that in these two cases, our choices of irregular stencils coincide the stencils proposed by [Oswald & Schröder 2003]. Further investigation on the structure of matrix (4.1) shows that we need to modify other weights except for the weights for children triangles of the first 1-ring. While failure of injectivity of S_2 may yield 2-forms of less smoothness, it does not violate the conditions that assure H^1 regularity of S^1 as given in Theorem 3.40.

4.2 Designing S_1 via Commutative Relations

Given S_0 and S_1 as defined in the previous section, it is now straightforward to get S_1 that satisfies commutative relations with S_0 and S_1. We set fully parameterized stencils surrounding irregular vertices (see Figure 4.5) by assuming size of stencils as well as symmetries. We also assume that irregular vertices are separated such that each edge has at most one irregular endpoint. Solving the commutative relations uniquely determines those stencils. The resulting weights that are the same as regular weights are marked in Figure 4.5. Those weights that differ from regular ones are given by equations (4.4)–(4.13). The resulting 1-form bases of different vertex valences are visualized in Figures 4.6–4.7,

$$\gamma_0 = -\frac{3}{32} + \frac{\beta_0}{8}, \tag{4.4}$$

$$\gamma_j = -\frac{1}{8} + \frac{\beta_0}{8} + \frac{1}{4}\sum_{k=1}^{j}\beta_k, \quad \text{for } 0 \le j \le \left\lfloor \frac{n}{2} \right\rfloor, \tag{4.5}$$

$$\gamma_j = -\gamma_{n-j-1}, \quad \text{for } \left\lfloor \frac{n}{2} \right\rfloor + 1 \le j \le n-1, \tag{4.6}$$

$$\sigma_0 = \frac{3}{8} - \alpha + 2\gamma_0 + \epsilon, \tag{4.7}$$

$$\sigma_1 = \frac{3}{32} - \alpha + \frac{1}{4}\beta_1, \tag{4.8}$$

$$\sigma_j = -\alpha + \frac{1}{4}\beta_j \quad \text{for } 2 \le j \le \left\lfloor \frac{n}{2} \right\rfloor, \tag{4.9}$$

$$\sigma_j = \sigma_{n-j-1} \quad \text{for } \left\lfloor \frac{n}{2} \right\rfloor + 1 \le j \le n-1, \tag{4.10}$$

$$\theta = \frac{1}{4} - \epsilon, \tag{4.11}$$

$$\eta = -\frac{3}{32} - \epsilon, \tag{4.12}$$

$$\xi = -\frac{3}{32} + \epsilon. \tag{4.13}$$

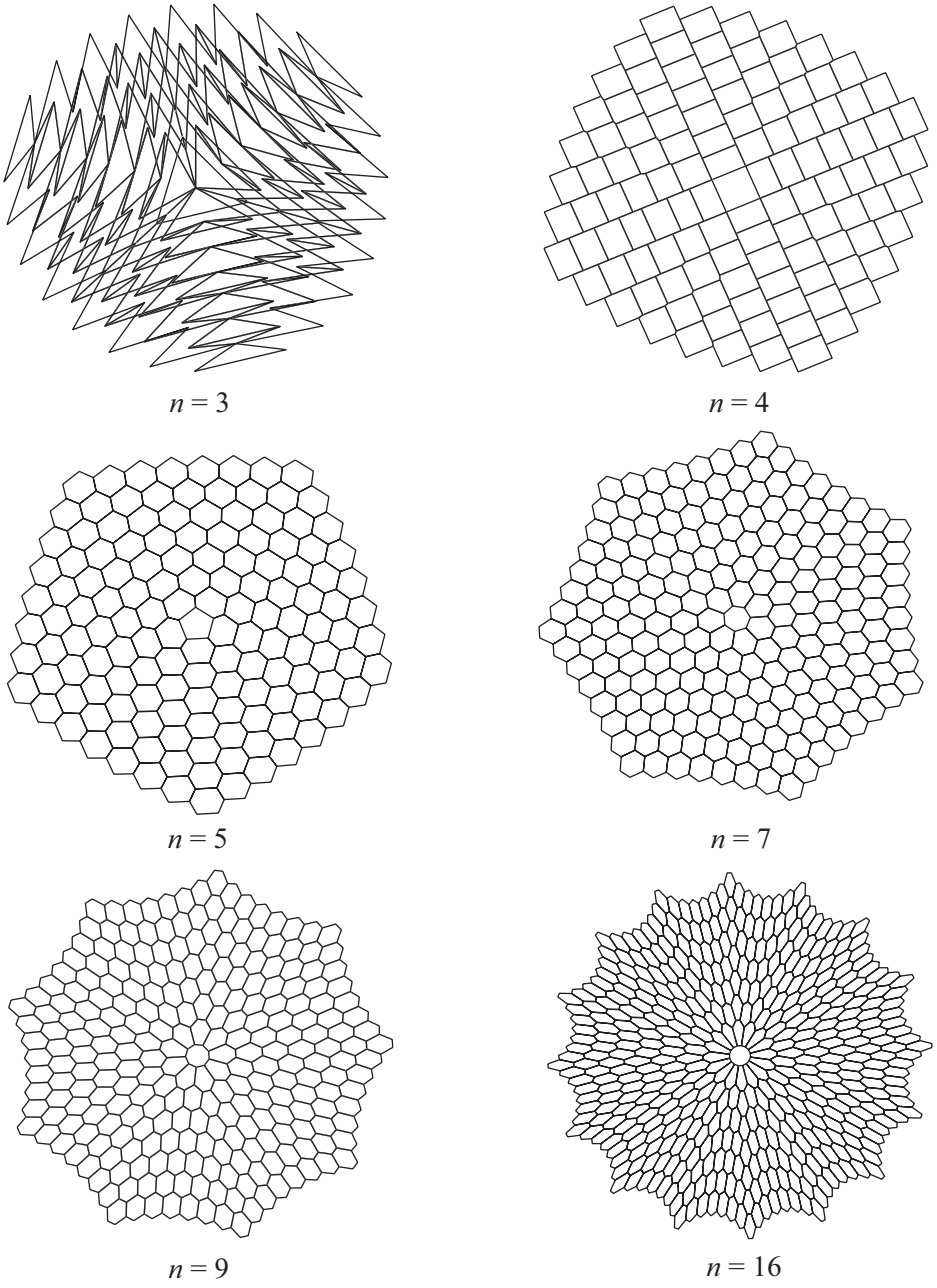

Figure 4.4: *Characteristic maps of S_2 surrounding irregular vertices of different valences n.*

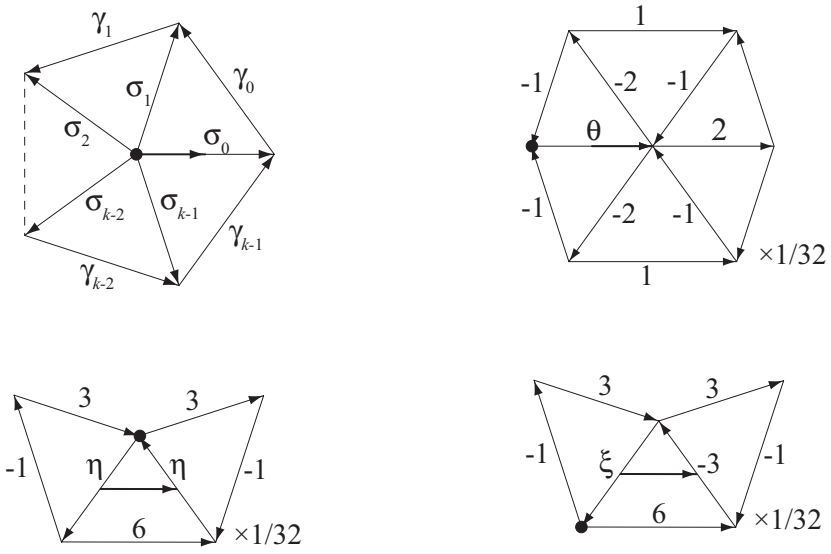

Figure 4.5: *Stencils surrounding irregular vertices. The irregular vertices are marked in black dots.*

4.3 Computational Tools

We discuss in this section some of the computational tools necessary for the application of 1-forms and in particular their use in the intrinsic design of vector fields. Our implementation of the proposed subdivision schemes is based on CGAL and extends the polyhedron example code [Shiue *et al.* 2005]. The use of a half-edge data structure is advantageous since the direction of edges and orientation of faces matters in terms of the meaning of 1- and 2-form coefficients as they change sign under orientation reversal.

4.3.1 Evaluation

Exact Evaluation Since our triple of subdivision schemes produces piecewise polynomial splines in the regular setting one can use these to implement exact evaluation of all quantities at arbitrary parameter locations in the regular setting, and with suitable eigen decompositions, in the irregular setting (for details see [Zorin & Kristjansson 2002] and [Stam 1998]). As these ideas are by now well understood we focus here only on the evaluation of vector field proxies of 1-forms. Due to the support of the 1-form edge bases, evaluation anywhere within a triangle requires the coefficients on all edges within a 1-ring of the triangle. Using these coefficients, one can use a Bézier representation (in the regular setting, or the eigen representation in the irregular setting) to compute a 2-vector value at the desired paramet-

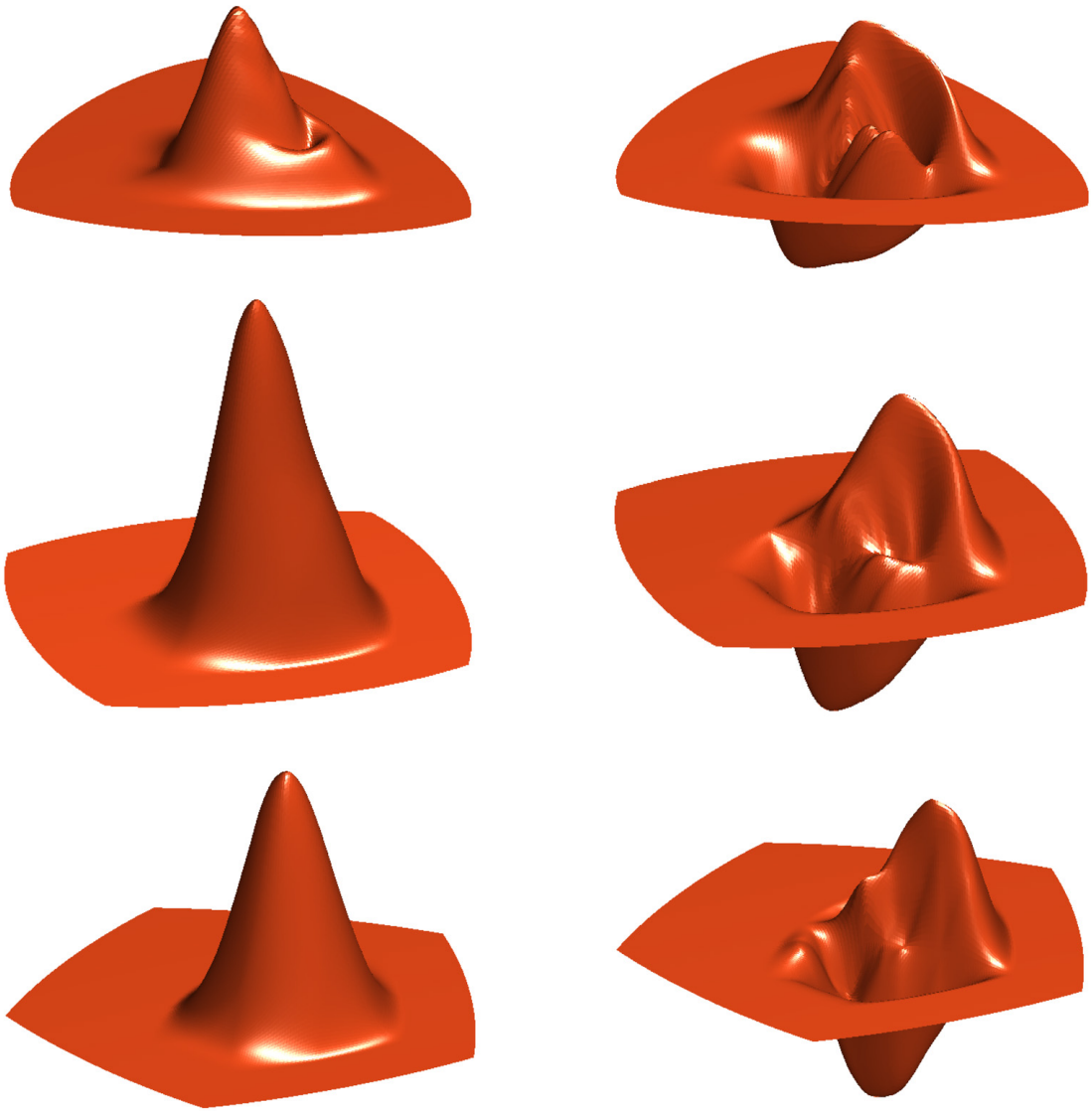

Figure 4.6: *Visualization (x resp. y component of vector proxy) of 1-form bases. Left column: x-component; right column: y-component. From top to bottom:* $n = 3, 4, 5$.

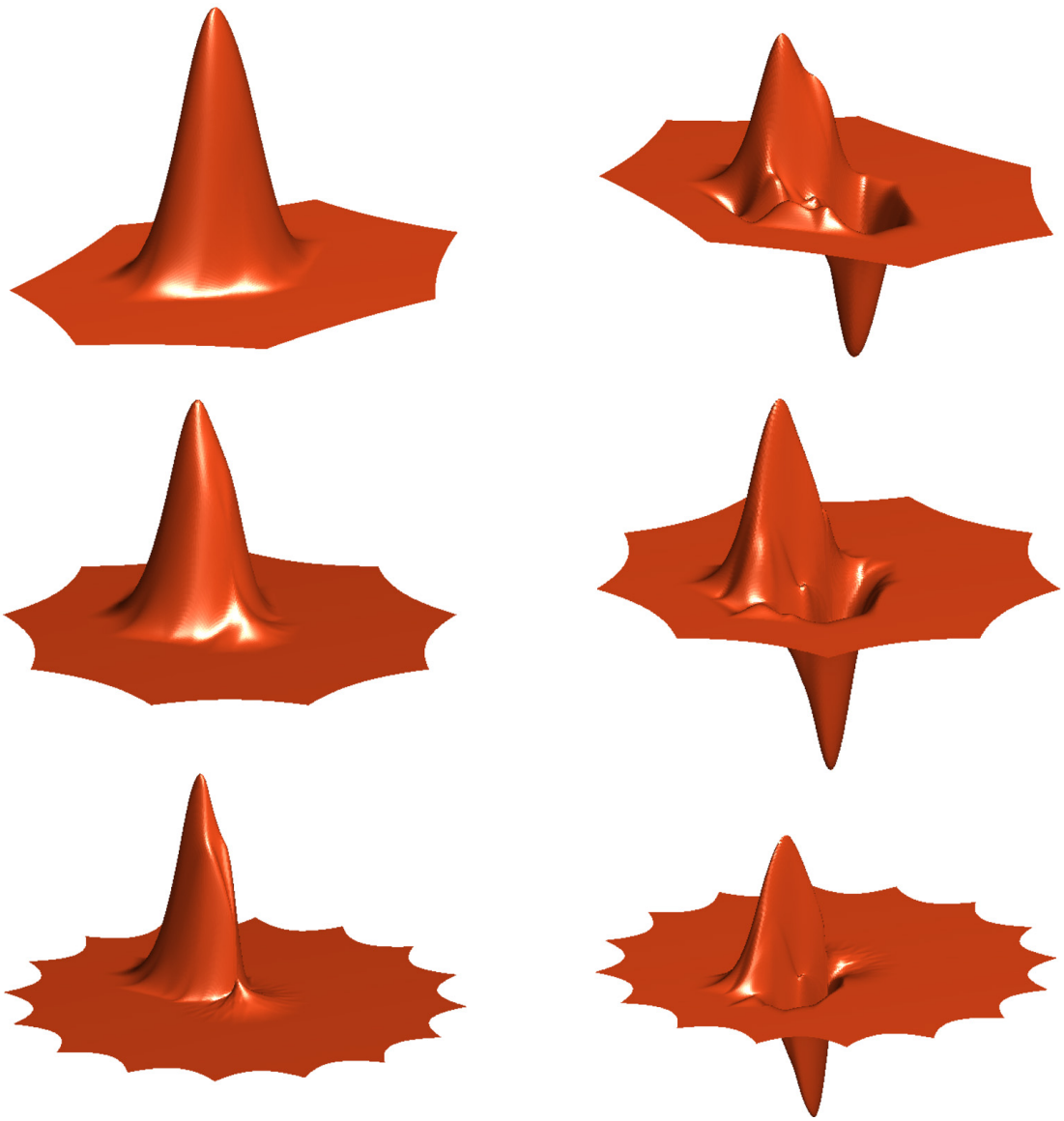

Figure 4.7: *Visualization (x resp. y component of vector proxy) of 1-form bases. Left column: x-component; right column: y-component. From top to bottom:* $n = 7, 9, 16$.

ric location. This 2-vector represents a tangent vector in the domain, which must now be pushed forward into the tangent space induced by the underlying 0-form at that parametric location. This requires evaluation of the parametric derivatives of the underlying 0-form data (the Loop surface in our case) at that point. Given such a tangent space basis the final tangent vector is given as the linear combination of the basis covectors $\{dx, dy\}$ with the coefficients from the 1-form evaluation.

Fast Evaluation In practice, for visualization especially, we have found far simpler to just employ the subdivision method itself to refine the mesh to a suitable level. In this scenario we refine the mesh through quadrisection and apply 0-form subdivision to the vertex positions and 1-form subdivision to the edge data. The 0-form data are then displayed through piecewise linear interpolation over each triangle, in effect using the Whitney 0-forms. This is the mesh as usually visualized in subdivision algorithms for surfaces. The 1-form data are similarly interpolated over each triangle piecewise linearly with the Whitney 1-forms. The advantage of this approach is that there is no need to explicitly push tangent vectors forward from the domain to the surface. In effect the underlying metric is "pulled along" through the subdivision of the 0-form data. Given vertex positions $\boldsymbol{a}$, $\boldsymbol{b}$, $\boldsymbol{c}$ of the three corners of a refined triangle together with the scalar coefficients a, b, c on the edges opposite $\boldsymbol{a}$, $\boldsymbol{b}$, $\boldsymbol{c}$ produces a vector field at any point inside the triangle. Given barycentric coordinates u, v, w we get

$$\boldsymbol{V}(u,v,w) = \tfrac{1}{2A}\{[v(a+b+c)-b]\overrightarrow{\boldsymbol{ab}}^{\perp} + [w(a+b+c)-c]\overrightarrow{\boldsymbol{ac}}^{\perp}\},$$

where A denotes the area of triangle $\boldsymbol{abc}$ and $^{\perp}$ indicates a CCW rotation by 90° in the plane of the triangle. This method of evaluation is used throughout our examples. We typically draw a single (3D embedded) arrow at the centroid of each triangle (see Figures 4.8, 4.9, 4.10, 4.11 and 4.12).

Limit Circulation Stencil For 0-form subdivision one typically requires a limit stencil to move vertices to the limit surface. Since 1-forms are treated as quantities integrated along curves the corresponding notion is that of a *limit circulation stencil*, *i.e.*, the computation of the circulation of the limit vector field on the limit edge of the surface. These can be computed analytically using the Bézier representation for a regular edge [Wang 2006]

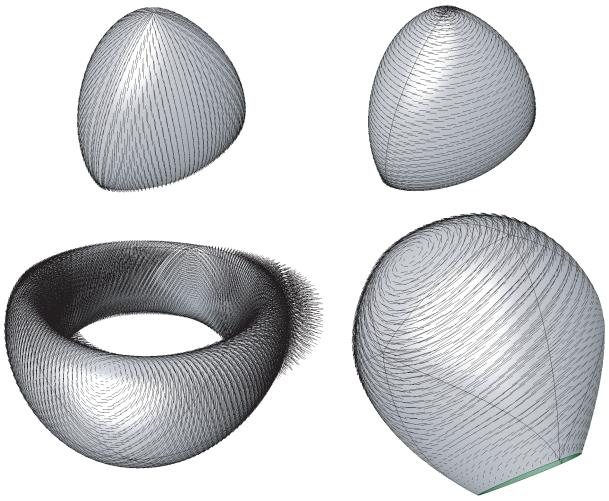

Figure 4.8: *Gallery of vector fields. Top: tetrahedron with 3 edges incident to a vertex set to* $+1$ *(left) resp. 3 edges incident on a face set to* $+1$ *(right); torus with 2 vortices and an open surface with 1 vortex.*

and extended to the irregular setting through a geometric series argument [Halstead *et al.* 1993]. Just as 0-form limit stencils are useful for approximation of a given surface with a subdivision surface (see for example [Litke *et al.* 2001]) the limit circulation stencils are useful for the approximation of given vector fields over a surface.

4.3.2 Design of Vector Fields

In surface modeling one manipulates control points to change the shape of the surface. To model a desired tangent vector field (over the underlying surface), one now manipulates *control coefficients on edges*. These coefficients have rather intuitive meaning, making design of a desired field simple. Placing a single coefficients of 1 on a given oriented edge produces a smooth vector field whose overall direction is roughly aligned with this edge and which decays smoothly to zero over the 1-ring of the two triangles incident to the edge. The magnitude of the vectors is directly controlled by the magnitude of the coefficient. Similarly, typical tasks in vector field design such as the placement of sinks, sources, and vortices becomes extremely easy. Sinks (and sources) at a vertex are where the divergence of a 1-form has negative (sink) or positive (source) value at the selected vertex. Vortices are similarly characterized by a positive (CW vortex) or negative (CCW vortex) curl (valued at a face) of a 1-form (see Figure 4.8).

However, setting only a few non-zero coefficients creates tangent vector fields that vanish

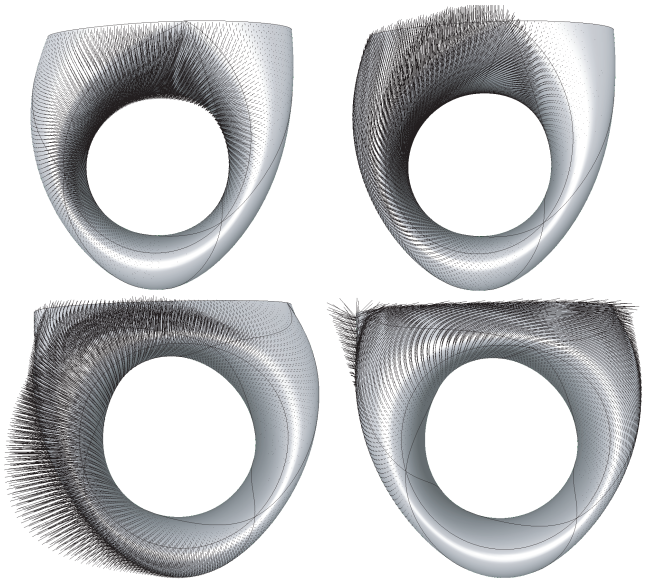

Figure 4.9: *1-form basis forms on an open surface near the boundary.*

over large parts of the surface since the basis 1-forms have finite support. In many scenarios one would like to place only a few select sources/sinks and/or CCW/CW vortices and then directly find a global vector field which satisfies these sparse features. This problem can be seen as the converse of the traditional Hodge decomposition of vector fields [Tong *et al.* 2003; Desbrun *et al.* 2005a].

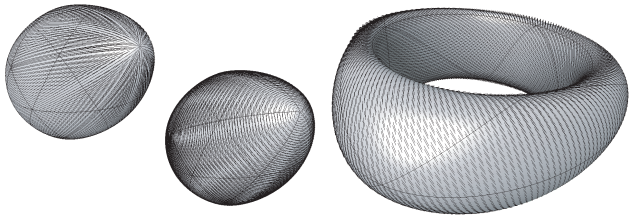

Figure 4.10: *Vector fields resulting from sparse interpolation. Top left: placing* ± 1 *at two opposing vertices results in a global (curl-free) vector field with a single source and sink. Placing* ± 1 *at selected faces results in a global (divergence-free) vector field with two opposing CCW/CW vortices. To produce a nontrival* harmonic *field on a higher genus surface (here, a torus), selected edge coefficients were set to* $+1$ *(right).*

Hodge Composition A simple design tool that we have employed proceeds as follows. Given the coarse control mesh of a surface (assumed genus-0 for now), the user places sources and sinks at some chosen vertices (and implicitly zeros at all other vertices). A 0-form is then solved for by using this data as the right hand side of Laplace's equation

over the vertices. CCW and CW vortices are placed at selected faces (and implied zeros at all other faces). Using Laplace's equation for 2-forms with the given data as rhs we get a corresponding global 2-form. (Any other sparse interpolation technique could of course be used as well.) If boundaries are present one may also supply Dirichlet or Neumann data there to enforce tangential or normal vector fields (or a mixture) at the boundary. Once 0-form (c_v) and 2-form data (c_t) are defined on all 0- respectively 2-simplices the final 1-form data c_e for all edges e_{ij} are set as

$$c_e = d^0 c_v + \delta^2 c_t.$$

Here δ^2 is the *co-differential* defined as follows. Letting t_{ijk} and t_{ijl} be the two triangles (with areas A_{ijk} and A_{ijl}) incident to e_{ij} and angles $\hat{k}$ and $\hat{l}$ at v_k and v_l we get

$$(\delta^2 c_t)_{ij} = (c_{t_{ijk}}/A_{ijk} + c_{t_{ijl}}/A_{ijl})/(\cot \hat{k} + \cot \hat{l}).$$

Figures 4.10 and 4.11 demonstrate examples of this approach. Here we only used a low-order approximation of the Laplace operator since it is sufficient for our experiments. For applications requiring high accuracy (*e.g.*, physical modeling) one can use exact Laplace stencils with wider support [Wang 2006].

While this approach allows for the flexible placement of sources, sinks, and vortices, some vector fields, in particular when the surface has non-trivial topology, are neither the differential of a 0-form nor the co-differential of a 2-form. Figure 4.10 (right) shows such an example, a non-vanishing harmonic vector field which is specified by setting edge coefficients directly. Importantly, for arbitrary topology surfaces *any* vector field can be specified with a combination of 0-, 1-, and 2-form data placed at the appropriate simplices.

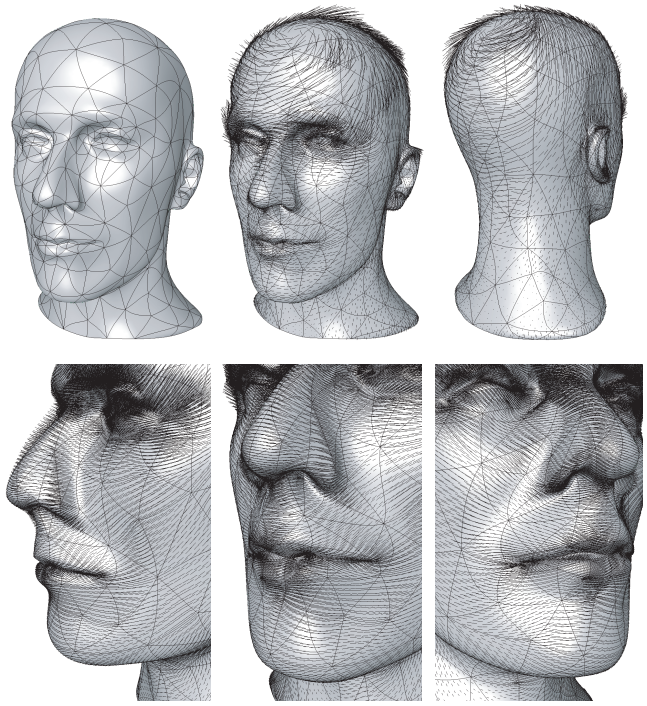

Figure 4.11: *Fun with the mannequin head. Two vortices were placed on the head and a global vector field interpolated on the dual graph with zero Neumann boundary conditions. Note in the close ups the smooth variation of the vector field even in the presence of irregular vertices.*

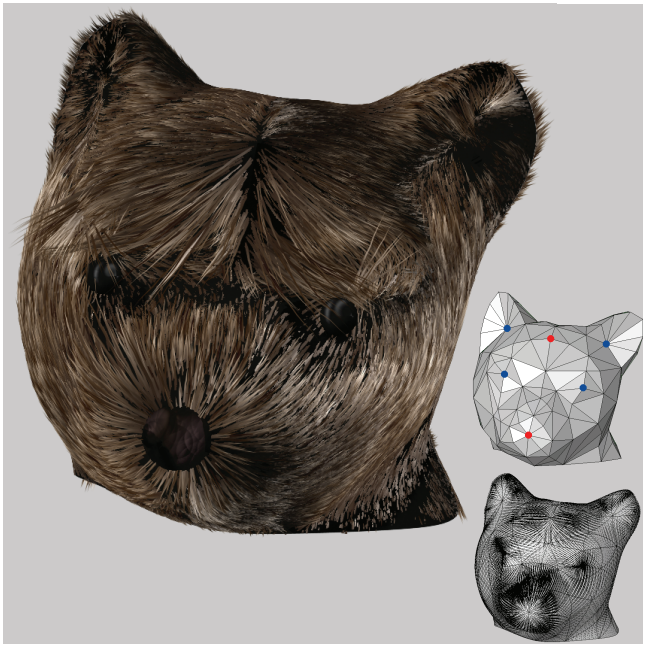

Figure 4.12: *Example of vector field design for use in a fur shader. The user marks selected vertices as sources (red) and sinks (blue) on the control mesh. Loop subdivision together with our novel 1-form subdivision results in a tangent vector field which interpolates the given sparse constraints over the subdivision surface (visualized on the bottom right). Such fields can be used directly to control standard fur shaders (here using Autodesk Maya).*

Chapter 5

Laplace and Bi-Laplace Equations of 1-Forms on Riemannian Surfaces

In this chapter, we demonstrate a numerical solver of Laplace and bi-Laplace equations of 1-forms on a simplicial surface M (with or without boundary) with a Riemannian metric. Recall that M becomes a C^2 differential manifold when it is equipped with the C^2-atlas $\{U_\alpha \colon |N_1(v_\alpha)| \to \mathbb{R}^2\}$ induced by Loop's subdivision scheme. Under $\{U_\alpha\}$ the subdivision 1-form basis is C^1 everywhere except irregular vertices at which only continuity is ensured. Therefor Dirichlet energy of the 1-form bases are finite which makes them a proper finite element space. Throughout we will be only concerned with such an atlas. The metric, however, is not necessarily generated by the subdivision scheme used for the atlas. It can be any admissible function which has the required regularity under the choice of atlas.

This chapter is organized as follows. Section 5.1 introduces the Hodge $\star$ operator on M. As a result, the generalized Laplace operator of differential forms can be written as composition of the coboundary operator $\boldsymbol{d}$ and $\star$. In Section 5.2 we set up the framework of finite element solutions for 1-form Laplace equations. Section 5.3 demonstrates convergence rate of the subdivision 1-form bases. We discuss applications of the subdivision 1-form bases to bi-Laplace equations in Section 5.4.

5.1 The Hodge Laplace Operator

We briefly review some elementary definitions. Let M be a closed oriented Riemannian n-manifold. We avoid technical discussions regarding the boundary. The reader is referred to [Morrey 1966; Spivak 1975] for details. A Riemannian metric tensor g is represented by

$\sum g_{ij}(u)du_i \otimes du_j$ under any admissible coordinate system $\{u\}$. The metric g determines an inner product on $V_p \equiv T_p^*M$ for all $p \in M$, and hence an inner product $(,)_p$ for each r on $V_p^r \equiv \bigwedge^r T_p^*M$. Precisely, let r-forms ω and η given by

$$\omega = \sum_{i_1<\cdots<i_r} \omega_{i_1\ldots i_r}(u)du_{i_1}\wedge\ldots\wedge du_{i_r}, \quad \eta = \sum_{j_1<\cdots<j_r} \eta_{j_1\ldots j_r}(u)du_{j_1}\wedge\ldots\wedge du_{j_r}.$$

Then

$$(\omega,\eta)_p = \sum_{\substack{i_1<\cdots<i_k \\ j_1<\cdots<j_k}} \begin{vmatrix} g^{i_1j_1}(u) & \ldots & g^{i_1j_k}(u) \\ g^{i_kj_1}(u) & \ldots & g^{i_kj_k}(u) \end{vmatrix} \omega_{i_1\ldots i_k}(u)\eta_{j_1\ldots j_k}(u).$$

where the g^{ij} matrix denotes the inverse of the matrix g_{ij} and $|\cdot|$ is the determinant. The unit volume form associated with the metric is $\mathrm{Vol}(g) = \sqrt{|g|}du_1\wedge\ldots\wedge du_r$. Here $|g|$ denotes $\det(g_{ij})$. Given $\omega \in V_p^r$, we obtain a linear map $L_\omega\colon V_p^{n-r} \to \mathbb{R}$, by composing the map $\eta \mapsto \omega\wedge\eta$ with the canonical isomorphism of V_p^n onto $\mathbb{R}$ (given by $c\mathrm{Vol}(g) \mapsto c$). By the Riesz representation theorem, there exists an element $\star\omega \in V_p^{n-r}$ such that $L_\omega(\eta) = (\star\omega,\eta)_p$ (see [Arnold *et al.* 2006a]). In other words, we have the following.

Definition 5.1. The Hodge start operator $\star\colon V_p^r \to V_p^{n-r}$ is defined by

$$(\star\omega,\eta)_p\mathrm{Vol}(g) = \omega\wedge\eta, \quad \omega \in V_p^r,\ \eta \in V_p^{n-r}, \tag{5.1}$$

or equivalently,

$$(\omega,\eta)_p\mathrm{Vol}(g) = \omega\wedge\star\eta = \eta\wedge\star\omega, \quad \omega \in V_p^r,\ \eta \in V_p^{n-r}. \tag{5.2}$$

We define the inner product $\langle,\rangle$ on $\Omega^r(M)$ by the integration

$$\langle\star\omega,\eta\rangle = \int_M (\star\omega,\eta)_p\mathrm{Vol}(g) = \int_M \omega\wedge\eta. \tag{5.3}$$

Definition 5.2. The adjoint of $\boldsymbol{d}$, denoted by $\boldsymbol{\delta}$, is defined by

$$\langle\boldsymbol{\delta}\omega,\eta\rangle = \langle\omega,\boldsymbol{d}\eta\rangle. \tag{5.4}$$

Note that $\boldsymbol{\delta}\colon \Omega^r(M) \to \Omega^{r-1}(M)$. The following relations hold among $\star$, $\boldsymbol{d}$ and $\boldsymbol{\delta}$. See [Spivak 1975; Wilson 2005].

Theorem 5.3. *As maps from Ω^r to their respective ranges:*

$$\begin{aligned}
\star\, \boldsymbol{d} &= (-1)^{r+1}\boldsymbol{\delta}\star, \\
\star\, \boldsymbol{\delta} &= (-1)^{r}\boldsymbol{d}\star, \\
\boldsymbol{\delta} &= (-1)^{n(r+1)+1}\star\, \boldsymbol{d}\star, \\
\star\star &= (-1)^{r(n-r)} Id.
\end{aligned}$$

Definition 5.4. The Laplacian is defined to be $\Delta = \boldsymbol{\delta d} + \boldsymbol{d\delta}$.

Finally, we state the Hodge decomposition theorem for $\Omega(M)$. Let $\mathcal{H}^r(M) = \{\omega \in \Omega^r(M) | \Delta\omega = \boldsymbol{d}\omega = \boldsymbol{\delta}\omega = 0\}$ be the space of harmonic k-forms.

Theorem 5.5. *There is an orthogonal direct sum decomposition*

$$\Omega^r(M) \cong \boldsymbol{d}\Omega^{r-1}(M) \oplus \mathcal{H}^r(M) \oplus \boldsymbol{\delta}\Omega^{r+1}(M),$$

and $\mathcal{H}^r(M) \cong H^r_{DR}(M)$, the de Rham cohomology of M in degree r.

In what follows, we assume that M is a two-dimensional simplicial surface equipped with the C^2 atlas $\{U_\alpha \colon |N_1(v_\alpha)| \to \mathbb{R}^2\}$ induced by Loop's scheme S_0. We assume two initial subdivision steps so that the surface can be treated as the union of patches parameterized over triangle faces with at most one irregular vertex incident on each face. We assume a local parametrization of a surface patch $\boldsymbol{x} \colon T \to \mathbb{R}^3$:

$$\boldsymbol{x}(\boldsymbol{u}) = \boldsymbol{x}(u_1, u_2) = \big(x_1(u_1, u_2), x_2(u_1, u_2), x_3(u_1, u_2)\big)^T,$$

where

$$T = \big\{\boldsymbol{u} = (u_1, u_2) \in [0,1]^2 \colon u_1 + u_2 \leq 1\big\}.$$

We emphasize that the component functions $x_i(u)$ may or may not be subdivision functions generated by S_0. The only requirement is that M is at least C^1 under the atlas U_α. The metric tensor $g(u_1, u_2) = \sum_{ij} g_{ij}(u_1, u_2) du_1 \otimes du_2$ can be written as

$$g_{ij}(u_1, u_2) = \sum_{k=1}^{3} \partial_i x_k(u_1, u_2) \partial_j x_k(u_1, u_2). \tag{5.5}$$

We list some technical results which will be used for numerical computation. Given 0-forms ω and η on M, their inner product reads as

$$\langle \omega, \eta \rangle = \sum_T \int_T \omega(u)\eta(u)\sqrt{|g|}du_1 \wedge du_2. \tag{5.6}$$

Similarly, for 1-forms $\omega = \omega_1 du_1 + \omega_2 du_2$ and $\eta = \eta_1 du_1 + \eta_2 du_2$ we have

$$\langle \omega, \eta \rangle = \sum_T \int_T \big(g^{11}\omega_1\eta_1 + g^{22}\omega_2\eta_2 + g^{12}\omega_1\eta_2 + g^{21}\omega_2\eta_1\big)\sqrt{|g|}du_1 \wedge du_2. \tag{5.7}$$

and, for 2-forms $\omega = \omega_{12} du_1 \wedge du_2$ and $\eta = \eta_{12} du_1 \wedge du_2$, we have

$$\langle \omega, \eta \rangle = \sum_T \int_T \omega_{12}(u)\eta_{12}(u)\frac{1}{\sqrt{|g|}}du_1 \wedge du_2. \tag{5.8}$$

In terms of the coordinate system, the Hodge star operator reads as

$$\star 1 = \sqrt{|g|}du_1 \wedge du_2, \tag{5.9}$$

$$\star du_1 = \sqrt{|g|}(-g^{12}du_1 + g^{11}du_2), \tag{5.10}$$

$$\star du_2 = \sqrt{|g|}(-g^{22}du_1 + g^{21}du_2), \tag{5.11}$$

$$\star(du_1 \wedge du_2) = \frac{1}{\sqrt{|g|}}. \tag{5.12}$$

As a result, we have the following expressions:

$$\star\omega = \sqrt{|g|}\big((-\omega_1 g^{12} - \omega_2 g^{22})du_1 + (\omega_1 g^{11} + \omega_2 g^{21})du_2\big), \tag{5.13}$$

$$\boldsymbol{d}\omega = (\partial_{u_1}\omega_2 - \partial_{u_2}\omega_1)du_1 \wedge du_2, \tag{5.14}$$

$$\begin{aligned}\boldsymbol{\delta}\omega &= - \star \boldsymbol{d} \star \omega \\ &= -\frac{1}{\sqrt{|g|}}\big\{\partial_{u_1}[\sqrt{|g|}(\omega_1 g^{11} + \omega_2 g^{21})] + \partial_{u_2}[\sqrt{|g|}(\omega_1 g^{12} + \omega_2 g^{22})]\big\}.\end{aligned} \tag{5.15}$$

5.2 Finite Element Solutions for 1-Form Laplace Equations

We consider the Laplace equation $\Delta\omega = f$ for r-form ω on M under boundary constraints. For $r = 0, 2$, the Laplace equation is a second-order elliptic equation of scalar fields on M whose finite element solutions have been extensively studied. Meanwhile relatively fewer

attempts have been made to solve 1-form Laplace equations. A formula based on mixed finite element is discussed in [Arnold *et al.* 2006a]. As an alternative we present a finite element solver based on the smooth 1-form bases developed in the previous chapter. Our approach has several advantages. Firstly it has no need for the mixed formula which leads to a larger indefinite system. Secondly the 1-form bases are C^1 on regular mesh and have higher approximation order. Therefore we expect higher rate of convergence.

The Dirichlet energy is defined as

$$D(\omega_h) = \langle \boldsymbol{d}\omega, \boldsymbol{d}\omega \rangle + \langle \boldsymbol{\delta}\omega, \boldsymbol{\delta}\omega \rangle. \tag{5.16}$$

Now consider the constrained minimization problem

$$\min_{\omega \in \Omega^1(M)} \frac{1}{2} D(\omega) + \langle f, \omega \rangle \quad \text{subject to} \tag{5.17}$$

$$t\omega = t\eta, \ n\omega = n\eta \quad \text{on } \partial M, \tag{5.18}$$

where $t\omega$ and $n\omega$ denotes the tangential and normal components along the boundary, respectively, and η is a given 1-form on ∂M. By the variational principle, the Euler-Lagrange equation of (5.17) and (5.18) is the boundary-value problem consisting of

$$(\boldsymbol{\delta d} + \boldsymbol{d\delta})\omega = f \quad \text{in } M, \tag{5.19}$$

together with the Dirichlet boundary conditions (5.18). Existence and uniqueness of the boundary-value problem (5.18)–(5.19) are proved in [Morrey 1966].

First we need to choose a finite element basis to represent 1-form ω. The obvious way is through the coordinate system $\{du_1, du_2\}$. One can use scalar finite element basis to represent its two component functions ω_1 and ω_2 under the coordinates and, for instance, we can associate the DoFs with coefficients at vertices. However, when the metric of M changes, in order to represent the same ω, the coefficients have to be changed accordingly. Indeed, the Hodge star operator and hence $\boldsymbol{\delta}$ are metric dependent. But representations of differential 1-forms should be metric independent, as is expected. Therefore it is more appropriate to use the subdivision 1-form basis $\{\Phi^e\}$ developed in the previous chapter, where the DoFs are associated with coefficients on edges of the triangle mesh and are

independent of the metric on M.

The second question is why Whitney 1-forms cannot be used in the minimization problem (5.17). Recall that the vector field proxy of Whitney 1-form Φ^W is discontinuous along the normal of element boundary. As a result, $\boldsymbol{\delta}\Phi^W$ is not square integrable and hence $D(\Phi^W)$ is not finite[1]. On the other hand, our smooth subdivision 1-form basis $\{\Phi^e\}$ is C^1 on regular mesh and C^0 at irregular vertices, $D(\Phi^e)$ is well defined.

Let $\{\Phi_i\}$ be the subdivision 1-form basis and assume the approximation of 1-form $\omega \in \Omega^1(M)$:

$$\omega_h = \sum_{i \in \text{Edge}(M)} c_i \Phi_i. \tag{5.20}$$

The Dirichlet energy of ω_h is then given by

$$D_h(\omega) = \sum_{i,j \in \text{Edge}(M)} \{\langle \boldsymbol{d}\Phi_i, \boldsymbol{d}\Phi_j \rangle + \langle \boldsymbol{\delta}\Phi_i, \boldsymbol{\delta}\Phi_j \rangle\} c_i c_j. \tag{5.21}$$

And the linear term

$$\langle f, \omega_h \rangle = \sum_{i \in \text{Edge}(M)} \langle f, \Phi_i \rangle c_i. \tag{5.22}$$

Hence the Ritz approximation of the variational problem (5.17)–(5.18)

$$\min_{\boldsymbol{\omega}_h} \frac{1}{2} \boldsymbol{\omega}_h^t \mathbf{D}_h \boldsymbol{\omega}_h + \mathbf{f}_h \boldsymbol{\omega}_h \quad \text{subject to} \tag{5.23}$$

$$\mathbf{T}_h \boldsymbol{\omega}_h = \boldsymbol{\eta}_h, \ \mathbf{N}_h \boldsymbol{\omega}_h = \boldsymbol{\eta}_h^{\perp}, \tag{5.24}$$

where, by a slight abuse of notations, here we take $\boldsymbol{\omega}_h$ to denote the array of DoFs $\{c_i\}$, $\mathbf{D}_h^{ij} = \langle \boldsymbol{d}\Phi_i, \boldsymbol{d}\Phi_j \rangle + \langle \boldsymbol{\delta}\Phi_i, \boldsymbol{\delta}\Phi_j \rangle$ is the stiffness matrix, and $\mathbf{f}_h$ is the array with entries $\langle f, \Phi_i \rangle$. The entries of matrix $\mathbf{T}$ and $\mathbf{N}$ are the contributions to the tangential and normal integration along ∂M. Precisely, they are given by

$$\mathbf{T}_h^{ij} = \int_{e_i} \Phi_j, \quad \mathbf{N}_h^{ij} = \int_{e_i} \star \Phi_j, \tag{5.25}$$

$$\boldsymbol{\eta}_h^i = \int_{e_i} \eta, \quad \boldsymbol{\eta}_h^{\perp,i} = \int_{e_i} \star \eta. \tag{5.26}$$

[1]Whitney forms can still be used to solve the 1-form Laplace equation, however, under the formula of mixed finite element methods.

The computation of element arrays requires the evaluation of integrals on the domain of each element. We need numerical quadrature rules to efficiently compute those integrals without compromising the order of convergence. Numerical experiments showed that a 1-point quadrature rule or trapezoid rule is not enough for the stability and convergence of the finite element solution. Therefore we have chosen the 4-point quadrature rule on triangles for the numerical demonstration. The barycentric coordinates ξ_i and the corresponding weights w_i of the quadrature points are (*e.g.*, [Carey & Oden 1984]),

$$\begin{aligned}
\xi_1 &= \frac{1}{3}(1,1,1), \quad w_1 = -27/48 \\
\xi_2 &= \frac{1}{5}(3,1,1), \quad w_2 = 25/48 \\
\xi_3 &= \frac{1}{5}(1,3,1), \quad w_3 = 25/48 \\
\xi_4 &= \frac{1}{5}(1,1,3), \quad w_4 = 25/48.
\end{aligned}$$

As for numerical integration on the boundary, we adopt the two-point Legendre–Gauss quadrature formula (the interval is scaled into $[-1,1]$):

$$\xi_1 = -\frac{\sqrt{3}}{3},\ w_1 = 1, \quad \xi_2 = \frac{\sqrt{3}}{3},\ w_2 = 1.$$

By applying the expressions (5.5)–(5.15) together with the choice of quadrature rule, we can fully discretize the Ritz approximation (5.23)–(5.24) for the given metric (g_{ij}). In order to get full approximation order on the boundary, artificial edges are introduced within one layer of triangles outside the boundary. The boundary constraints are imposed by the penalty method, with a penalty stiffness equal to 100 times the maximum diagonal component of the stiffness matrix [Carey & Oden 1984].

5.3 Numerical Demonstration

5.3.1 Rate of Convergence on Regular Mesh

We consider a regular triangle mesh with regular boundary. In particular, we consider the uniform regular triangulation of $[0,1] \times [0,1]$ with Cartesian coordinate system $\{dx, dy\}$.

The matrix g_{ij} of metric is identity. In test problem I, we take

$$f = 4\pi^2(\cos(2\pi x) - 4\sin(4\pi y))dx + 4\pi^2(\cos(2\pi x) + 4\sin(4\pi x))dy \tag{5.27}$$

in (5.19). The exact solution is

$$\omega = (-\sin(4\pi y) + \cos(2\pi x))dx + (\sin(4\pi x) + \cos(2\pi x))dy. \tag{5.28}$$

As shown in Figures 5.1–5.3, we observed that the rate of convergence in the L^2 norm and the strain energy norm is h^3 and respectively h^2, where h represents the side length of elements. Notice that, on a regular triangular mesh, our smooth 1-form bases span all linear and quadratic 1-forms. It is well known that a finite element space that contains the complete quadratic polynomials satisfies the error bound [Strang & Fix 1973]:

$$\|\omega - \omega_h\|_1 \leq Ch^2\|\omega\|_3, \tag{5.29}$$

where $\|\cdot\|_s$ denotes the norm over H^s. Therefore the optimal rate of convergence in the strain energy norm is h^2 and it is attained in the experiments we performed.

For test problem II, we take

$$f = 16\pi^2 \sin(4\pi x)dx + 4\pi^2 \cos(2\pi y - \pi)dy, \tag{5.30}$$

with the exact solution being

$$\omega = \sin(4\pi x)dx + \cos(2\pi y - \pi)dy. \tag{5.31}$$

The finite element solution ω_h is visualized in Figure 5.4. The same rate of convergence as shown in Figure 5.1 is observed.

Next we consider a smooth non-identity metric on M which is induced by a one-to-one regular mapping $F\colon [0,1]^2 \to \mathbb{R}^2$. For instance, we can take

$$F(x,y) = \begin{pmatrix} F_1 \\ F_2 \end{pmatrix} = \begin{pmatrix} x + y + \frac{1}{4\pi}\sin(\pi y) \\ y + \frac{1}{4\pi}\sin(\pi x) \end{pmatrix}. \tag{5.32}$$

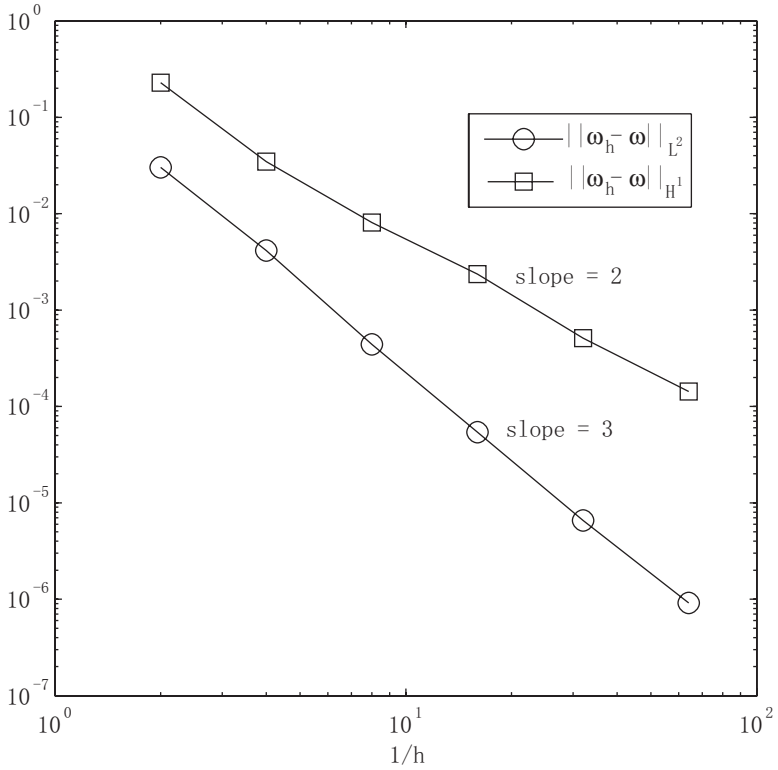

Figure 5.1: *Rate of convergence in L^2 norm and H^1 norm for the finite element approximation of Laplace equations.*

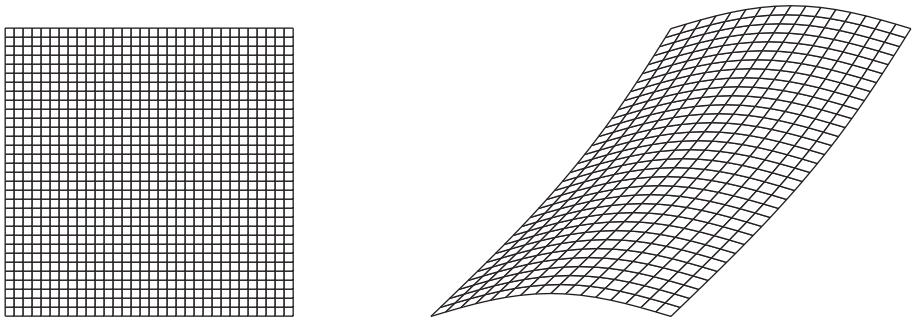

Figure 5.2: *Deformation under the injective and regular mapping* $F(x, y)$.

Figure 5.2 shows the deformation of a square under the mapping $F(x, y)$. The metric g_{ij} induced by F is given by

$$g_{ij} = \sum_{k=1}^{2} \frac{\partial F_k}{\partial x_i} \frac{\partial F_k}{\partial x_j}.$$

We take ω in test problem I as the exact solution and let $f = -\Delta\omega$ be the right side of the Laplace equation with metric (g_{ij}). The optimal rate of convergence shown in Figure 5.1 is attained. Figure 5.5 shows the vector field proxy of ω_h under deformation of metric (g_{ij}). Note that ω_h here approximates the same 1-form as test problem II, and hence their solutions of edge coefficients share the same value, up to the order of approximation.

5.3.2 Degradation of Convergence Rate on L-Shaped Domain

It is interesting to consider the performance of 1-form basis over a domain with singularities. We consider an L-shaped domain Ω with a concave corner P. Our numerical experiments showed that, if a smooth solution exists, our method is able to capture it with the optimal rate of convergence. Figure 5.6 visualizes one of the component functions of the smooth 1-form which solves the Laplace equation on Ω.

It is well known that, the following boundary value problem,

$$\Delta\omega = -1, \text{ in } \Omega, \quad \omega = 0 \text{ on } \partial\Omega$$

has a singularity at the point P. In terms of polar coordinate (r, θ) centered at P, the dominant term in the singularity is $r^{2/3} \sin \frac{2}{3}\theta$. Singular functions need to be included into the finite element space to maintain optimal rate of convergence. In our numerical experiment with the 1-form basis, the rate of convergence in the L^2-norm is degraded to

h (Figure 5.7). It shows that the 1-form basis is too smooth to handle the singularity efficiently.

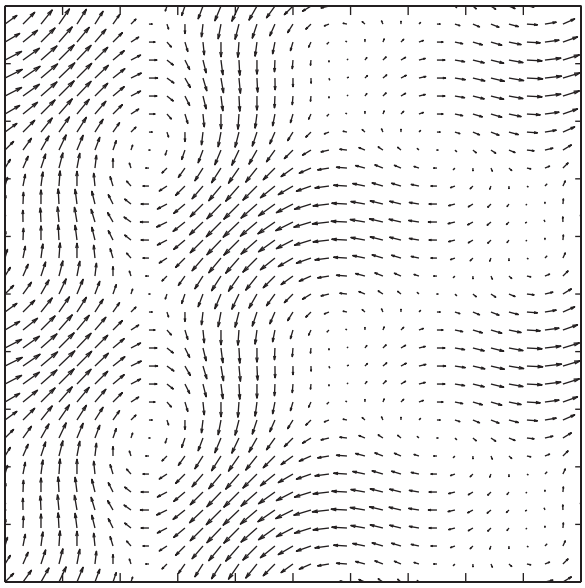

Figure 5.3: *Finite element approximation of problem I. The component functions of ω_h are visualized as a vector field. Rotations are well captured.*

5.4 Applications to Bi-Laplace Equations

The bi-Laplace equation of r-form on M is defined as

$$\Delta\Delta\omega = f \quad \text{on } M, \tag{5.33}$$

subject to certain boundary constraints along ∂M. For example, we consider the Dirichlet boundary condition,

$$\omega = \eta \text{ and } \partial_n\omega = \theta \quad \text{on } \partial M, \tag{5.34}$$

where η and θ are 1-forms defined on the boundary. Here $\omega = \eta$ has the same meaning as (5.18) (*i.e.*, the normal and tangential components are equal respectively), and $\partial_n\omega$ denotes the normal derivative of the normal and tangential components of ω along ∂M. The variational principle shows that the solution of (5.33) subject to (5.34) is the minimizer

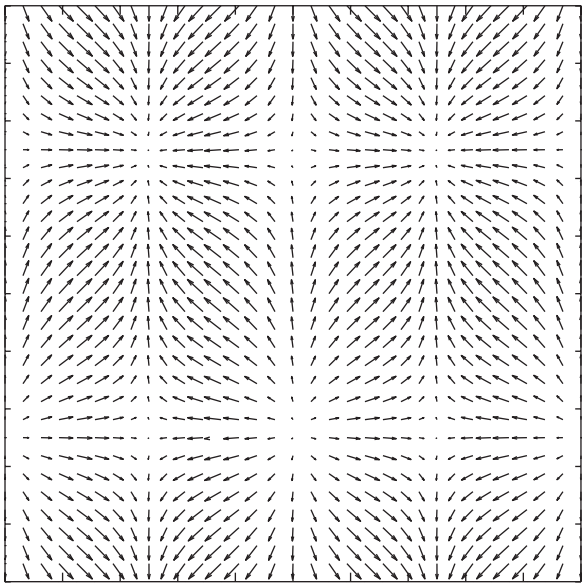

Figure 5.4: *Finite element approximation of problem II. The component functions of ω_h are visualized as a vector field. Sinks and sources are well captured.*

of following constrained minimization problem

$$\min_{\omega \in \Omega^1(M)} \frac{1}{2} B(\omega) - \langle f, \omega \rangle, \tag{5.35}$$

subject to the boundary constraint (5.34). Here the energy functional $B(\omega)$ is defined as

$$B(\omega) = \langle \boldsymbol{\delta d}\omega, \boldsymbol{\delta d}\omega \rangle + \langle \boldsymbol{d\delta}\omega, \boldsymbol{d\delta}\omega \rangle. \tag{5.36}$$

For the finite element approximation, we assume the approximation (5.20) of ω in the finite element space spanned by $\{\Phi_i\}$. The energy functional $B(\omega)$ is therefore given by

$$B_h(\omega_h) = \sum_{i,j \in \mathrm{Edge}(M)} \{\langle \boldsymbol{\delta d}\Phi_i, \boldsymbol{\delta d}\Phi_j \rangle + \langle \boldsymbol{d\delta}\Phi_i, \boldsymbol{d\delta}\Phi_j \rangle\} c_i c_j. \tag{5.37}$$

All that follows is completely analogous to the Ritz approximation of the Laplace equation. According to the approximation theory of finite element method [Strang & Fix 1973], the error estimate for solving the bi-Laplace equation on a regular triangle mesh is give by

$$\|\omega - \omega_h\|_2 \leq Ch \|\omega\|_3, \tag{5.38}$$

due to the fact that the subdivision 1-form bases span all quadratic 1-forms on the regular

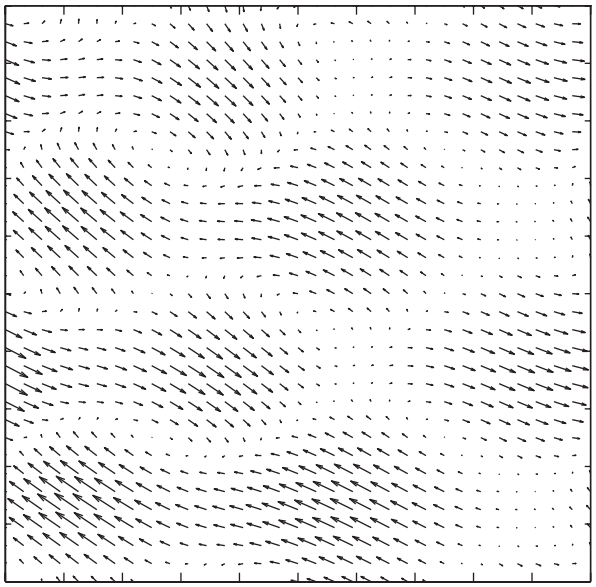

Figure 5.5: *Finite element approximation of problem I with deformed metric induced by* $F(x, y)$*. Component functions of* ω_h *are visualized under the deformed metric.*

mesh. Therefore the optimal rate of convergence in H^2 norm is linear.

As an example, we consider the uniform regular triangulation of $[0, 1] \times [0, 1]$, and take the exact solution to be

$$\omega = \sin(\pi x) * \sin(\pi y)dx + \sin(2\pi x)\sin(\pi y)dy. \tag{5.39}$$

We let $f = \Delta\Delta\omega$ and let the boundary conditions coincide with the boundary values of ω and $\partial_n\omega$. The finite element approximation of ω using the subdivision 1-form bases is visualized in Figure 5.8. The linear convergence rate in H^2 norm is verified in this example (see Figure 5.9).

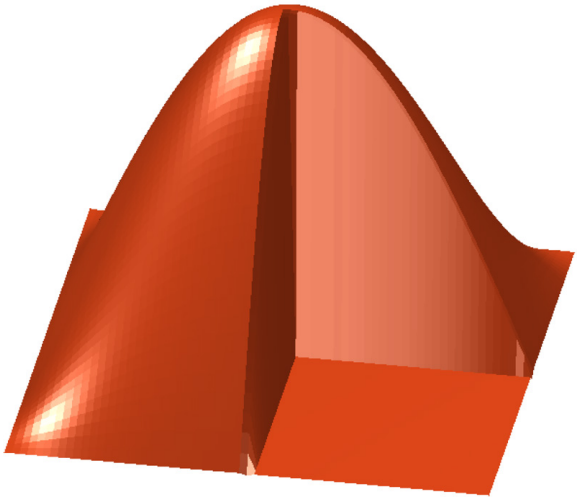

Figure 5.6: *Smooth solution is well captured on an L-shaped domain. One component function is visualized.*

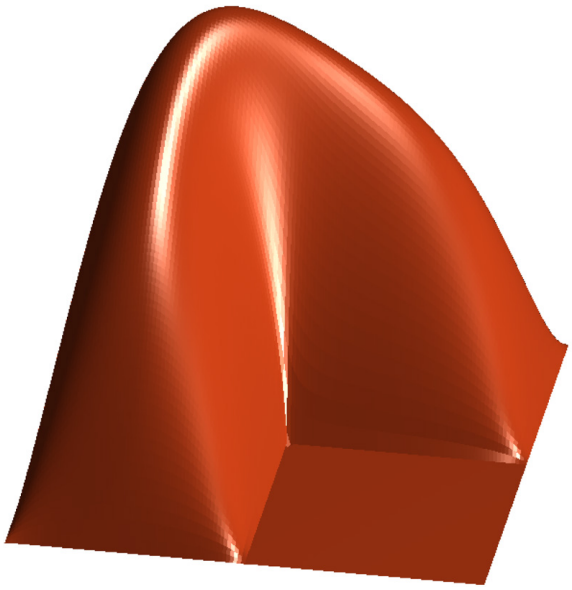

Figure 5.7: *Approximation to singular solution on an L-shaped domain. Rate of convergence in the* L^2 *norm is degraded to* h.

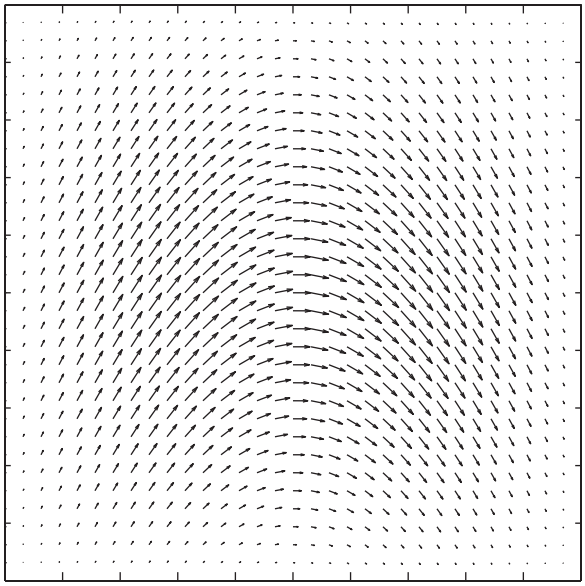

Figure 5.8: *Finite element approximation ω_h of the bi-Laplace equation with the exact solution being* (5.39)*. The vector field proxy is visualized.*

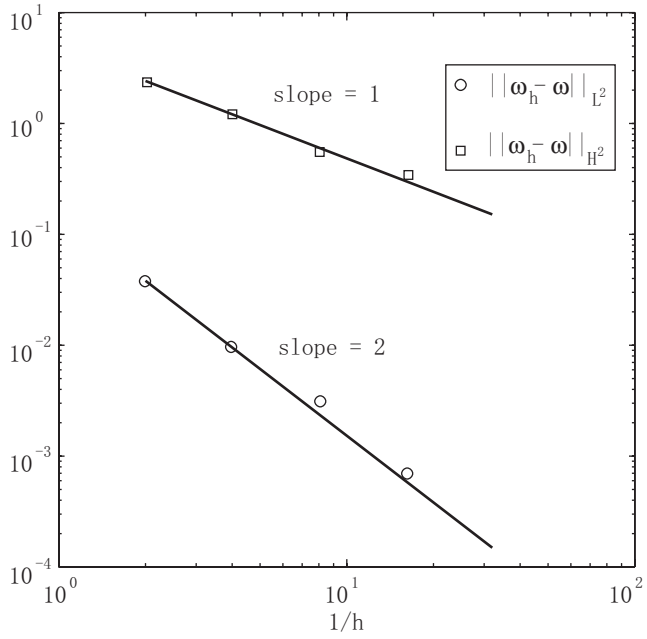

Figure 5.9: *Rate of convergence in L^2 norm and H^2 norm for the finite element approximation of bi-Laplace equations.*

Chapter 6

Extension to 3-D Subdivision

The subdivision approach we proposed in this thesis built a connection between Whitney forms and the theory of subdivision. As a result, edge-based subdivision schemes are constructed as a natural extension of classic primal and dual subdivision schemes, and they converge to a limit 1-form. Abstractly there are two essential ingredients in this approach. The first one is the recursive refinement of mesh primitives which maps the mesh from coarse level to fine level (*e.g.*, the 4-to-1 quadrisection for triangle meshes). Second, the commutative relations links subdivision schemes of r-cells and $r+1$-cells through the coboundary operator:

$$dS_r = S_{r+1}d, \quad r = 0, 1, \ldots, n-1, \tag{6.1}$$

where n is the mesh dimension. While the previous chapters are mainly devoted to two-dimensional simplicial meshes, this framework is general enough to handle higher-dimensional or non-simplicial cases. Its applications on quadrilateral mesh can be found in the appendix. In this chapter we will show its extension to the octet mesh which consists of tetrahedra and octahedra.

In Section 6.1 we will introduce the tetrahedral subdivision scheme proposed by [Schaefer *et al.* 2004], which avoids the choice of a preferred diagonal in splitting octahedra into tetrahedra. Following this line, vertices of the mesh are identified with the well-known face-centered cubic (FCC) lattice. In order to perform convolution process to get smoother schemes, we regard FCC lattice as a sheared $\mathbb{Z}^3$ lattice. Section 6.2 is devoted to technical calculations on constructing linear subdivision schemes of Whitney r-forms on octet meshes by solving the commutative relations (6.1). The resulting schemes are uniquely determined up to one parameter. In Section 6.3 we perform spectrum analysis to optimize the choice

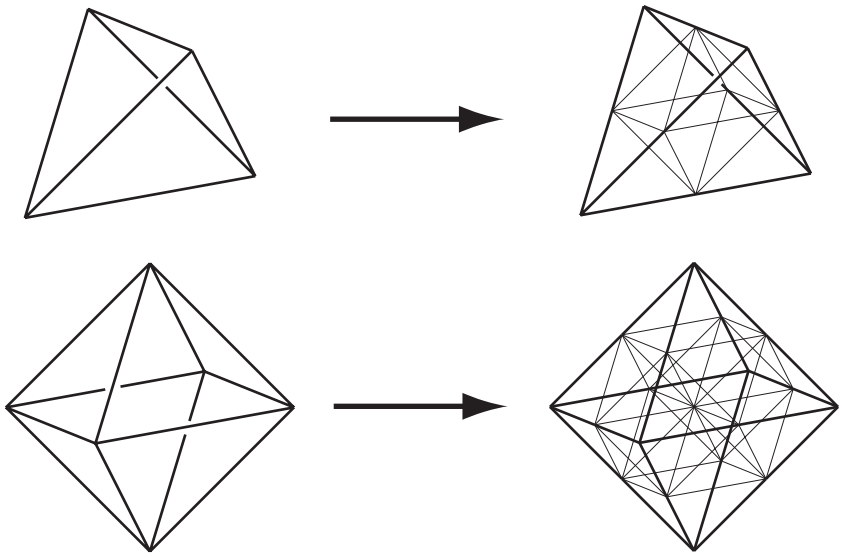

Figure 6.1: *A tetrahedron is split into four tetrahedra and an octahedron (top). An octahedron is split into six octahedra and eight tetrahedra (bottom).*

of this parameter. Finally Section 7.2 shows how to get smoother schemes by convolving the linear schemes obtained in Section 6.2.

6.1 Tetrahedral Subdivision Scheme

To perform linear subdivision on a tetrahedral mesh, we need to define a split on a single tetrahedron, which is then applied to all tetrahedra in the mesh. The split we will be describing is proposed in [Schaefer *et al.* 2004]. Given a tetrahedron, we insert new vertices at the midpoints of each edge followed by connecting them within each face of the tetrahedron. Four new tetrahedra are formed at the corners of the original tetrahedron. Chopping these four children off the parent tetrahedron leaves an octahedron (see Figure 6.1, top). We then face two choices of splitting the resulting octahedron.

One choice is to split the octahedron into four tetrahedra by cutting through two of its three diagonal planes. This is equivalent to choose a preferred diagonal for the octahedra. This choice of diagonal causes the resulting tetrahedral mesh to contain a preferred direction associated with the choice of diagonal. More crucially, each tetrahedron in the base mesh must be assigned such a diagonal. As a result, it leads to substantial complications in smoothness analysis of associated subdivision schemes.

The other choice is to leave the octahedron alone and develop a linear subdivision for

octahedra. We split a tetrahedron into four new tetrahedra and an octahedron (Figure 6.1). To refine an octahedron, we insert vertices at the middle points of each edge on the octahedron called edge vertices, and at the centroid of the octahedron, which is the average of the six vertices of the octahedron. Next we connect the centroid vertex with each edge vertex, and connect edge vertices within each face of the original octahedron. This way we formed six new children octahedra at the six corner of the parent octahedron, and eight new tetrahedra corresponding to the eight faces of the original octahedron. Together with the split of a tetrahedron, we obtained a refinement process for octet meshes (Figure 6.1).

6.2 Construction of Whitney Forms on Uniform Octet Meshes

6.2.1 Numeration of Vertices, Edges, Triangles, and Volumes

Our objective is to construct r-cell subdivision schemes on octet meshes for $r = 0, 1, 2, 3$. First we need to label each r-cell of the mesh such that a subdivision scheme can be represented by its symbol, as a common practice in surface subdivision. Starting with a regular base tetrahedron (octahedron), the octet refinement rule (Figure 6.1) generates a uniformly structured mesh, called uniform octet mesh, in the interior of the base tetrahedron (octahedron) (see Figure 6.2). And each triangle of the mesh is the common face of a tetrahedron and an octahedron. Each edge of the mesh is shared by two tetrahedra and two octahedra. Each vertex is surrounded by eight tetrahedra and six octahedra. This structure can be identified with the well-known face-centered cubic lattice. FCC lattice is a common crystal structure, which can be generated in the following way. Given a regular cubic mesh with vertices being identified with $\mathbb{Z}^3$ lattice, we insert new vertices at the centroid of each square of the mesh, called centroid vertices. Next we connect each vertex with all of its neighboring vertices of distance $\frac{\sqrt{2}}{2}$ to the vertex. The FCC lattice consists of $\mathbb{Z}^3$ vertices, centroid vertices and edges of length $\frac{\sqrt{2}}{2}$. Furthermore, the vertices of the FCC lattice can again be identified with a sheared $\mathbb{Z}^3$ lattice (see Figure 6.3).

We demonstrate a consistent way of numerating all edges, triangles and volumes (tetrahedra and octahedra) of the uniform octet mesh. As shown in Figure 6.4, given a base vertex marked with grey circle, six edges that emanate from the base vertex are grouped together and attached to that vertex. Similarly, eight triangles that are adjacent to the base vertex are grouped together and attached to that vertex. Finally two tetrahedra and

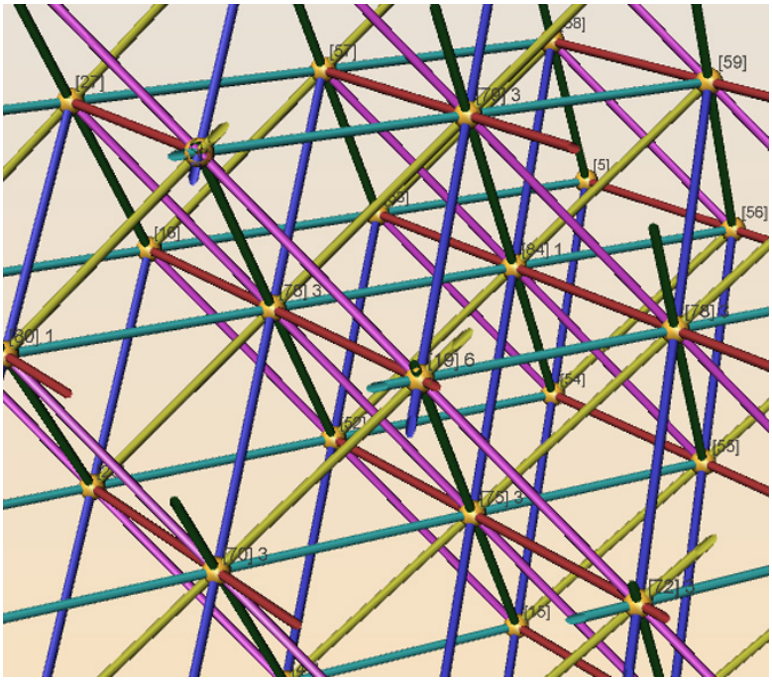

Figure 6.2: *Zoom view into the interior of a regular base octahedron after a number of octet subdivisions. The screenshot is generated by jReality Viewer.*

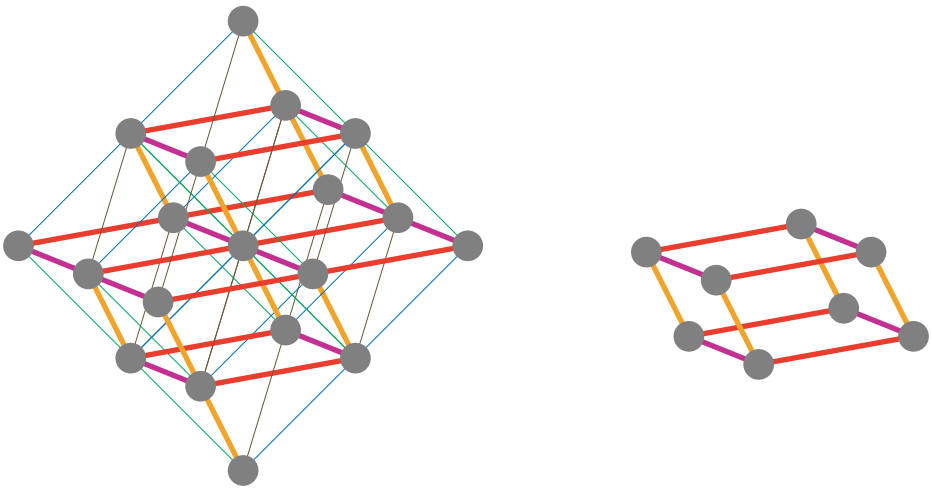

Figure 6.3: *Vertices of a uniform octet mesh, marked with grey circles, can be identified with a sheared $\mathbb{Z}^3$ lattice (left). Building block of the sheared $\mathbb{Z}^3$ lattice with x, y, z axes being highlighted (right).*

one octahedron are grouped together and attached to the base vertex. By traversal over all vertices followed by counting components in group associated with each vertex, each r-cell of the uniform mesh get counted once and only once. Orientations of edges are indicated by arrows. Notice that parallel edges receive the same orientation. Since each triangle is the common face a tetrahedron and an octahedron, we define a positive direction on each triangle as the direction pointing from the octahedron to the tetrahedron. All tetrahedrons and octahedrons receive positive orientation.

Under the convention of Figure 6.4, 0-, 1-, 2- and 3-cochains on the octet mesh can be interpreted as scalar, 6-, 8- and 3-vectors on the $\mathbb{Z}^3$ lattice. Therefore the theory of matrix subdivision applies.

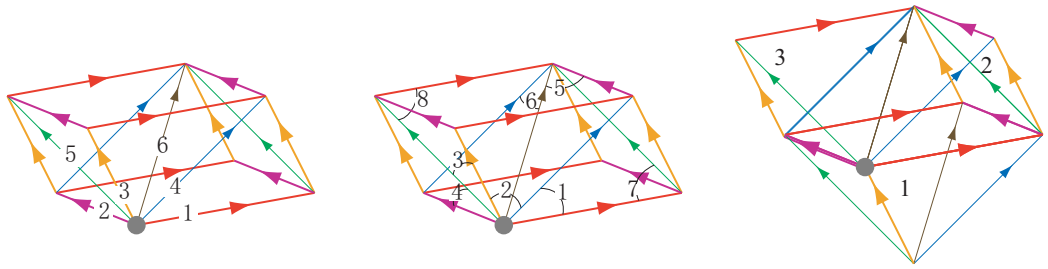

Figure 6.4: *Numeration of oriented r-cells of the uniform octet mesh. Edges are grouped as* 6*-vectors (left), triangles are grouped as* 8*-vectors (middle) and volumes are grouped as* 3*-vectors.*

6.2.2 Solving Commutative Relations

There are four types of cochain subdivision schemes on a uniform octet mesh, S_r for r-cochains, $r = 0, 1, 2, 3$. To construct Whitney forms on a uniform octet mesh, we solve for linear subdivision schemes S_r that satisfy (6.1) under two assumptions. First we assume that, given dimension r, S_r has different actions on splitting a tetrahedron than a octahedron while the common face shared by tetrahedra and octahedra must receives the same coefficient. The second assumption is that, when restricted on a triangle, S_r must coincide with the subdivision schemes of Whitney forms on triangles. Recall that Whitney forms on a tetrahedron is given by the formula (3.2) and they satisfy (6.1). We emphasize that we do not presume formula (3.2) in our construction.

Consider the splitting rule of a tetrahedron. Let S_0 be the linear subdivision scheme on the tetrahedron and S_3 the constant volumetric subdivision. That is to say, a child

tetrahedron is weighted by $\frac{1}{8}$ from its parent octahedron, and a child octahedron is weighted by $\frac{1}{2}$. Actions of S_1 and S_2 on boundary of the tetrahedron are determined by 1- and 2-cochain subdivision schemes of Whitney forms on triangles, respectively. Weights for the interior child triangle are uniquely determined by the commutative relations (see Figure 6.5). The resulting weights, $h_1 = 1/8$ and $h_2 = -1/8$, agree with the formula (3.2) of Whitney forms on tetrahedra. Therefore actions of S_r on splitting a tetrahedron are completely determined.

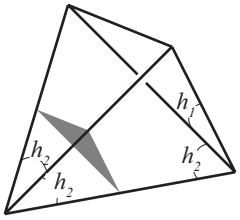

Figure 6.5: *Weights for the interior child triangle in splitting of a tetrahedron, with triangle orientation pointing inwards to tetrahedra,* $h_1 = 1/8$, $h_2 = -1/8$.

Actions of S_r on splitting an octahedron are more subtle. S_0 is simply the linear subdivision scheme proposed by [Schaefer *et al.* 2004]. The centroid of the octahedron is the average of its six vertices with weight $\frac{1}{6}$. We also assume constant volumetric subdivision for S_3. That is to say, a child octahedron is weighted by $\frac{1}{8}$ from its parent octahedron, and a child tetrahedron is weighted by $\frac{1}{32}$. Taking into account symmetry, we assume fully parameterized masks for S_1 and S_2 (see Figure 6.6). Solving the commutative relations yields the following one parameter solution where c is to be determined:

$$a_1 = -\frac{c}{48} - \frac{1}{48},\ a_2 = 0,\ a_3 = \frac{c}{96} + \frac{17}{96},\ a_4 = \frac{c}{96} + \frac{3}{32}, \tag{6.2}$$

$$f_1 = \frac{7}{96},\ f_2 = \frac{c}{96},\ f_3 = -\frac{c}{48} - \frac{19}{96}, \tag{6.3}$$

$$f_4 = -\frac{c}{48} - \frac{1}{32},\ f_5 = \frac{c}{96} + \frac{1}{12},\ f_6 = -\frac{1}{96}. \tag{6.4}$$

Remark 6.1. We start with a base tetrahedron and apply S_r to get sequences of r-cochains in the interior of the tetrahedron at arbitrarily refined level. It can be verified that the sequences of r-cochains are independent of the free parameter c, and coincide with the interpolation by the formula of Whitney forms on tetrahedra. Therefore actions of S_1 and S_2 on a base tetrahedron is uniquely determined by the commutative relations and the choice of S_0 and S_3.

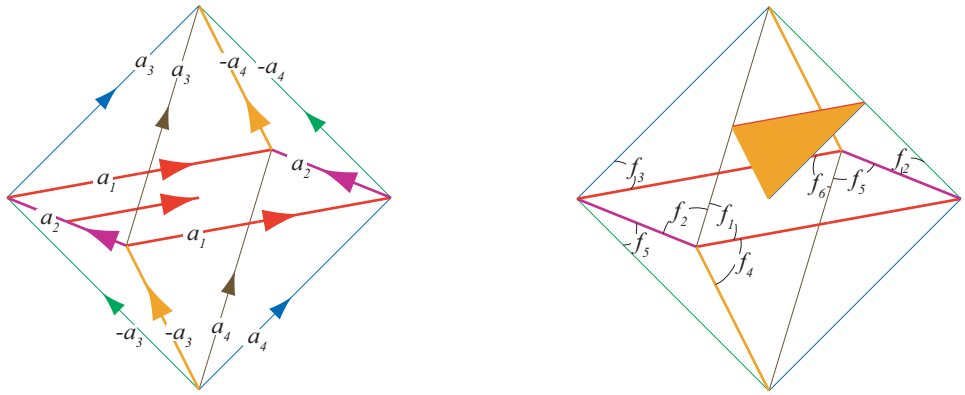

Figure 6.6: *Mask parameters of S_1 for the child edge pointing from middle point of one edge to the centroid of the octahedron (left). Mask parameters of S_2 for the shaded child triangle (right).*

Remark 6.2. The equations (6.2)–(6.4) together with the choice of S_0 and S_2 define subdivision schemes S_r of Whitney r-forms on an octahedron, up to choices of parameter c. Sine S_r agree with Whitney r-forms on a base tetrahedron, the limit r-cochain generated by S_r on a base octahedron can be represented as linear combination of infinitely many Whitney r-cochains on all subdivided tetrahedra contained in the base octahedron.

Remark 6.3. Our construction can be extended to pyramids/tetrahedra with the choice of a preferred diagonal through which an octahedron is split. For the same reason as above, the resulting limit r-cochains on a base pyramid is represented as infinite sum of Whitney r-cochains on subdivided tetrahedra contained in the base pyramid. Gradinaru & Hiptmair [1999] proposed explicit formulae of Whitney elements on pyramids. They are not linear in any tetrahedra that are contained in the base pyramid, and hence do not admit a subdivision scheme S_r. In other words, the Whitney forms proposed by Gradinaru & Hiptmair are not refinable on pyramids/tetrahedra mesh.

6.3 Fixing c by Spectrum Analysis of S_r

We need to choose the parameter c for r-cochain subdivision schemes S_r on a uniform octet mesh. Theoretically, the parameter has no influence upon the interior of a base tetrahedron. However, the choice of c may affect stability of the subdivision algorithm since an octahedron within the base tetrahedron may not receive the exact coefficients as they should be due to round-off error. The difference will mimic the actions of S_r on

a base octahedron. Should S_r have unstable eigenvectors, they will eventually grow up and deteriorate numerical results. Second, S_r are newly discovered r-cochain subdivision schemes of Whitney forms on octahedra, and hence deserve further investigation to have as high regularity as possible through the choice of c.

Recall that r-cochains on an octet mesh at level j can be regarded as vectors $f^j \equiv \{f^j_\alpha \colon \alpha \in \mathbb{Z}^3\}$ (see Figure 6.4), and r-cochains at level $j+1$ are recursively generated by $f^{j+1} = S_r f^j$:

$$f^{j+1}_\alpha = \sum_{\beta \in \mathbb{Z}^3} P^r_{\alpha - 2\beta} f^k_\beta, \quad \alpha \in \mathbb{Z}^3. \tag{6.5}$$

See Section 3.2.3 for details of matrix subdivision. As before, the *symbol* of the matrix refinement equation of S_r is defined as, thanks to $\mathbb{Z}^3$ lattice,

$$P^r(\gamma) = \frac{1}{8} \sum_{\alpha \in \mathbb{Z}^3} P^r_\alpha e^{-i\alpha\cdot\gamma}. \tag{6.6}$$

The convergence of S_r in the distributional sense is determined by the matrix

$$\Delta^r = P^r(0) = \frac{1}{8} \sum_{\alpha \in \mathbb{Z}^3} P^r_\alpha. \tag{6.7}$$

Subdivision schemes S_0 and S_3 generate a scalar functional space that include constant functions while S_1 and S_2 generate a cochain space that include the coordinate basis $\{dx, dy, dz\}$ of $\mathbb{R}^3$. Due to Theorem 3.6, Δ^0 must have dominant eigenvalue 1 of multiplicity 1, Δ^1 dominant eigenvalue $1/2$ of multiplicity 3, Δ^2 dominant eigenvalue $1/4$ of multiplicity 3 and Δ^3 dominant eigenvalue $1/8$ of multiplicity 1. Let Λ^r be the vector of eigenvalues of Δ^r. We have

$$\begin{aligned}
\Lambda^0 &= \{1\}, \\
\Lambda^1 &= \left\{\frac{1}{2},\ \frac{1}{2},\ \frac{1}{2},\ -\frac{1}{48}(c+1),\ -\frac{1}{48}(c+1),\ -\frac{1}{48}(c+1)\right\}, \\
\Lambda^2 &= \left\{\frac{1}{4},\ \frac{1}{4},\ \frac{1}{4},\ \frac{1}{16},\ \frac{1}{32},\ -\frac{1}{48}(c+1),\ -\frac{1}{48}(c+1),\ -\frac{1}{48}(c+1)\right\}, \\
\Lambda^3 &= \left\{\frac{1}{8},\ \frac{1}{16},\ \frac{1}{32}\right\}.
\end{aligned}$$

Theorem 3.6 requires that

$$\frac{|-c-1|}{48} < \frac{1}{4}. \tag{6.8}$$

The commutative relations can be written in symbols

$$\begin{aligned} d^0(\boldsymbol{z})P^0(\boldsymbol{z}) &= P^1(\boldsymbol{z})d^0(\boldsymbol{z}), \\ d^1(\boldsymbol{z})P^1(\boldsymbol{z}) &= P^2(\boldsymbol{z})d^1(\boldsymbol{z}), \\ d^2(\boldsymbol{z})P^2(\boldsymbol{z}) &= P^3(\boldsymbol{z})d^2(\boldsymbol{z}). \end{aligned}$$

for $\boldsymbol{z} \equiv \exp(-i\gamma)$. Based on the same argument of Proposition 3.31, we have a similar condition on c:

$$\frac{|-c-1|}{48} < \frac{1}{8}. \tag{6.9}$$

The invariant neighborhood of S_r at vertex v consists of six octahedra and eight tetrahedra that share vertex v. We can write down the subdivision map of S_r on the invariant neighborhood. We claim that similar eigenstructures of the subdivision maps as given by Lemma 3.32 also hold in octet subdivision. Calculation shows that S_1 has eigenvalue $-\frac{1}{24}(c+5)$ and it is passed to S_2 through the commutation relation. To assure dominance of eigenvalue $1/2$ for S_1, eigenvalue $1/4$ for S_2 and eigenvalue $1/8$ for S_3 (see proof of Proposition 3.31), we must have

$$\frac{|-c-5|}{24} < \frac{1}{8}. \tag{6.10}$$

Further we want to avoid negative eigenvalues which means

$$-c-1 \geq 0 \text{ and } -c-5 \geq 0. \tag{6.11}$$

Putting conditions (6.8)–(6.11) together, we have

$$-7 < c \leq -5. \tag{6.12}$$

In practice we took $c = -5$ to get numerical results (see Figure 6.7). It is important to notice that coefficients are uniformly bounded at all subdivision levels.

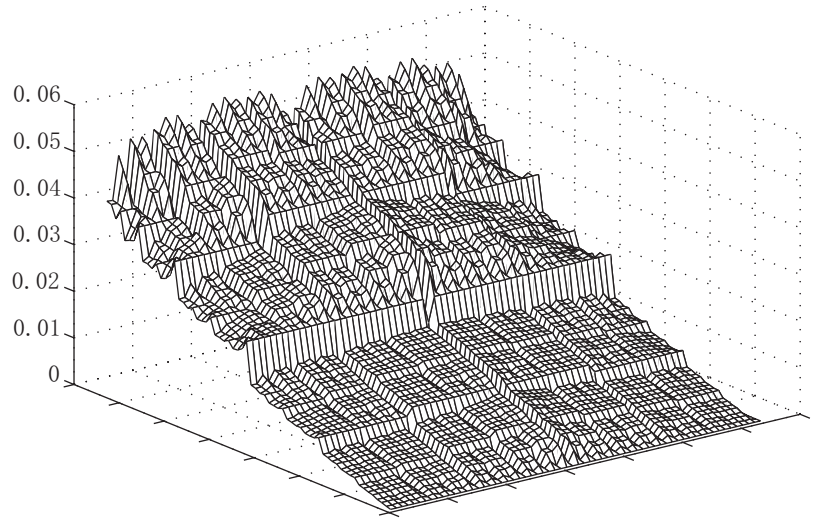

Figure 6.7: *One component of* 8*-vectors at uniform grids generated by* S_2 *with initial data being a single nonzero coefficient on a base octahedron. Visualized is a volumetric slice plot.*

Chapter 7

Conclusion and Future Work

7.1 Conclusion

We presented in this thesis a novel subdivision method of constructing smooth differential forms on simplicial complexes. We have the following conclusions:

(a) The r-cochain subdivision schemes we introduced in this thesis generalizes classic primal/dual subdivision schemes to subdivision schemes based on r-simplexes. The limit of an r-cochain subdivision corresponds to a differential r-form on the mesh.

(b) On a regular mesh, we established the convergence and regularity criteria for r-cochain subdivision schemes by utilizing the theory and techniques of matrix subdivision schemes.

(c) We proved that exactness preserving of the mappings from r-cochains to forms is equivalent to the commutative relations between r-cochain subdivision schemes and the discrete exterior derivative d. Using the commutative relations as a guiding principle we extended our construction to arbitrary topology. we treat r- and $(r+1)$-cochain subdivision schemes as a pair and enforce the commutative relations. Convergence and regularity analysis surrounding irregular vertices are established under the characteristic atlas. As a result, our low-order construction recovers classic Whitney forms, while the high-order construction yields a new class of high-order Whitney forms which form a smooth de Rham complex. In practice, this means that one can do usual vector calculus operations simply through local operations on coefficients associated with simplexes.

(e) We presented a concrete construction of smooth 1-form bases on simplicial surfaces through the edge subdivision scheme. Design of tangent vector fields on a subdivision surface

is now as simple as choosing coefficients on edges without having to worry about coordinate frames. As finite element bases, such 1-form bases exhibit optimal rate of convergence in solving Laplace equations of 1-forms on Riemannian surfaces.

(f) Our method is general enough to accommodate three-dimensional subdivision as well as non-simplicial meshes, such as quadrilaterals and octahedra.

7.2 Further Work: Smooth 3D Schemes

With the linear r-cochain subdivision schemes S_r at hand, it is now straightforward to generate smooth r-cochain subdivision schemes on a uniform octet mesh. As proposed by [Schaefer *et al.* 2004], the smooth 0-cochain scheme $\tilde{S}_0$ is obtained by convolving S_0 with itself. Written in symbols, we have

$$\tilde{P}^0(\boldsymbol{z}) = P^0(\boldsymbol{z})P^0(\boldsymbol{z}), \quad \boldsymbol{z} \in \mathbb{Z}^3.$$

Let $\tilde{P}^r \equiv P^0(\boldsymbol{z})P^r(\boldsymbol{z})$. Since $P^0(\boldsymbol{z})$ is a scalar polynomial, it commutates with the coboundary operator $d(\boldsymbol{z})$. Therefore we have

$$d^r(\boldsymbol{z})\tilde{P}^r(\boldsymbol{z}) = \tilde{P}^{r+1}(\boldsymbol{z})d^r(\boldsymbol{z}), \quad \text{for } r\text{=0,1,2.} \tag{7.1}$$

It is also shown that, in the interior of a base tetrahedron, the resulting $\tilde{S}_0$ is C^2. As a result, we can expect C^1 smoothness for $\tilde{S}_r$, for $r = 1, 2, 3$. The following subjects may be worthwhile to pursue as future work.

7.2.1 Regularity Analysis of S_r on Uniform Octet Meshes

On a base octahedron, the traditional criteria for continuity will not work directly for S_0 since its symbol $P^0(\boldsymbol{z})$ has no factors of $(1+z_i)$ for $i = 1, 2, 3$. Regularity analysis in Sobolev spaces is involved and more advanced tools for analyzing regularities of matrix subdivision schemes are needed (*e.g.*, [Jiang & Oswald 2003]). Unfortunately, software that works for three-dimensional domains is not well developed yet. When proper tools are available, we can perform further investigation on S_r on uniform octet meshes to get optimal Sobolev regularity by varying parameter c.

7.2.2 Design of Schemes on Irregular Tetrahedra Meshes

As demonstrated by [Schaefer *et al.* 2004], smoothness analysis of $\tilde{S}_0$ on the faces of the base tetrahedra mesh can be accomplished by joint spectral radius test. And it already becomes challenging to analyze $\tilde{S}_0$ on edges, or surrounding vertices of the base mesh. In construction of $\tilde{S}_r$ on irregular meshes, the commutative relations must be respected. How should one design $\tilde{S}_r$ on irregular configurations with appearance of commutative relations so as to get optimal regularity there?

7.2.3 3D Simulations and Vector Field Design with Smooth Form Bases

We have demonstrated some promising properties of smooth form bases in simulations on surfaces. Such form bases respect geometry of physical quantities, and at the same time can achieve optimal rate of convergence. Therefore we expect interesting applications when smooth three-dimensional form bases developed above come into use. In particular, design of vector fields in a volume will become more pleasant with our smooth subdivision based on coefficients on edges (triangles).

Appendix A

Bézier Representations

A.1 Bézier Representations

In the regular setting all basis forms have explicit piecewise polynomial representations which we give here. Together with an eigen decomposition around irregular vertices these can be used to implement exact evaluation at arbitrary parameter values in the arbitrary topology setting following the ideas demonstrated by Stam [1998] and Zorin & Kristjansson [2002].

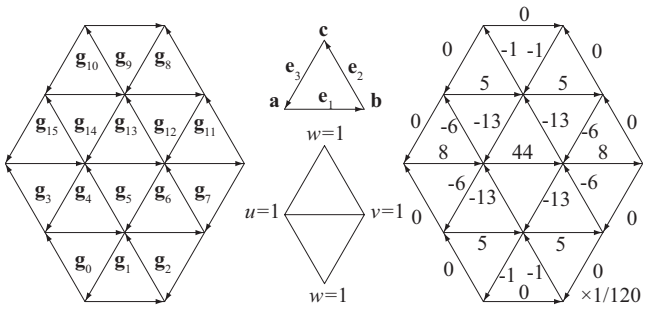

Figure A.1: *Notation and regular limit circulation stencil (right).*

To give the Bézier coefficients we must fix a reference configuration. Let $\mathbf{a}, \mathbf{b}, \mathbf{c} \in \mathbb{R}^2$ be the vertices of a reference triangle and define the edge vectors

$$\mathbf{e}_1 \equiv \mathbf{b} - \mathbf{a},\ \mathbf{e}_2 \equiv \mathbf{c} - \mathbf{b},\ \mathbf{e}_3 \equiv \mathbf{a} - \mathbf{c},\ \bar{\mathbf{e}}_i \equiv \mathbf{e}_i / |\mathbf{e}_i|$$

as well as parameters θ, η and ζ

$$\theta \equiv \langle \bar{\mathbf{e}}_1, \mathbf{e}_2 \rangle,\ \eta \equiv \langle \bar{\mathbf{e}}_1, \mathbf{e}_3 \rangle,\ \zeta \equiv 2A/|\mathbf{e}_1|,$$

where $A \equiv \text{Area}(\triangle\mathbf{abc})$. The restriction $\mathbf{g}_k$ to patch k of the C^1 vector field proxy of the smooth 1-form basis is then given by:

$$\mathbf{g}_k = \frac{1}{2A}\left(g_{k,1}(u,v,w)\bar{\mathbf{e}}_1 + g_{k,2}(u,v,w)\bar{\mathbf{e}}_1^{\perp},\right)$$

where $g_{k,t}(u,v,w) \equiv \frac{1}{24}\sum_{i\geq 0, j\geq 0, i+j\leq 4} m_{k,t}^{ij} u^i v^j w^{4-i-j}$ are functions supported on patch k and (u,v,w) are the barycentric coordinates (see Figure A.1). Due to symmetry we have $\mathbf{g}_{k+8}(u,v,w) = \mathbf{g}_k(v,u,w)$. The values of $m_{k,t}^{ij}$ are listed below (with trailing rows and columns of all zeros elided for brevity), where $M_k \equiv \begin{pmatrix} \binom{ij}{m_{k,1}} \\ \binom{ij}{m_{k,2}} \end{pmatrix}$:

$$M_0 = \begin{pmatrix} \begin{pmatrix} 0 & 0 & 0 & 0 & 2\zeta \\ 0 & 0 & 0 & 8\zeta & 0 \\ 0 & 0 & 6\zeta & 0 & 0 \end{pmatrix} \\ \begin{pmatrix} 0 & 0 & 0 & 0 & \eta-\theta \\ 0 & 0 & 0 & 4(\eta-\theta) & 0 \\ 0 & 0 & -6\theta & 0 & 0 \end{pmatrix} \end{pmatrix}, \; M_1 = \begin{pmatrix} \begin{pmatrix} 2\zeta \end{pmatrix} \\ \begin{pmatrix} \eta-\theta \end{pmatrix} \end{pmatrix},$$

$$M_2 = \begin{pmatrix} \begin{pmatrix} 0 & 0 & 0 \\ 0 & 0 & 0 \\ 0 & 0 & 6\zeta \\ 0 & 8\zeta & 0 \\ 2\zeta & 0 & 0 \end{pmatrix} \\ \begin{pmatrix} 0 & 0 & 0 \\ 0 & 0 & 0 \\ 0 & 0 & 6\eta \\ 0 & 4(\eta-\theta) & 0 \\ \eta-\theta & 0 & 0 \end{pmatrix} \end{pmatrix}, M_3 = \begin{pmatrix} \begin{pmatrix} 0 & 0 & 6\zeta & 16\zeta & 6\zeta \\ 0 & 0 & 12\zeta & 8\zeta & 0 \end{pmatrix} \\ \begin{pmatrix} 0 & 0 & -6\theta & 8(\eta-\theta) & 3(\eta-\theta) \\ 0 & 0 & -12\theta & 4(\eta-\theta) & 0 \end{pmatrix} \end{pmatrix},$$

$$M_4 = \begin{pmatrix} \begin{pmatrix} 6\zeta & 32\zeta & 42\zeta & 16\zeta & 2\zeta \\ 16\zeta & 48\zeta & 36\zeta & 8\zeta & 0 \\ 6\zeta & 12\zeta & 6\zeta & 0 & 0 \end{pmatrix} \\ \begin{pmatrix} 3(\eta-\theta) & 16(\eta-\theta) & 18\eta-24\theta & 8(\eta-\theta) & \eta-\theta \\ 8(\eta-\theta) & 24(\eta-\theta) & 12\eta-24\theta & 4(\eta-\theta) & 0 \\ 6\eta & 12\eta & 6\eta & 0 & 0 \end{pmatrix} \end{pmatrix},$$

$$M_5 = \begin{pmatrix} \begin{pmatrix} 2\zeta & 16\zeta & 42\zeta & 32\zeta & 6\zeta \\ 16\zeta & 96\zeta & 132\zeta & 40\zeta & 0 \\ 42\zeta & 132\zeta & 72\zeta & 0 & 0 \\ 32\zeta & 40\zeta & 0 & 0 & 0 \\ 6\zeta & 0 & 0 & 0 & 0 \end{pmatrix} \\ \begin{pmatrix} \eta-\theta & 8(\eta-\theta) & 24\eta-18\theta & 16(\eta-\theta) & 3(\eta-\theta) \\ 8(\eta-\theta) & 48(\eta-\theta) & 72\eta-60\theta & 20(\eta-\theta) & 0 \\ 18\eta-24\theta & 60\eta-72\theta & 36(\eta-\theta) & 0 & 0 \\ 16(\eta-\theta) & 20(\eta-\theta) & 0 & 0 & 0 \\ 3(\eta-\theta) & 0 & 0 & 0 & 0 \end{pmatrix} \end{pmatrix},$$

$$M_6 = \begin{pmatrix} \begin{pmatrix} 6\zeta & 16\zeta & 6\zeta \\ 32\zeta & 48\zeta & 12\zeta \\ 42\zeta & 36\zeta & 6\zeta \\ 16\zeta & 8\zeta & 0 \\ 2\zeta & 0 & 0 \end{pmatrix} \\ \begin{pmatrix} 3(\eta-\theta) & 8(\eta-\theta) & 6\eta \\ 16(\eta-\theta) & 24(\eta-\theta) & 12\eta \\ 24\eta-18\theta & 24\eta-12\theta & 6\eta \\ 8(\eta-\theta) & 4(\eta-\theta) & 0 \\ \eta-\theta & 0 & 0 \end{pmatrix} \end{pmatrix}, M_7 = \begin{pmatrix} \begin{pmatrix} 0 & 0 \\ 0 & 0 \\ 6\zeta & 12\zeta \\ 16\zeta & 8\zeta \\ 6\zeta & 0 \end{pmatrix} \\ \begin{pmatrix} 0 & 0 \\ 0 & 0 \\ 6\eta & 12\eta \\ 8(\eta-\theta) & 4(\eta-\theta) \\ 3(\eta-\theta) & 0 \end{pmatrix} \end{pmatrix}.$$

A.2 Limit Circulations

Evaluation of the limiting positions of vertices of the initial mesh can be written as a linear operator which takes the control points can returns their limiting positions on the subdivision surface. This is the basic operator to interpolate/approximate data by subdivision surfaces.

Using the Bézier representations of the 1-form proxy, we consider projections of $\mathbf{g}_k$ to unit reference vectors $\bar{\mathbf{e}}_i$, $i = 1, 2, 3$:

$$
\begin{aligned}
C_{k,1}(u, v, w) &\equiv \langle \mathbf{g}_k, \bar{\mathbf{e}}_1 \rangle = \frac{1}{2A|\mathbf{e}_1|}(-\theta - \eta) g_{k,1}, \\
C_{k,2}(u, v, w) &\equiv \langle \mathbf{g}_k, \bar{\mathbf{e}}_2 \rangle = \frac{1}{2A|\mathbf{e}_2|}(\theta g_{k,1} + \zeta g_{k,2}), \\
C_{k,3}(u, v, w) &\equiv \langle \mathbf{g}_k, \bar{\mathbf{e}}_3 \rangle = \frac{1}{2A|\mathbf{e}_3|}(\eta g_{k,1} - \zeta g_{k,2}).
\end{aligned}
$$

With a straightforward but tedious computation one can verify that $C_{k,i}(u, v, w)|\mathbf{e}_i|$ is *independent* of the parameters θ, η, ζ and A, as expected. This shows that circulations of $\mathbf{g}_k$ on triangle edges aligned with reference vectors $(\mathbf{e}_1, \mathbf{e}_2, \mathbf{e}_3)$ are invariant under affine transforms. Circulation on, for instance, the center edge is calculated by the formula

$$
\int_0^1 C_{5,1}(1 - t, t, 0)|e_1| dt = \frac{11}{30}.
$$

Circulations on other edges are calculated in a similar manner and their values are listed in Figure A.1 (right). (It is clear that all circulations vanish on the boundary of the support.)

We can also obtain the limit circulations in regular setting simply through the refinement mask of the 1-form basis. Consider the limit circulation operator $\mathcal{I}$. Due to the symmetry of edges, $\mathcal{I}$ is completely determined by 6 coefficients which are circulations on the 6 edges in the northeast by putting a single 1 on the central edge (see Figure A.1). Given the 1-form subdivision matrix S_1, we have the following relation

$$
R\mathcal{I}S_1 = \mathcal{I},
$$

where R takes the sum along the two fine pieces of a coarse edge. Therefore the operator $\mathcal{I}$ can be seen as an eigenvector, with eigenvalue 1, of the linear operator F defined through

$F(\mathcal{I}) \equiv R\mathcal{I}S_1$. Computation shows that F has a simple eigenvalue 1 and the associated eigenvector $\{44, 8, -13, -6, 5, -1\}$ which exactly recovers, up to a constant scaling factor, the circulations in Figure A.1. To fix this constant factor, we consider the coefficients on coarse edges given by dx where x is the 0-form data that lead to the linear coordinate function on $\mathbb{R}^2$. Edge subdivision of dx yields a constant vector field parallel to the x-axis and its circulations on coarse edges can be easily calculated. Fixing this constant factor, we end up with the same limit circulation operator as given by Bézier representations.

To compute circulations near irregular vertices one may follow the treatment of Halstead *et al.* [1993] essentially verbatim and we will not repeat it here.

Appendix B

Boundary Rules

The design of suitable boundary rules is more subtle since the boundary rules of Loop subdivision are fixed so that the boundary curve depends only on the boundary data. Additionally the cross boundary second derivative vanishes. Consequently we expect a reduced approximation power of the 1-forms near the boundary. To use the commutative relations (3.56), we also need to fix suitable boundary rules for the 2-form scheme.

In what follows, k is used to denote the number of triangles adjacent to vertex v on the boundary. We call a boundary vertex v regular when $k = 3$, irregular otherwise. Boundary vertices are marked in black while interior vertices are marked in white. Vertices without markers may or may not be on the boundary.

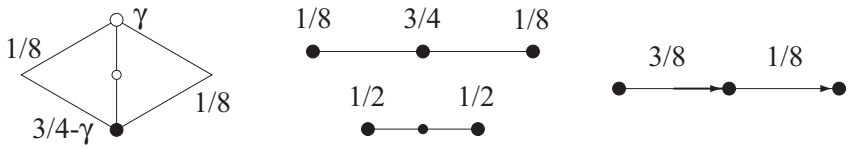

Figure B.1: *Odd stencil for interior edges adjacent to irregular boundary vertices (left) and the even/odd boundary rules for 0-forms (middle). On the right the 1-form boundary stencil.*

B.1 0- and 2-Form Boundary Rules

For the boundary 0-form rules we follow Biermann *et al.* [2000]. In particular we assume the γ modified odd rules for interior edges incident on boundary irregular vertices (see Figure B.1, left). To design boundary rules for 2-forms, we wish to preserve the maximal size of the odd stencil. This simple constraint results in a 7-parameter family of 2-form stencils

(with $A, B, C, D, F_0, F_1, F_2$ as parameters) near the boundary as shown in Figure B.2 (here we consider only $k \geq 3$).

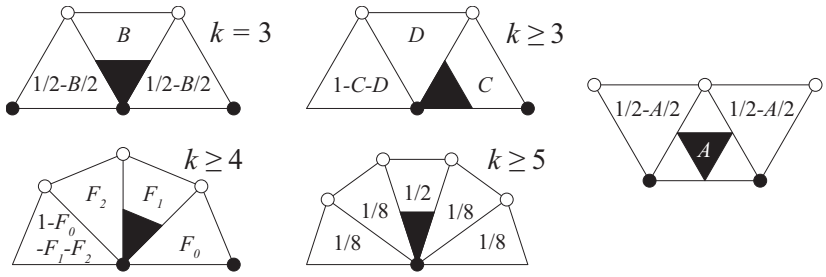

Figure B.2: *Fixing the 2-form stencil support near the boundary we have four cases for odd children (left) and a single case for the even child (right).*

B.2 1-Forms Near the Boundary

The even 1-form boundary rules are simple as they must commute with the 0-form boundary rules which reproduce cubic splines along the boundary. Consequently even 1-form stencils along the boundary are the rules for quadratic splines up to a factor of 1/2 (see Figure B.1, right). With these fixed, and a fully parameterized set of 1-form stencils near the boundary, we can solve the commutative relations. If we require that the even 2-form stencil near the boundary does not depend on the valence of either boundary vertex we find that B, F_0, F_1, F_2 become linear functions of C and D only, giving us a 2-parameter family of stencils overall.

To tie down a particular choice for C and D we ask for a "nice" spectrum for the 2-form near the boundary. In the regular case ($k = 3$) the spectrum consists of a single one, three quarters, four eighths and the remaining eigen values $\{1 - 3D, 1 - C - D, 1 - C - D, -1 + 2C + D\}$. Choosing $C = 2/3$ and $D = 1/6$ yields the particularly nice spectrum $\{1, 1/2, 1/2, 1/4, 1/4, 1/4, 1/6, 1/6, 1/8, 1/8, 1/8, 1/8\}$ and weights

$$A = \tfrac{1}{2}, B = \tfrac{2}{3}, C = \tfrac{2}{3}, D = \tfrac{1}{6}, F_0 = \tfrac{5}{24}, F_1 = \tfrac{7}{12}, F_2 = \tfrac{1}{12}.$$

The corresponding 1-form stencils are depicted in Figure B.3 and Figure B.4 visualizes representative basis forms on the boundary.

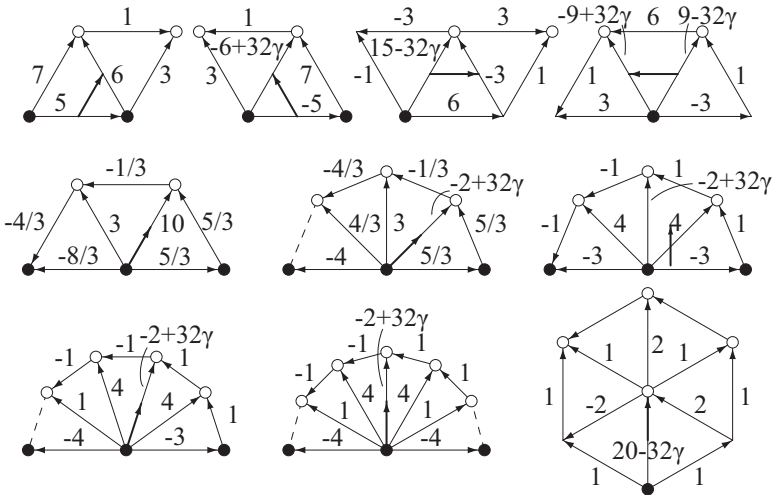

Figure B.3: *1-form stencils (times 32) near the boundary derived from the γ modified boundary rules from [Biermann* et al. *2000].*

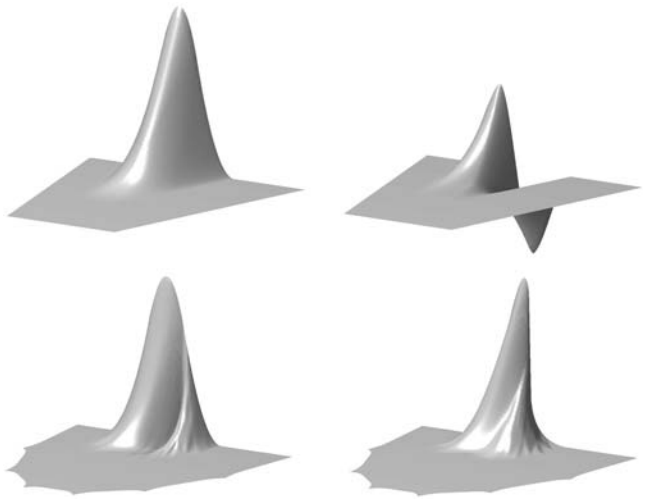

Figure B.4: *Vector proxy visualization of 1-form bases at the boundary. Top: regular ($k = 3$), x & y; bottom: irregular ($k = 7$), x & $-y$.*

Appendix C

Extension to Quads

Our approach to the construction of smooth differential 1-forms on triangle meshes extends naturally to quad meshes. (In fact it is simpler: quad meshes have only two preferred directions rather than three.) We fix the 0-forms on quads to be bilinear functions and 2-forms to be piecewise constant. To find the missing 1-forms in the middle, we simply construct an edge subdivision scheme satisfying the commutative relations. Taking into account the size of support, we assume fully parameterized 1-form stencils. Solving for the commutative relations uniquely determines those stencils (see Figure C.1):

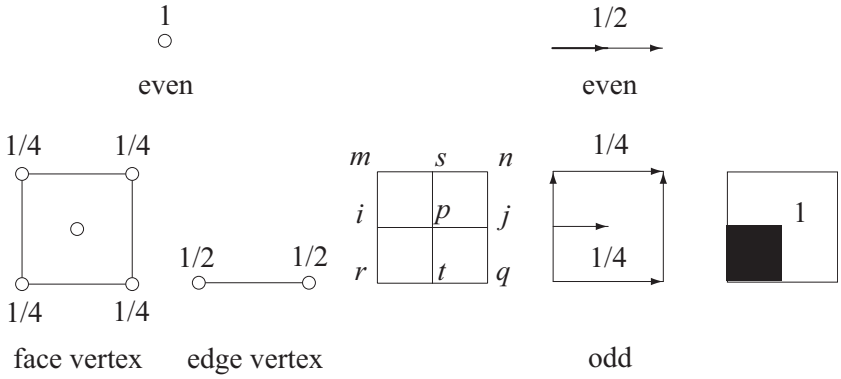

Figure C.1: *Stencils for Whitney 0-, 1-, and 2-forms on quads.*

This gives the following refinement equation for Whitney 1-forms on quad meshes:

$$\phi_{ij} = \frac{1}{2}(\phi_{ip} + \phi_{pj}) + \frac{1}{4}(\phi_{ms} + \phi_{sn} + \phi_{rt} + \phi_{tq}).$$

(recalling the edge elements proposed in Welij [1985]). We consider the quad in 2D to be the image of the unit square under a bilinear transform $x(s)$ where x and s are two-dimensional

vectors. Restricted to the quad the inverse mapping exists as well. Assuming edge ij is the image of interval $\{s_2 = 0,\ 0 \leq s_1 \leq 1\}$, the edge element for ij is defined as

$$\phi_{ij} = (1 - s_2)\boldsymbol{d}s_1. \tag{C.1}$$

Applying this formula to parallelogram meshes which are affine transforms of the $\mathbb{Z}^2$ lattice, it is easy to see that ϕ_{ij} satisfies the above refinement equations.

We now increase the smoothness of 0-, 1-, and 2-forms in the regular setting by twofold convolution along two principal directions. This results in bicubic and biquadratic splines for 0- and 2-forms, respectively. For the arbitrary topology setting, we require our 1-form schemes to commute with Catmull-Clark and Doo-Sabin schemes according to the commutative relations. Given the parameters in the Catmull-Clark and Doo-Sabin subdivision

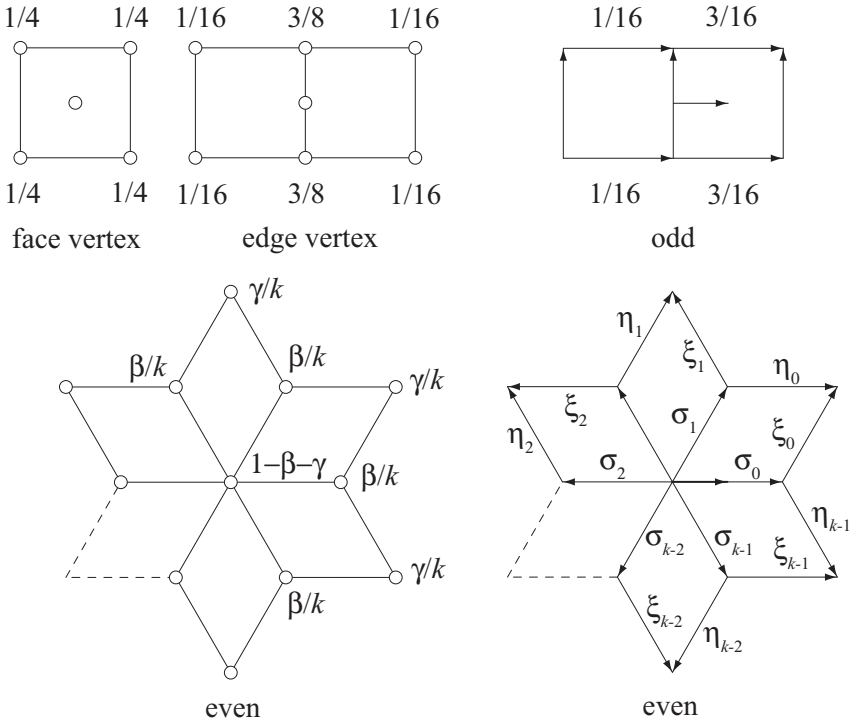

Figure C.2: *Stencils for 0-forms (Catmull-Clark) subdivision (left) and stencils for smooth 1-forms (right).*

schemes β, γ and α_i, we list here the *unique* solution for parameters of the smooth 1-form

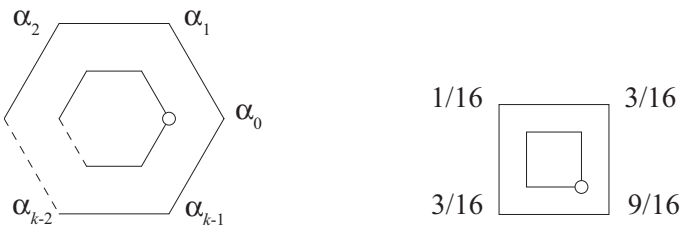

Figure C.3: *Stencils for 2-form (Doo-Sabin) subdivision.*

subdivision scheme (see Figures C.2 and C.3):

$$
\begin{aligned}
&\xi_0 = -\frac{1}{16} - \frac{\gamma}{2k} + \frac{\alpha_0}{8}, \\
&\xi_m = -\frac{1}{8} - \frac{\gamma}{2k} + \frac{\alpha_0}{8} + \frac{1}{4}\sum_{j=1}^{m}\alpha_j,\ 1 \le m \le k-2, \\
&\xi_{k-1} = \xi_{k-2} + \frac{1}{4}\alpha_1, \\
&\eta_m = \xi_{k-m-1},\ 0 \le m \le k-1, \\
&\sigma_0 = \frac{3}{8} - \frac{\beta}{k} + 2\xi_0, \\
&\sigma_1 = \frac{1}{16} - \frac{\beta}{k} + \xi_1 + \xi_{k-1}, \\
&\sigma_m = -\frac{\beta}{k} + \xi_m + \xi_{k-m},\ 2 \le m \le k-2, \\
&\sigma_{k-1} = \sigma_1.
\end{aligned}
$$

To get numerical results, we fix the parameters to be:

$$\beta = \frac{3}{2k},\ \gamma = \frac{1}{4k},$$

$$\alpha_0 = \frac{1}{2} + \frac{1}{4k},\ \alpha_1 = \alpha_{k-1} = \frac{1}{8} + \frac{1}{4k},\ \alpha_j = \frac{1}{4k},\ j = 2, \cdots, k-2,$$

and visualize in the following the smooth 1-form in the image domain of the characteristic map. Given 4 edge values of a quad, we compute the vector at its centroid ($s_1 = s_2 = 1/2$) using (C.1) (see Figure C.4).

Corresponding boundary rules can be derived similar to the case for triangle meshes.

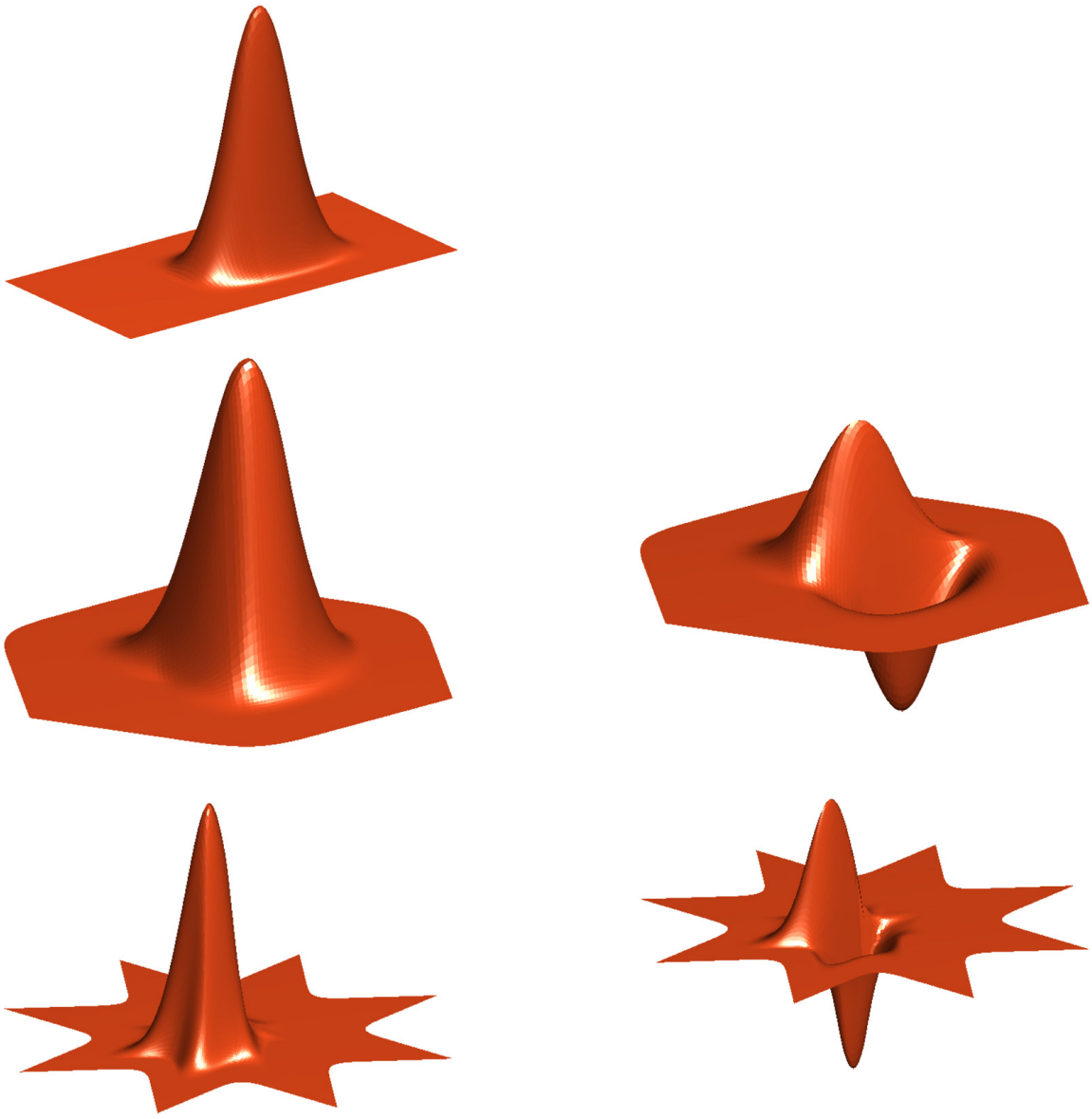

Figure C.4: *Visualization (x resp. y-component of vector proxy) of 1-form bases in the regular ($k = 4$, top; here the y component is identically zero) and irregular ($k = 3$, middle; $k = 8$, bottom) setting. A single edge coefficient incident to the (ir-)regular vertex is set to* 1. *The edge is aligned with the x-axis.*

Bibliography

Arden, G. (2001). *Approximation Properties of Subdivision Surfaces*. Ph.D. thesis, University of Washington.

Arnold, D.N., Falk, R.S. & Winther, R. (2006a). Finite Element Exterior Calculus, Homological Techniques, and Applications. *Acta Numerica*, **15**.

Arnold, D.N., Falk, R.S. & Winther, R. (2006b). Differential complexes and stability of finite element methods. I. The de Rham complex. *The IMA Volumes in Mathematics and its Applications*, **142**, 23–46.

Biermann, H., Levin, A. & Zorin, D. (2000). Piecewise Smooth Subdivision Surfaces with Normal Control. *Comp. Graphics (ACM/SIGGRAPH Proc.)*, 113–120.

Bossavit, A. (1988). Whitney forms: a class of finite elements for three-dimensional computations in the electromagnetism. vol. 135, 493–500.

Bossavit, A. (1990). Solving Maxwell's Equations in a Closed Cavity and the Question of Spurious Modes. *IEEE Trans. Mag.*, **26**, 702–705.

Bossavit, A. (1998). *Computational Electromagnetism*. Academic Press, Boston.

Bossavit, A. (2001). 'Generalized Finite Differences' in Computational Electromagnetics. *Progress in Electromagnetics Research*, **PIER 32**, 45–64.

Bossavit, A. (2002). Generating Whitney Forms of Polynomial Degree One and Higher. *IEEE Transactions on Magnetics*, **38**, 341–344.

Carey, G.F. & Oden, J.T. (1984). *Finite Elements–Computational Aspects*, vol. III. Prentice-Hall, Inc., Englewood Cliffs, N.J.

Catmull, E. & Clark, J. (1978). Recursively Generated B-Spline Surfaces on Arbitrary Topological Meshes. *Comp. Aid. Des.*, **10**, 350–355.

Cavaretta, A.S., Dahmen, W. & Micchelli, C.A. (1991). Stationary subdivision. *Memoirs of the American Mathematical Society*, **93**.

Cendes, Z.J. (1991). Vector Finite Elements for Electromagnetic Field Computation. *IEEE Transactions on Magnetics*, **27**, 3958–3966.

Charina, M., Conti, C. & Sauer, T. (2005). Regularity of Multivariate Vector Subdivision Schemes. *Numerical Algorithms*, **39**, 97–113.

Cirak, F., Ortiz, M. & Schröder, P. (2000). Subdivision surfaces: a new paradigm for thin-shell finite-element analysis. *International Journal for Numerical Methods in Engineering*, **47**, 2039–2072.

Cohen, A., Dyn, N. & Levin, D. (1995). Matrix Subdivision Schemes.

Desbrun, M., Kanso, E. & Tong, Y. (2005a). Discrete Differential Forms for Computational Modeling. In E. Grinspun, P. Schröder & M. Desbrun, eds., *Discrete Differential Geometry*, Course Notes, ACM SIGGRAPH.

Desbrun, M., Leok, M. & Marsden, J.E. (2005b). Discrete Poincaré Lemma. *Applied Numerical Mathematics*, **53**, 231–248.

Dodziuk, J. (1976). Finite-Difference Approach to the Hodge Theory of Harmonic Forms. *American Journal of Mathematics*, **98**.

Dodziuk, J. & Patodi, V.K. (1976). Riemannian structures and triangulations of manifolds. *Journal of the Indian Mathematical Society*, **40**, 1–52.

Doo, D. & Sabin, M. (1978). Analysis of the Behaviour of Recursive Division Surfaces near Extraordinary Points. *Comp. Aid. Des.*, **10**, 356–360.

Elcott, S., Tong, Y., Kanso, E., Schröder, P. & Desbrun, M. (2007). Stable, Circulation-Preserving, Simplicial Fluids. *ACM Transactions on Graphics*, **26**.

Gradinaru, V. & Hiptmair, R. (1999). Whitney Elements on Pyramids. *Electronic Transactions on Numerical Analysis*, **8**, 154–168.

Grinspun, E., Krysl, P. & Schröder, P. (2002). CHARMS: A Simple Framework for Adaptive Simulation. *ACM Trans. on Graph.*, **21**, 281–290.

Halstead, M., Kass, M. & DeRose, T. (1993). Efficient, Fair Interpolation using Catmull-Clark Surfaces. *Comp. Graphics (ACM/SIGGRAPH Proc.)*, 35–44.

Heil, C. & Colella, D. (1996). Matrix Refinement Equations: Existence and Uniqueness. *The Journal of Fourier Analysis and Applications*, **2**, 363–377.

Hiptmair, R. (1999). Canonical Construction of Finite Elements. *Mathematics of Computation*, **68**, 1325–1346.

Hiptmair, R. (2001). Higher-Order Whitney Forms. *Progress in Electromagnetics Research*, **32**, 271–299.

Hirani, A.N. (2003). *Discrete Exterior Calculus*. Ph.D. thesis, California Institute of Technology.

Jiang, Q. & Oswald, P. (2003). Triangular $\sqrt{3}$-subdivision schemes: The Regular Case. *J. Comput. Appl. Math.*, **156**, 47–75.

Khodakovsky, A., Schröder, P. & Sweldens, W. (2000). Progressive Geometry Compression. *Comp. Graphics (ACM/SIGGRAPH Proc.)*, 271–278.

Kobbelt, L. (2000). $\sqrt{3}$ Subdivision. *Comp. Graphics (ACM/SIGGRAPH Proc.)*, 103–112.

Litke, N., Levin, A. & Schröder, P. (2001). Fitting Subdivision Surfaces. In *Visualization '01*, 319–324.

Loop, C. (1987). *Smooth Subdivision Surfaces Based on Triangles*. Master's thesis, University of Utah, Department of Mathematics.

Morrey, C.B. (1966). *Multiple Integrals in the Calculus of Variations*. Springer-Verlag New Yor Inc.

Nédélec, J.C. (1980). Mixed finite elements in $\mathbb{R}^3$. *NUMERISCHE MATHEMATIK*, **35**, 315–341.

Oswald, P. & Schröder, P. (2003). Composite Primal/Dual $\sqrt{3}$ Subdivision Schemes. *Comput. Aided Geom. Des.*, **20**, 135–164.

Peters, J. & Reif, U. (1998). Analysis of Algorithms Generalizing B-spline Subdivision . *SIAM J. Numer. Anal.*, **35**, 728–748.

Raviart, P. & Thomas, J. (1977). A Mixed Finite Element Method for 2nd Order Elliptic Problems. In A. Dold & B. Eckmann, eds., *Lecture Notes in Mathematics*, vol. 606, Springer-Verlag, New York.

Reif, U. (1995). A Unified Approach to Subdivision Algorithms Near Extraordinary Points. *Comput. Aided Geom. Des.*, **12**, 153–174.

Reif, U. (1999). *Analyse und Konstruktion von Subdivisionsalgorithmen für Freiformflächen beliebiger Topologie*. Shaker Verlag, habilitationsschrift.

Reif, U. & Schröder, P. (2001). Curvature Integrability of Subdivision Surfaces. *Advances in Computational Mathematics*, **14**, 103–193.

Schaefer, S., Hakenberg, J. & Warren, J. (2004). Smooth subdivision of tetraheral meshes. *Eurographics Symposium on Geometric Processing*.

Shiue, L.J., Alliez, P., Ursu, R. & Kettner, L. (2005). A Tutorial on CGAL Polyhedron for Subdivision Algorithms.

Spanier, E.H. (1989). *Algebraic topology*. Springer-Verlag, New York.

Spivak, M.A. (1975). *Comprehensive Introduction to Differential Geometry*, vol. IV. Publish or Perish Inc., Boston, MA.

Stam, J. (1998). Exact Evaluation of Catmull-Clark Subdivision Surfaces at Arbitrary Parameter Values. *Comp. Graphics (ACM/SIGGRAPH Proc.)*, 395–404.

Stam, J. (2003). Flows on Surfaces of Arbitrary Toplogy. *Comp. Graphics (ACM/SIGGRAPH Proc.)*, 724–731.

Strang, G. & Fix, G.J. (1973). *An Analysis of the Finite Element Method*. Prentice-Hall, Inc., Englewood Cliffs, New Jersey.

Tong, Y., Lombeyda, S., Hirani, A.N. & Desbrun, M. (2003). Discrete Multiscale Vector Field Decomposition. *ACM Trans. on Graph.*, **22**, 445–452.

Umlauf, G. (2000). Analyzing the Characteristic Map of Triangular Subdivision Schemes. *Constructive Approximation*, **16**, 145–155.

Wallace, A.H. (1970). *Algebraic Topology Homology and Cohomology*. W. A. Benjamin, Inc, New York.

Wang, K. (2006). Online Companion to "Edge Subdivision Schemes and the Construction of Smooth Vector Fields". Tech. rep., Caltech.

Wang, K., Weiwei, Tong, Y., Desbrun, M. & Schröder, P. (2006). Edge Subdivision Schemes and the Construction of Smooth Vector Fields. *Proceedings of ACM SIGGRAPH*, **25**, 1041 – 1048.

Warren, J. (1994). Subdivision methods for geometric design.

Warren, J. & Weimer, H. (2001). *Subdivision Methods for Geometric Design: A Constructive Approach*. Morgan Kaufman Publishers, 1st edn.

Welij, J.V. (1985). Calculation of Eddy Currents in Terms of H on Hexahedra. *IEEE Transactions on Magnetics*, **21**, 2239–2241.

Whitney, H. (1957). *Geometric Integration Theory*. Princeton University Press.

Wilson, S.O. (2005). Geometric Structures on the Cochains of a Manifold.

Zorin, D. (1998). *Stationary Subdivision and Multiresolution Surface Representations*. Ph.D. thesis, California Institute of Technology, Pasadena, California.

Zorin, D. (2000a). A Method for Analysis of C^1-Continuity of Subdivision Surfaces. *SIAM J. Numer. Anal.*, **37**, 1677–1708.

Zorin, D. (2000b). Smoothness of Subdivision on Irregular Meshes. *Constructive Approximation*, **16**, 359–397.

Zorin, D. & Kristjansson, D. (2002). Evaluation of Piecewise Smooth Subdivision Surfaces. *Visual Computer*, **18**, 299–315.

Zorin, D. & Schröder, P., eds. (2000). *Subdivision for Modeling and Animation*. Course Notes, ACM SIGGRAPH.